

General Disclaimer

One or more of the Following Statements may affect this Document

- This document has been reproduced from the best copy furnished by the organizational source. It is being released in the interest of making available as much information as possible.
- This document may contain data, which exceeds the sheet parameters. It was furnished in this condition by the organizational source and is the best copy available.
- This document may contain tone-on-tone or color graphs, charts and/or pictures, which have been reproduced in black and white.
- This document is paginated as submitted by the original source.
- Portions of this document are not fully legible due to the historical nature of some of the material. However, it is the best reproduction available from the original submission.

Multiple Pages Intentionally Left
Blank

DEPARTMENT OF CIVIL ENGINEERING
SCHOOL OF ENGINEERING
OLD DOMINION UNIVERSITY
NORFOLK, VIRGINIA

(NASA-CR-158159) MATHEMATICAL MODEL N79-18478
INVESTIGATION OF LONG-TERM TRANSPORT OF
OCEAN-DUMPED SEWAGE SLUDGE RELATED TO REMOTE
SENSING Final Report, 18 Jul. 1977 - 17 HC A08 / MF A01
Feb. 1979 (Old Dominion Univ. Research) Unclas
G3/45 16329

MATHEMATICAL MODEL INVESTIGATION OF LONG-TERM TRANSPORT
OF OCEAN-DUMPED SEWAGE SLUDGE RELATED TO REMOTE SENSING

by

Chin Y. Kuo, Principal Investigator

and

Thomas D. Modena

Final Report - Part I
For the period July 18, 1977 - February 17, 1979

Prepared for the
National Aeronautics and Space Administration
Langley Research Center
Hampton, Virginia



Under
Research Grant NSG 1441
Robert W. Johnson, Technical Monitor
Marine and Applications Technology Division

February 1979



Page intentionally left blank

ACKNOWLEDGMENT

This research project was funded by the NASA/Langley Research Center, as part of the continuous effort to develop the capability of monitoring water quality in estuarine and coastal waters using remote sensing techniques. Kind assistance received from Dr. Robert W. Johnson, Technical Monitor, is sincerely appreciated. We would also like to acknowledge graduate students, Mr. Raymond S. Chapman, Mr. Henry F. N. Wong, Mr. W. C. Wang and undergraduate student, Mr. Richard G. Smith, for their assistance on this project.

TABLE OF CONTENTS

	<u>Page</u>
ACKNOWLEDGMENT	
SUMMARY	1
1. INTRODUCTION	1
1.1. General Scope of the Study	1
1.2. Remote Sensing	3
1.3. Oceanic Dumping Studies	4
1.4. Oceanic Mathematical Models	6
2. MATHEMATICAL MODELS	13
2.1. History Before University of Rhode Island (URI) Model . .	13
2.2. Development of WAPIC Equations	13
2.3. The WAPIC Algorithm	15
2.4. Considerations in Operating the Model	19
2.5. Old Dominion University (ODU) Modifications	21
2.6. Parametric Studies	21
3. MATHEMATICAL MODEL RESULTS	24
3.1. Results of Parametric Studies for Instantaneous Release .	24
3.2. NASA Remote Sensing Data	28
3.3. Results of Parametric Studies for Continuous Release . . .	30
4. LABORATORY STUDIES OF SLUDGE DUMPING IN VARIOUS AMBIENT DENSITY CONDITIONS	36
4.1. Laboratory Setup	36
4.2. Sludge	37
4.3. Experimental Results	38
4.4. Discussion	41
5. CONCLUSIONS	43
REFERENCES	113
APPENDIX	

PRECEDING PAGE BLANK NOT FILMED

LIST OF TABLES

<u>Table</u>	<u>Page</u>
1 Typical data for settling velocity of sewage sludge and dredged material	45
2 Typical data for horizontal diffusion coefficients	46
3 Typical data for vertical diffusion coefficients	47

LIST OF FIGURES

<u>Figure</u>	
1 Particle size distribution measured by NOAA	48
2 Particle size distribution fitted by a Gaussian curve	49
3 Relative maximum concentration vs. horizontal diffusion coefficient, level 1	50
4 Relative maximum concentration vs. horizontal diffusion coefficient, levels 1 to 2	51
5 Relative maximum concentration vs. horizontal diffusion coefficient, levels 1 to 4	52
6 Relative maximum concentration vs. vertical diffusion coefficient, level 1	53
7 Relative maximum concentration vs. vertical diffusion coefficient, levels 1 to 2	54
8 Relative maximum concentration vs. vertical diffusion coefficient, levels 1 to 4	55
9 Relative maximum concentration vs. particle specific density, level 1	56
10 Relative maximum concentration vs. particle specific density, levels 1 to 2	57
11 Relative maximum concentration vs. particle specific density, levels 1 to 4	58

(CONTINUED)

LIST OF FIGURES (Continued)

<u>Figure</u>		<u>Page</u>
12	Plume width vs. horizontal diffusion coefficient, level i (equal concentration line = 1.0)	59
13	Plume width vs. horizontal diffusion coefficient, levels 1 to 2 (equal concentration line = 1.0)	60
14	Plume width vs. horizontal diffusion coefficient, levels 1 to 4 (equal concentration line = 1.0)	61
15	Plume width vs. horizontal diffusion coefficient, level 1 (equal concentration line = 0.1)	62
16	Plume width vs. horizontal diffusion coefficient, levels 1 to 2 (equal concentration line = 0.1)	63
17	Plume width vs. horizontal diffusion coefficient, levels 1 to 4 (equal concentration line = 0.1)	64
18	Plume width vs. vertical coefficient, level 1	65
19	Plume width vs. vertical coefficient, levels 1 to 2	66
20	Plume width vs. vertical coefficient, levels 1 to 4	67
21	Plume width vs. particle specific density, level 1	68
22	Plume width vs. particle specific density, levels 1 to 2	69
23	Plume width vs. particle specific density, levels 1 to 4	70
24	Plume width vs. time, $E_z = 4.645 \text{ cm}^2/\text{sec}$	71
25	Plume width vs. time, $E_z = 9.29 \text{ cm}^2/\text{sec}$	72
26	Plume width vs. time, $E_z = 23.23 \text{ cm}^2/\text{sec}$	73
27	Plume width vs. time, $E_z = 46.45 \text{ cm}^2/\text{sec}$	74
28	Plume width vs. time, $E_z = 69.68 \text{ cm}^2/\text{sec}$	75
29	Plume width vs. time, $E_z = 92.90 \text{ cm}^2/\text{sec}$	76
30	Settling velocity vs. particle specific density	77
31	Advection and diffusion of plume, level 1	78

LIST OF FIGURES (Continued)

<u>Figure</u>	<u>Page</u>
32 Advection and diffusion of plume, levels 1 to 2	79
33 Advection and diffusion of plume, levels 1 to 4	80
34 Vertical profile of plume for instantaneous release (time = 15 min)	81
35 Vertical profile of plume for instantaneous release (time = 45 min)	82
36 Vertical profile of plume for instantaneous release (time = 75 min)	83
37 Quantitative distribution of suspended solids concentra- tions, mg/l, in a "spot" sewage sludge dump in the NY bight on July 15, 1976, 15 minutes after dump	84
38 Quantitative distribution of suspended solids concentra- tions, mg/l, in a "spot" sewage sludge dump in the NY bight on July 15, 1976, 30 minutes after dump	85
39 Quantitative distribution of suspended solids concentra- tions, mg/l, in a "spot" sewage sludge dump in the NY bight on July 15, 1976, 45 minutes after dump	86
40 Quantitative distribution of suspended solids concentra- tions, mg/l, in a "spot" sewage sludge dump in the NY bight on July 15, 1976, 60 minutes after dump	87
41 Quantitative distribution of suspended solids concentra- tions, mg/l, in a "spot" sewage sludge dump in the NY bight on July 15, 1976, 75 minutes after dump	88
42 Variation of averaged relative maximum concentration with time ($U_x = 3$ cm/sec, $E_x = E_y = 929$ cm ² /sec)	89

LIST OF FIGURES (Continued)

<u>Figure</u>		<u>Page</u>
43	Variation of averaged relative maximum concentration with time ($U_x = 3$ cm/sec, $E_x = E_y = 929$ cm ² /sec)	90
44	Variation of averaged relative maximum concentration with time ($U_x = 6$ cm/sec, $E_x = E_y = 4645$ cm ² /sec)	91
45	Variation of averaged relative maximum concentration with time ($U_x = 6$ cm/sec, $E_x = E_y = 4645$ cm ² /sec)	92
46	Variation of averaged relative concentration with depth ($U_x = 3$ cm/sec, $E_x = E_y = 929$ cm ² /sec)	93
47	Variation of averaged relative concentration with depth ($U_x = 6$ cm/sec, $E_x = E_y = 4645$ cm ² /sec)	94
48	Equiconcentration lines for continuous release, first case (time = 15 min)	95
49	Equiconcentration lines for continuous release, first case (time = 30 min)	96
50	Equiconcentration lines for continuous release, first case (time = 45 min)	97
51	Equiconcentration lines for continuous release, first case (time = 60 min)	98
52	Equiconcentration lines for continuous release, first case (time = 75 min)	99
53	Equiconcentration lines for continuous release, second case (time = 10 min)	100
54	Equiconcentration lines for continuous release, second case (time = 20 min)	101
55	Equiconcentration lines for continuous release, second case (time = 30 min)	102

LIST OF FIGURES (Concluded)

<u>Figure</u>		<u>Page</u>
56	Vertical equiconcentration lines, first case (time = 15 min)	103
57	Vertical equiconcentration lines, first case (time = 45 min)	104
58	Vertical equiconcentration lines, first case (time = 75 min)	105
59	Vertical equiconcentration lines, second case (time = 10 min)	106
60	Vertical equiconcentration lines, second case (time = 20 min)	107
61	Vertical equiconcentration lines, second case (time = 30 min)	108
62	The relationship between water depth and salinity for the case of linear density stratification	109
63	Laboratory setup	110
64	Wastewater treatment plant flowsheet	111

MATHEMATICAL MODEL INVESTIGATION OF LONG-TERM TRANSPORT OF OCEAN-DUMPED SEWAGE SLUDGE RELATED TO REMOTE SENSING

By

Chin Y. Kuo¹ and Thomas D. Modena²

SUMMARY

An existing, three-dimensional, Eulerian-Lagrangian finite-difference model was modified and used to examine the transport processes of dumped sewage sludge in the New York Bight. Both in situ and laboratory data were utilized in an attempt to approximate model inputs such as mean current speed, horizontal diffusion coefficients, particle size distributions, and specific gravities. The results presented are a quantitative description of the fate of a negatively buoyant sewage sludge plume resulting from continuous and instantaneous barge releases. Concentrations of the sludge near the surface were compared qualitatively with those remotely sensed. Laboratory study was performed to investigate the behavior of sewage sludge dumping in various ambient density conditions.

1. INTRODUCTION

1.1. General Scope of the Study

The disposal of concentrated wastes, such as dredged spoils, sewage sludge, industrial wastes, construction and demolition debris, and solid wastes by barging and dumping in the open ocean is a long-standing practice. Because it is an economical disposal method, a great amount of waste has been disposed of in the ocean environment (e.g. off the Atlantic and Gulf Coasts). For example, over five million tons of municipal sewage sludge were dumped in 1976 at a site near the apex of the New York Bight (ref. 1).

¹ Associate Professor of Civil Engineering and Oceanography, Department of Civil Engineering, Old Dominion University, Norfolk, Virginia 23508.

² Graduate Research Assistant, Department of Civil Engineering, Old Dominion University, Norfolk, Virginia 23508.

The environmental impact of dumping has been recognized, especially when the amount of disposed material is enormous. Because of this, this method cannot be indiscriminately adopted in spite of its obvious economic advantage. An overall environmental impact evaluation of this practice is necessary to assess its impact on the aquatic life and the quality of the water environment. Even if the existing dumping site is adequate at present, a comprehensive monitoring program should be maintained and an alternate site should be designated. The alternate site would be used when and if the monitoring program indicates that the existing site cannot safely accommodate any more sewage sludge. The Environmental Protection Agency (EPA) and National Oceanic and Atmospheric Administration (NOAA) have been working hand in hand toward this end.

For such assessments, knowledge of the physical, chemical, and biological behavior of the dumped material is necessary. As part of the continuous effort in monitoring the program for the sludge dumping in the New York Bight, NOAA coordinated a study, Sludge Tracking Acoustics Experiment (STAX II), during July 11 to 16, 1976. The experiment was multidisciplinary in nature, studying various aspects of the sludge plume after the dumping. NASA/LARC was part of the study team. NASA's primary interest was the application of remote sensing techniques to monitor the concentration field of the sewage sludge at ocean surface.

The research reported herein was aimed at the interpretation and evaluation of data related to remote sensing of ocean-dumped sewage sludge. The results of the study concerning the physical aspect of the dumped sludge are presented in this report. Specifically, the far-field transport processes were investigated by means of an existing mathematical model. A concentration field as predicted by the computer model was used for comparison with the results derived from the remote sensing method. Input data required were velocity field, sea conditions, diffusion coefficients, detailed in situ characteristics of the dumped sewage sludge and its dumping rate. STAX II was planned and conducted with no attempt to gather all pertinent data for the use of mathematical model; hence, the results of the mathematical model study on far-field transport of the sludge were compared qualitatively with the remote sensing data. In other words, the behavior of a sewage sludge plume was studied for general trends of spreading, both vertically and horizontally,

contours of equal concentration, maximum sludge concentration within the plume at a given time after the dumping, etc. Efforts were also devoted to the computer model parametric studies for various diffusion rates, current speeds, and settling rates of the sludge. The results of study on chemical and biological aspects of the sewage sludge are presented in Part II of the final report (ref. 2). A laboratory exploratory study of sewage sludge dumping in various ambient density structures was performed, and the results are documented in this report.

The overall objective of this study is to better understand the transport processes of the dumped sewage sludge and therefore provide more information to assist the interpretation of remotely sensed data. Although direct comparison between the results of the computer model and the remote sensing data is not available at this time, the results of the computer model parametric study will be useful to help the planning of a future joint field experiment involving remote sensing and in situ measurements. A long-term objective is to develop the remote sensing techniques to assess the efforts of ocean dumping of wastes on the marine environment.

1.2. Remote Sensing

Remote sensing from aircraft and satellites, called platforms, offered a promising method of studying synoptic surface distributions of features such as suspended solids associated with ocean dumping of sewage sludge. Remote sensing has significant advantages over conventional in situ measuring techniques because of large area coverage, availability of synoptic data, and reduction in the requirements for personnel, instrumentation and boats. Spectral anomalies of signatures from sensors such as Modular Multispectral Scanner (M2S) have already been used to locate and qualitatively and quantitatively map readily identifiable features such as suspended solids in estuaries and coastal areas. For example, multiple regression techniques were used by Johnson to correlate ERTS-1 data with measured values of suspended sediment. Using the derived regression equation, suspended sediment contours were plotted for the Potomac River, Virginia, using Chesapeake Bay deep water for atmospheric calibration (ref. 3). A multispectral scanner onboard an aircraft was also employed by Johnson in the James River, Virginia to qualitatively map suspended sediment (ref. 4). Similar techniques have been applied to study

industrial waste plumes at Hopewell, Virginia (ref. 5), acid waste and sewage sludge dumping off Cape Henlopen, Delaware and in the New York Bight area (refs. 6, 7, 8, 9). Remote sensing from both aircraft and satellite has been applied to the monitoring of water quality parameters in the Great Lakes area (refs. 10, 11, 12).

1.3. Oceanic Dumping Studies

Ketchum and Ford (ref. 13) presented a one-dimensional analysis of the dispersion of a liquid waste discharged at sea in the wake of a barge. They considered vertical dispersion to be instantaneous and only horizontal diffusion perpendicular to the axis of the wake to be effective. The problem was treated as though all of the liquid discharged was concentrated along the wake median line at the initial time $t = 0$. It was also assumed that the distribution of waste along lines perpendicular to the axis was Gaussian. With these simplifications, a simple expression for the concentration, using a diffusion coefficient independent of the dimensions of the mixing field, was obtained:

$$Y = \frac{N}{2\sqrt{K\pi t}}$$

where Y equals the quantity of pollutant in grams in a column of water (a square cross section); N equals pollutants discharged in gm/cm of barge travel; K equals horizontal dispersion coefficient, cm^2/sec ; and t equals time in seconds.

This relationship also provided a means of estimating the rate of discharge of pollutants necessary to meet specific concentration limits. This equation is simple to use, but is expected to give conservative results.

Hood (cited by Ball and Reynolds, ref. 14) carried out studies of the ocean disposal of industrial waste off the coast of Texas in 1961 and 1962. His concentration-time data fit an exponential relationship well. He studied the effects of the speed of the barge dumping the wastes. His conclusions were similar to those of Ketchum and Ford.

Ball and Reynolds (ref. 14) carried out ocean dispersal studies off the coast of Texas on industrial waste dumped by barge with a tracer dye added.

They determined concentration-time relationships with regard to the potential harm to the environment of specific wastes and discharge techniques. They also provided additional field data to help define the dispersion phenomenon.

They concluded that the immediate dilution of the waste in seawater was found to be a function of the speed of the barge and the rate of release. Their data agreed with eddy diffusion theory, but the parameters varied exponentially with concentration rather than directly. Concentration of waste in the water appeared to be a function of the difference in density between the waste and seawater, and was related to the time after discharge (to a power) rather than exponentially as presented in the eddy diffusion theory.

Duedall et al. (ref. 9) studied the fate of sludge-derived ammonium in the water column and the fate of sewage sludge as measured by carbon and nitrogen in sediment samples collected from the sewage sludge disposal site. Proni et al. (ref. 9) studied the distribution of sewage sludge in the water column as measured by an acoustical system.

A joint study of NOAA, State University of New York at Stony Brook (SUNY), and NASA on the sewage sludge dumping in the New York Bight was conducted in July 1976 (ref. 15). Physical and chemical processes which occur during the first few hours after sewage sludge is dumped into a stratified ocean were examined by a variety of remote and direct sampling techniques such as acoustic tracking.

EPA reported a series of studies conducted between 1973 and 1975 on the dispersion of sewage sludge subsequent to its disposal at a site near the apex of New York Bight (refs. 16 to 19). Concentrations of suspended material were measured. Current data and temperature-salinity-density profiles were taken. Laboratory analyses on the settling characteristics, densities, and optical properties of sewage sludge from the New York City area were made. By far, this was the most comprehensive field study on the ocean dumping of sewage sludge. Unfortunately, the study was not coordinated with the over-flight for the remote sensing purpose.

For the interpretation and evaluation of field experiment data related to remote sensing of ocean-dumped sewage sludge, Usry et al. (ref. 20) have performed laboratory upwelled spectral signature measurements of sewage sludge. This was to support the studies reported by Johnson (refs. 6 to 9).

1.4. Oceanic Mathematical Models

Much work has been done in the area of mathematical and numerical modeling of transport phenomena in fluids. However, most models are concerned only with the water quality parameters, such as dissolved oxygen and biochemical oxygen demand and, therefore, do not consider the transport of material containing different groups of particulate matter.

Since 1971, some models have been developed which can handle this form of transport. Many of these, however, are appropriate only for a river or estuary environment. Johnson, in reference 21, provided a review of those models which can be used in a coastal or open ocean area.

The model developed by Koh and Chang (ref. 22) for EPA was a three-dimensional mathematical and numerical model by which the short-term dispersion of barge-disposed wastes could be determined, given the waste characteristics, the ocean environmental conditions, and the method of disposal. The waste was assumed to consist of two phases. The first was a solid phase characterized by up to four constituents with different densities, void ratios, and concentrations, each with as many as two different fall velocities. The second phase was a liquid assumed to be miscible with the ambient water. The model could estimate the concentration of waste material in suspension, in solution, and the distribution of deposited solids.

The model was able to handle three types of barge discharge operations: instantaneous bottom-opening hopper release, discharge through a nozzle under the barge bottom, and discharge continuously in the wake of a moving barge. The ocean conditions incorporated in the model were horizontal currents, a stratified density structure, and a variation of vertical and horizontal diffusion coefficients.

After initial mixing, the model assumed that the descent of the waste cloud takes place in three stages, each stage being governed by a different mechanism. The first stage was convective descent and entrainment. With an initial momentum, the negatively buoyant waste cloud descended and entrained water until it became neutrally buoyant. It was assumed that the particle-laden waste cloud could be treated as a liquid of equivalent density, falling through a less dense ambient liquid.

The second stage was the cloud collapse. The cloud was now neutrally buoyant and spread horizontally at a constant vertical position due to liquid entrainment. The model assumed that the governing mechanism was the difference in hydrostatic pressure between the cloud and the ambient fluid. The collapse phase could be replaced by or include a bottom spreading phase. Under certain circumstances the collapse phase was bypassed.

The last stage was long-term cloud transport and settling which occurred after the horizontal spreading stopped. The dynamically passive waste cloud undergoes vertical settling and long-term horizontal advection by the ambient current and turbulent diffusion. It was assumed that the ambient current was horizontally unidirectional and steady and might only vary in magnitude in the vertical direction. The governing equation was the turbulent diffusion equation with settling processes built in. This equation was transformed by the Aris method of moments, which integrated over the horizontal plane. The location of the centroid, variance of the cloud, and the volume of solids versus depth were given by the equation. The form of distribution (such as uniform or Gaussian) had to be assumed in order to determine the height of material deposited on the bed.

A series of preliminary laboratory experiments was performed by Koh and Chang (ref. 22) to verify the assumptions made. A good comparison was achieved between the experimental results and the theoretical prediction.

The major limitation of the model was the use of the Aris method of moments in the long-term diffusion-settling phase. This does not allow diffusion coefficients, currents, and other ambient conditions to be functions of time or horizontal position. Because of this, the effects of temporal variation could not be obtained, and the model could not be used in more dynamic environments.

Another limitation of using the Aris method lay in the area of comparing recorded field data with computed results from the long-term phase. With this equation the detailed distribution of the dumped material was ignored and only the gross characteristics of the dispersent as a function of time and depth were given.

An additional limitation of the model lay in the fact that there was no provision for a vertical ambient velocity. This would be necessary if lateral boundaries were needed for a location close to a coastline. Lateral boundaries would probably prohibit the use of the Aris method.

Edge (ref. 23) devised a mathematical model similar to that of Koh and Chang. This model could describe the transport of barge-dumped fine grained clay and silt dredge materials and also wastewater sludges from municipal or industrial sources. However, their model could only handle one method of discharge: pumping through nozzles from a moving barge. They divided the motion of the waste plume into two separate stages, eliminating the collapse stage that Koh and Chang used. Their first stage was convective descent, as was that of Koh and Chang. Again the dumped material was treated as a liquid medium whose density was equal to the average equivalent density of the waste material. The second and last stage was settling with dispersion. This was based on Koh's method in which solid particles settle with their fall velocities while undergoing horizontal spreading due to turbulent diffusion. The four-thirds power law was used for the horizontal diffusion, and vertical diffusion was neglected. Their modifications made for a simplification of calculations, but provided less detail than Koh's method.

B. G. Krishnappan (ref. 24) developed a mathematical model which used the principle of superposition to calculate the motion of granular dredged material when instantaneously dumped near the surface of deep water with a turbulent, one-dimensional, steady flow field. The dredged material was considered to consist of various fractions of uniform size particles with varying negative buoyancies. These different fractions have a weighted influence on the total behavior of the dredged material. The behavior of the particles had been formulated using the theory of dimensional analysis and laboratory experiments.

His experiments indicated that the spreading rate of solid particles moving in a liquid medium was different from that of a denser liquid moving in a liquid medium. The model of Koh-Chang and Edge used the liquid mixture in a liquid mechanism in the initial stages. As the particle size decreased, the difference between the behavior of solid and liquid particle clouds also decreased. Therefore, Krishnappan maintained that treating the dredged material as a liquid medium was not valid, especially when the dredged material consisted of larger size particles.

Treating the dumped material as dense liquid had further consequences. Such an assumption necessitated the design of the collapse stage as a separate

stage, even though the negative buoyancy of dredged material consisting mainly of sand particles would not become zero with any amount of entrainment of the external fluid.

The results of this research showed that the motion of the particles could be treated in two distinct phases: the initial entrainment and the final settling. During the entrainment phase, which completely described waste plumes in coastal waters, the size of the particle cloud grew due to entrainment of ambient liquid while the descent velocity decreased. During the settling phase, which occurred at depths of 1000 meters or more, the fall velocity of the cloud was the same as the average settling velocity of particles in the cloud. The cloud grew horizontally due to ambient turbulence until it reached the bottom.

This method permitted the evaluation of vertical height and horizontal size of the mound formed by the deposition of the dredged material at the bottom of deep water. It also indicated how the above characteristics of the mound depended on the volume of the dump, the size distribution of the dredged material, and the depth of the deep water, thereby providing guidance for the selection of optimum dump size and the location for disposal of the dredged material.

B. H. Johnson and B. W. Holliday (ref. 25) conducted a study in 1977 using and attempting to verify the Koh-Chang model. The model's predictions did not agree with the observed fate of dredged material that was dumped into the ocean off the Hawaiian Islands. The authors felt that this could have been caused by incorrectly characterizing the waste material.

A mathematical model was developed by Falk, Myers, and Thomann (ref. 26) for the study of dispersion of liquid wastes behind a moving barge. It was able to take into account the vertical temperature - density structure of the ocean and the density and settling characteristics of the waste. This model was a two-dimensional (lateral and vertical) diffusion-advection mass equation. It used a horizontal Lagrangian coordinate system which eliminated horizontal advective velocities. Longitudinal diffusion was also eliminated since the concentration gradient in this direction was smaller than in the lateral and vertical directions. Lateral diffusion was considered symmetrical and lateral concentration gaussian. Instantaneous mixing was assumed in the longitudinal direction, and the waste field was considered to be laid down

instantaneously. Discrete settling was included in the mass balance equation to incorporate the vertical settling characteristics of the waste. The nonlinear time variable equation was solved numerically using the finite difference approach.

The model's waste-settling routine was verified with laboratory studies, and the entire model was verified with several sets of field data obtained from a waste disposal area off the Delaware coast.

A.K. Deb (ref. 27) used the Koh-Chang model to study the characteristics of dispersion of liquid and solid fractions of industrial ocean-dumped wastes. The model was run under heavy thermocline and no thermocline conditions. Deb was satisfied with the results and used them in attempts to determine suitable disposal sites. The Koh-Chang model used by Deb was the original version which was also used by Rittall (ref. 28) to study the sludge dumping associated with EPA studies (refs. 16 to 19). No attempt was made to compare the model outputs with the field data collected.

G.W. Bowers and M.K. Goldblatt (ref. 29) described recent modifications to the Koh-Chang model by the J.B.F. Scientific Corporation and previous modifications by the U.S. Army Corps of Engineers. The recent modifications included improving the model's dynamic phase predictive capability through a program of laboratory calibration and model testing. Also, use of the model was simplified by simplifying inputs and outputs. Modifications of long-term diffusion equations were also made for fall velocities of fine particles. Previous modifications to the Koh-Chang model were primarily made to handle the prediction of the short-term fate of dredged material discharged in an estuarine environment (ref. 30).

The Aris method of moments was replaced by a convolution method which obtains material concentrations directly. The original model assumed horizontally uniform steady currents, and no horizontal boundaries were allowed. The revisions allowed nonuniform currents, horizontal boundaries, and unsteady flow. The short-term model for estuarine environments was evaluated and calibrated by the Corps of Engineers Waterways Experiment Station (ref. 31).

In the present study, a computer model was needed to predict the long-term advection and diffusion of ocean-dumped sewage sludge for comparison with remotely sensed data. At the time there were two models available: the original Koh-Chang model and the Pavish-Spaulling model. The Pavish-Spaulling model was chosen as the best for this study (ref. 32).

The Pavish-Spaulling model did not have the short-term routines of the Koh-Chang model, but this was felt to be acceptable. Sewage sludge has a combined density slightly heavier than water. Because of this the sewage would not go through an extensive descent and collapse, which are the short-term stages of the Koh-Chang model. Sewage sludge would quickly enter the long-term advection and diffusion phase at a relatively shallow depth. This is shown by the Alpha Contour Plots in Appendix C of the report by Teeter et al. (ref. 19).

The long-term phase of the original Koh-Chang model was limited by the use of the Aris method of moments. That routine did not allow a detailed description of sludge concentration since it integrated over the horizontal plane. The Pavish-Spaulling model gave concentration values in a three-dimensional grid form. Since the model was to be compared with data given over the horizontal plane, it was felt that the Koh-Chang model was inappropriate for this study which emphasized the detailed sewage sludge concentration distribution near the surface related to remote sensing study.

The Aris routine also did not allow diffusion coefficients, currents, and other ambient conditions to be functions of time or horizontal position. At the time it was felt that a detailed description of current and diffusion data would be supplied or could be calculated and used with the sludge concentration data; hence the Koh-Chang model was too limiting. The Pavish-Spaulling model had a velocity processor developed for the interpretation of velocities from a vertically averaged, two-dimensional velocity field of a finite-difference, hydrodynamical, numerical model. There were also options of diffusion coefficient routines in the model. Later in the study it became evident that detailed current and diffusion data would not be available, so these options in the model were not used in spite of these advantages.

The original Koh-Chang model also only allowed a horizontal lower boundary as the only permissible boundary condition, which was limiting in a coastal location. The Pavish-Spaulling model transformed the vertical coordinate into dimensionless space, then rearranged it into a flux conservative, pseudo-velocity form. This allowed an adaptation to flow situations with a time and spatially varying bottom topography and free surface. Although this routine was not used, it allowed more flexibility in the study.

Most recent literature, (ref. 29) shows that most of the limitations of the original Koh-Chang model have been eliminated in newer versions of the model. In addition, the model has been calibrated and verified in the laboratory to some extent for the initial phase of mixing, and work is underway to verify it in the field. The Pavish-Spaulling model has not been calibrated or verified to date. In the early stage of this study, the Pavish-Spaulling model was selected because of the stated limitations of Koh-Chang model. At that time it was not known that revision and laboratory verification on near-field plume behavior of the Koh-Chang would be made. Field verification of both Pavish-Spaulling and Koh-Chang models remains to be done.

2. MATHEMATICAL MODEL

2.1. History Before University of Rhode Island (URI) Model

Several simpler numerical models and calculation methods for fluids evolved to form the Pavish-Spauling model. In 1957 Evans and Harlow (cited in Pavish and Spaulding, ref. 32) developed the particle in cell (PIC) numerical method. This solved problems involving dynamics of compressible fluids in two dimensions. The flow area was a fixed Eulerian mesh of computational cells, and the moving fluid was represented by particles with physical mass, energy, and a velocity of motion. Sklarew developed the pseudo-total flux velocity method in 1970 (cited in ref. 32). This was an adaptation of PIC solutions to the turbulent, three-dimensional, incompressible, mass transport equation. Hotchkiss (cited in ref. 32) applied an explicit, finite-difference solution to the three-dimensional, incompressible Navier-Stokes equations. This was called the atmospheric heat and mass transport model of ADPIC. It produced a time-dependent, advective, atmospheric velocity field and used Lagrangian marker particles and Sklarew's pseudo-total velocity technique. Hirt et al. (cited in ref. 32) devised the alternating Lagrangian-Eulerian technique, called ALE. They also devised the translating and expanding grid system with a Lagrangian particle cloud. Finally, Pavish and Spaulding (ref. 32) developed the water advective particle in cell technique (WAPIC), which was a three-dimensional, explicit, finite difference, pseudo-total velocity solution to the turbulent, mass transport equation.

2.2. Development of WAPIC Equations

The main governing equation of the WAPIC algorithm was the Fickian turbulent advection diffusion equation. This was an ensemble time average of the three-dimensional mass transfer equation:

$$\frac{\partial C}{\partial t} + \frac{U\partial C}{\partial X} + \frac{V\partial C}{\partial Y} + \frac{W\partial C}{\partial Z} = \frac{\partial}{\partial X} \left(K_x \frac{\partial C}{\partial X} \right) + \frac{\partial}{\partial Y} \left(K_y \frac{\partial C}{\partial Y} \right) + \frac{\partial}{\partial Z} \left(K_z \frac{\partial C}{\partial Z} \right)$$

where U , V , and W were the X , Y , and Z time and spatially averaged velocity components; K_x , K_y , and K_z were the X , Y , and Z turbulent diffusion coefficients; and C was the time and spatially averaged concentrations. This equation could only be used when the scale of the current eddies

was much smaller than the dimensions of the waste field. The assumptions made in this equation were that the pollutant concentrations were dilute, nondecaying, and neutrally buoyant, and the flux terms due to molecular diffusivity were neglected. The flow field of the model was specified by time and spatially averaged velocity components, and the time and spatially averaged diffusion coefficients were determined either empirically or parametrically.

Settling was added to the turbulent advection diffusion equation. The advective mass flux in the Z direction was given by the still water terminal particle settling velocity, W_s , times the vertical concentration gradient, $\frac{\partial C}{\partial Z}$. This simulates the motion of a negatively buoyant dilute mass such as a sewage sludge slurry.

The flux conservative form of the mass transfer equation is the pseudo-total velocity equation:

$$\frac{\partial C}{\partial t} + \frac{\partial}{\partial X} (U_T C) + \frac{\partial}{\partial Y} (V_T C) + \frac{\partial}{\partial Z} (W_T C) = 0$$

where: $U_T = U + U_D$

$$V_T = V + V_D$$

$$W_T = W + W_D + W_s$$

and: $U_D = - \frac{K_x}{C} \frac{\partial C}{\partial X}$

$$V_D = - \frac{K_y}{C} \frac{\partial C}{\partial Y}$$

$$W_D = - \frac{K_z}{C} \frac{\partial C}{\partial Z}$$

This indicates that each marker particle is advected with the mean motion of the fluid field and diffused with a velocity proportional to the concentration gradient surrounding the particle.

2.3. The WAPIC Algorithm

The WAPIC algorithm modeled the long-term transport of ocean-dumped sludge by providing a solution to the pseudo-velocity equations by the Lagrangian marker particle in Eulerian cell technique. Long-term transport means that initial mixing has been completed so that there would be no momentum forces, only advection, diffusion, and settling, due to density differences. Falk, Myers, and Thomann (ref. 26) concluded from a 1977 study that initial mixing was completed 10 to 30 minutes after the release of acid waste from a barge.

The model, for the case of instantaneous release of sewage sludge, consisted of a system of equal volume boxes numbering 15 longitudinally, 15 laterally, and 10 vertically. These boxes, called Eulerian grid cells, collectively represented a portion of water. Boundaries could be defined on the faces of these cells. In the case of this study, the top of the collection or system of cells was considered to be the level sea surface, and the bottom was considered to be the thermocline. Particles called Lagrangian marker particles moved inside these Eulerian cells. These particles statistically represented a cloud or concentration of suspended or settling particles, and, in the case of this study, the particles represented a sewage sludge plume.

The cells were called Eulerian since, although the cells could expand and translate, the system was always referenced to a fixed point. The system of cells formed a framework by which the marker particles could be kept track of and given locating coordinates. The particles were called Lagrangian since they moved with the advective velocities, representing the prevailing ocean currents and particle settling, and the diffusive velocities, representing the spreading of the plume.

Each particle was given a volume equal to one grid cell and a dimensionless mass. When these particles or parts of particles in each grid cell were summed, a concentration could be calculated and defined at the center of each cell. A separate routine based on a specified particle diameter array and a particle density was used to calculate the settling velocities of the particles.

There were three different particle generation procedures in the WAPIC algorithm. The instantaneous Gaussian release particle generation procedure was used to simulate an instantaneous pollutant release. For this procedure, simplifying assumptions were made. The first assumption was that a finitely sized, evenly distributed, waste cloud, created by the turbid plume from a sewage sludge, could be represented in the long-term dispersion phase as if it had originally been an instantaneous point source. It was also assumed that turbulent diffusion from an instantaneous release point in a homogeneous, unidirectional, unbounded flow after sufficient initial dilution and diffusion time would form a three-dimensional Gaussian character. This implied that the concentration field had a normal distribution around a maximum concentration and that this could be described by standard deviations. It was also assumed that 99.5 percent of the pollutant concentration or marker particles would be within range of plus or minus three standard deviations from the mean or maximum concentration.

A continuous release was also simulated in this study by releasing a Gaussian particle distribution at a specified location for each successive time step. However, the Eulerian grid could not be allowed to expand or translate when this routine was used.

In the algorithm, given the distance of each Eulerian grid cell from the mean cloud position and standard deviation lengths of the cloud, a specified number of particles was placed in each Eulerian cell using a simple, analytical, probability function. This prevented an initial bunching of particles around the mean particle position. A uniform random number generator was then used to determine the location of the specified number of particles within each grid cell.

The time cycle of the algorithm consisted of a Eulerian step followed by a Lagrangian step. In the Eulerian step, concentrations defined at the center of each cell were used to calculate diffusion velocities, which were defined at the center of cell faces. The pseudo-diffusive velocities were approximated by a centered, finite-difference, calculation method written in Cartesian space. There was an optional calculation method using vertically transformed dimensional space which was not used since a flat sea surface and bottom were assumed. After the diffusion velocities were calculated, they were added to the advection velocities to give total velocity.

In the Lagrangian step, each marker particle was advected for one time step in three-space by the pure explicit form of the velocity field. The time-centered form was not used since the particles were assumed to be traveling with a constant unidirectional advective velocity as was specified in this study. A two-dimensional hydrodynamic velocity processor was not needed for the same reason. New Lagrangian coordinates were computed for each particle by adding a bilinear weighted velocity times the length of the time step to the old coordinate value. Every WAPIC grid was surrounded by a maximum of 26 cells. The particular cell in which a particle's coordinates were located was divided into eight equivolume octants, and the octant in which the particle was located was determined. Then each marker particle was given the fictitious volume of one Eulerian grid cell, which could overlap into eight surrounding grid cells. The particle's velocity was determined by the three-dimensional weight of the nearest eight surrounding pseudo-total velocities.

In the next part of the Lagrangian step, there was a selective expansion of the Eulerian grid with the diffusive growth of the marker particle cloud, and a selective translation of the grid with the mean motion of the advected cloud in any three dimensions in Cartesian space. The Y and Z direction translation was not used since only an X-direction current was specified. The Z-direction expansion was not used since the top of the grid was assumed to be the sea surface and the bottom of the grid a fixed depth.

In the expansion step, each particle was tested for placement within a certain distance of an outer grid system boundary in any given direction. If the particle was within that distance, then each grid cell expanded a specified percentage of the grid cell length in that direction. The combined expansion was about the grid system center. The grid origin's coordinates were updated from its original location at time equal to zero. For the translation step, the average distance that all the particles moved was calculated and the grid system origin was recalculated accordingly.

It was necessary to employ boundary conditions when the Eulerian grid no longer expanded or translated in a given dimension. Since the algorithm was part Eulerian and part Lagrangian, it was necessary to establish conditions for each: each Eulerian grid cell was assigned a boundary identification number. Vertical boundary cells, whose cell faces lay on the horizontal plane boundary, could be set for the Lagrangian conditions of no conditions

or particle reflection, deposition, or entrainment. When the fictitious volume of the marker particles overlapped more than halfway into an open boundary cell, the particle was reflected if it was a top boundary, or deposited if it was a bottom boundary. If deposited, then the particles were removed from the grid field by setting their Z coordinates to zero and storing the X and Y deposition coordinates. The vertical boundary cells could be set for the Eulerian conditions of velocity flux or no flux across the cell face. The top boundary was set for reflection since it was considered the sea surface, and the bottom boundary was set for deposition since particle settling was employed. Both top and bottom had no vertical velocity flux conditions employed. Horizontal cells with cell faces not on the horizontal plane could have the boundary conditions of land cell or open cell, both specifying Lagrangian reflection conditions and Eulerian, no horizontal velocity, flux conditions. The condition of a water cell, which specified no Lagrangian conditions and Eulerian velocity flux conditions across the cell face, was used since open-ocean conditions were being modeled.

The final part of the Lagrangian step was the calculation of the new concentration field from the new particle positions. Each marker particle was assigned a physical mass and a fictitious volume of one Eulerian grid cell. The WAPIC code located the Eulerian cell and the octant in the cell in which each particle was located. The fictitious volume was located, and a three-dimensional weighting scheme was employed to find which fraction lay in each of eight possible surrounding cells. All parts of the fictitious volumes in each grid cell were totaled, and the concentration in each grid was calculated.

In the WAPIC algorithm, an array of settling velocities for negatively buoyant particles could be imposed upon advective and diffusive particle velocities. The assumptions made were that the water column was vertically well mixed in density and homogeneous with respect to vertical turbulence. It was also assumed that a given Lagrangian marker particle statistically represented a given mass of sediment particles in the water column, that they all had an equal density, and that they could be described with a still water terminal settling rate.

The particle settling rate was calculated by Watson's empirically modified version of Rubey's analytically derived still water settling law for sand grains:

$$W_s = \frac{\left(9A^2 \mu^2 + \frac{4}{3} SR^3 (\rho_P - \rho_{FL})g - 3A\mu \right)}{SR\rho_{FL}}$$

where:

S = pressure drag coefficient = 0.5303 (dimensionless),

A = viscous drag coefficient = 0.623 (dimensionless),

R = particle radius (cm),

W = settling velocity (cm/sec),

μ = fluid viscosity (poise),

ρ = mass density (g/cm³), and

FL, P = subscripts for fluid or particle density.

Vertical settling velocity was added to vertical advective and diffusive velocities. The array of particle settling rates was calculated when the array of particle diameters, the percentage of particles of each diameter, and the particle specific gravity were given. The ambient fluid density and viscosity and drag coefficients were specified to match ambient conditions.

2.4. Considerations in Operating the Model

There were many interconnected factors which had to be considered to obtain reasonable results from the WAPIC model. An important consideration was that the Eulerian grid size be large enough and that the number of grid cells be sufficient to resolve the concentration gradient and therefore avoid diffusion velocity errors.

To achieve this end, Lange's estimation equation was used:

$$\frac{U_{\text{Finite Difference}}}{U_{\text{Exact}}} = 1 - \frac{1}{24} \left(\frac{X^2}{\sigma^2} - 3 \right) \frac{\Delta X^2}{\sigma^2}$$

where:

U = diffusion velocity,

X = particle cloud length,

ΔX = grid cell length, and

σ^2 = standard deviation.

Three times the standard deviation was substituted for the particle cloud length since 99 percent of all particles was assumed to be included in this range, giving:

$$\frac{U_{\text{F.D.}}}{U_{\text{Exact}}} = 1 - \frac{\Delta X^2}{4\sigma^2}$$

Using this equation, a $\frac{\sigma}{\Delta X}$ of 0.5 gave 100 percent accuracy in diffusion velocity; 1.0 gave 25 percent; 2.0 gave 6.25 percent; and 3.0 gave 2.78 percent accuracy. A ratio of 6.25 percent was considered an acceptable level of error.

Plus or minus 3 times the standard deviation was calculated to be 12 Eulerian grid lengths in the X and Y directions. Twelve grids were needed and 15 were provided so the concentration gradient could have the proper resolution inside the Eulerian grid system in the X and Y directions. Three grid lengths were needed in the Z direction, and 10 were used.

The relationship between the number of marker particles and the number of Eulerian grid cells used to resolve their distribution was also important to the model accuracy. As few as one marker particle per Eulerian cell yielded meaningful results. As many should be used as computer storage limitations will allow. Two thousand particles were used for 2250 grid cells. However, these were concentrated toward the center of the model, not evenly spaced out.

Finite difference techniques have either a dynamic stability or a time-step restriction. The fastest moving particle could translate no more than one-half cell length in a given time step. This restriction dampened the amplitude of high-frequency oscillations in the marker particle field present in the particle-in-cell method.

The number of marker particles used was important in producing a truly normal distribution. Estimated and actual standard deviation lengths versus grid size ratios were used as an indicator for normality. It was found that 1000 particles were needed to achieve an accuracy of 10 percent for the standard deviation to grid length ratio of 1.0, and 2000 particles were needed for a 10 percent accuracy for a ratio of 2.0.

In general, when the standard deviation-grid length ratio was decreased, accuracy was increased; when the number of marker particles was decreased, then accuracy was decreased.

2.5. Old Dominion University (ODU) Modifications

Modifications had to be made to the program which was written for an IBM 370, to adapt it to ODU's DEC-10 system. One adaptation was the replacement of the random number generator. A system program was called that gave the required random numbers when supplied with a seed number. Different seed numbers were tried to generate a set of numbers which located the three-space averaged particle position as close to the specified position as possible.

The particle array used in the settling routine was changed to reflect the material comprising the sewage plume modeled. R. A. Young (ref. 15) analyzed the particle size and distribution of typical sewage sludge for NOAA. An array of seven sizes similar to those he found was used, but the distribution was made to fit a Gaussian curve. The NOAA data and the Gaussian curve distribution of particle size are included in figures 1 and 2. The specific gravity of the particles used in this study was within a range determined by Browne and Callaway (ref. 33) for EPA. A value of 1.7 g/cm^3 was chosen for this study. (Table 1 shows the sample data for settling velocity compiled from various studies on sewage sludge and dredged material.)

Corrections had to be made to the particle settling routine coding in one of the program's subroutines. When a particle settled to the bottom of the Eulerian grid and was removed from the calculations, its assigned diameter was reassigned to the next marker particle in the calculations, a very unreasonable situation physically. This defect was corrected so that each particle retained its originally assigned diameter. A correction also had to be made in the average total vertical velocity values output by the program because the settling velocity was not included in the calculations in the URI model.

2.6. Parametric Studies

A parametric study was carried out after the model was working properly and adjusted to the conditions to be modeled. Since horizontal and vertical diffusion and particle settling rate in an oceanic environment differ, these

parameters were studied. The horizontal diffusion coefficients in the X and Y directions were selected equal and varied from 4.65 to 464500 cm²/sec. The vertical diffusion coefficient was varied from 0.93 to 92.9 cm²/sec. (Typical values on horizontal and vertical diffusion coefficients from other studies are summarized in tables 2 and 3.) The specific gravity of the marker particles was varied from 1.025 g/cm³, specified for the ambient fluid, to 2.65 g/cm³, approximately that of sand. For each of the parameters looked at, concentrations were calculated for depths integrated from the surface down to 0.61, 1.22, and 2.44 m (2, 4, and 8 ft). This had to be done to compare the data to remotely sensed data for which the depth of penetration was unknown.

An attempt was made to measure the horizontal diffusion rate from the equiconcentration plots of the sludge concentration obtained by NASA using remote sensing techniques (ref. 9 and figs. 37 through 41). Using a method given by F. J. Burgess (ref. 34), equations for nonsteady-state diffusion coefficients (D_x, D_y) were obtained. For X and Y:

$$D = \frac{1}{2} \frac{\Delta\sigma_i^2}{\Delta t}$$

where

$$\Delta\sigma_i^2 = \sigma_{1,i}^2 - \sigma_{2,i+c}^2$$

The subscripts 1 and 2 refer to flight numbers, i refers to the section number across the plume in flight one, and i+c is the section number in flight two adjusted for the movement of the waste field between flights; t is the time difference between the flights. Variance (σ^2) was estimated for a normal distribution from sample variance (S_y^2):

$$S_y^2 = \frac{\sum w(Y - \bar{Y})^2}{N} = \frac{1}{N} \left[\sum_{i=1}^n W_i Y_i^2 - \frac{\left(\sum_{i=1}^n W_i Y_i \right)^2}{N} \right]$$

where

$$N = \sum_{i=1}^n W_i$$

Y equals distance from the origin, and W equals concentration. The values used were scaled from an estimated center point on the equiconcentration plots around each contour. The calculations yielded a typical value of 417 cm²/sec, which was comparable with other data shown in table 2, but at the lower end of the range as cited in the table. Based on this available set of remote sensing data, this method proved to be very sensitive in terms of the direction of sections used to calculate standard deviations and the time sequence of flights selected.

3. MATHEMATICAL MODEL RESULTS

3.1. Results of Parametric Studies for Instantaneous Release

Relative maximum concentrations and plume sizes at different equal concentrations were determined for time equal to 0, 15, 30, 45, 60, and 75 min. These were given for depths integrated from the surface to 0.6096 m or level one, from the surface to 1.219 m or levels one through two, and from the surface to 2.438 m or levels one through four. This output was studied parametrically as horizontal and vertical diffusion and particle density were varied. The concentrations shown throughout this report are relative concentrations referring to an arbitrary unit. For example, if 1 unit is assigned 1 mg/l, then 2 units mean 2 mg/l.

Figures 3 through 5 show the maximum concentration of the plume at 15, 30, 45, 60, and 75 min, in level one, levels one through two, and levels one through four as the horizontal diffusion was varied. The vertical diffusion was held at $46.45 \text{ cm}^2/\text{sec}$, and the particle density was held at 1.7 g/cm^3 . The maximum concentration decreased as the horizontal diffusion increased, since diffusion spread the plume out, decreasing all concentrations. As time increased, the maximum concentration decreased because of diffusion and settling. Also, as the depth was integrated to a deeper level below the surface, the maximum concentration increased slightly. This was because the portion of the plume being considered, such as the fourth level, was above the injection source, the maximum concentration for the whole plume. The concentration increased towards the maximum. The integrated depth concentration increased as the level containing higher concentration was included. Figures 6 to 8 show the maximum concentrations as the vertical diffusion was varied, shown at the same time intervals and integrated depths as before. The horizontal diffusion was held at $4645 \text{ cm}^2/\text{sec}$, and the particle density was held at 1.7 g/cm^3 . As vertical diffusion increased, the maximum concentration increased to a point, then leveled off and decreased gradually. Larger vertical diffusion coefficients would diffuse more mass vertically and leave less mass to be diffused horizontally. As a result, a lot of mass was distributed at levels lower than the fourth level above which the integration was carried out. The maximum concentration detected in the upper levels decreased. As time increased, the maximum concentration decreased as before. Also, maximum concentration was slightly larger for

integrated depth levels integrated to a greater depth. This effect was more pronounced earlier in time, as was explained above. Figures 9 to 11 show the maximum concentration as the particle density was varied, at the same times and integrated depths as above. The horizontal diffusion was held at 4645 cm^2/sec and the vertical at 46.45 cm^2/sec . As the particle gravity was increased, the maximum concentration in the upper levels decreased almost linearly due to the linear increase in settling velocities. As time increased, the maximum concentration decreased due to settling and diffusion as mentioned above. The maximum concentration was larger for integrated depth levels integrated to a greater depth. This effect was more pronounced earlier in time and at higher densities. For a density of 1.025 g/cm^3 , the same as the ambient fluid, the program only allowed one particle size to be specified, instead of the usual seven used in this study. This caused a slight fluctuation in the concentrations for this value for the case of transport of neutrally buoyant pollutants.

Figures 12 to 14 show the width of the plume at an equal concentration of 1.0 as the horizontal diffusion was varied. The vertical diffusion was held at 46.45 cm^2/sec and the particle density at 1.7 g/cm^3 . For small values of horizontal diffusion, the plume width increased as the diffusion increased, and slightly increased as time increased. This was caused by a combination of vertical diffusion and settling. For intermediate values of horizontal diffusion, the width increased slightly as diffusion increased for time equal to 15 and 30 min. It increased, then decreased for time equal to 45 min and 60 min, and decreased for 75 min. The width increased with time to 30 min then decreased for this range of diffusion values. For large values of horizontal diffusion, the plume width increased to time equal to 15 min, then decreased. As the horizontal diffusion coefficient increased, the mass of sludge was diffused farther away from the release point. Because of the large volume of ambient water involved, the concentration decreased at a given level under consideration. The width of plume shown in figures 12 to 14 is for the averaged plume size of the equal concentration of one unit. The width was slightly larger for the integrated depth levels integrated to a greater depth. This was caused by the effect of including a layer closer to the maximum concentration as explained in figures 3 to 5. Figures 15 to 17 show the plume width at an equiconcentration of 0.1 as the horizontal diffusion was varied. The vertical diffusion was held at 46.45

cm^2/sec and the particle density at 1.7 g/cm^3 . The graphs have the same basic shape as the graphs for concentration equal to 1.0, figures 12 to 14. The main difference between the graphs is that maximum plume widths at each time interval occur at a larger horizontal diffusion coefficient for the 0.1 concentration graphs. Figures 18 to 20 show the plume width at an equiconcentration of 1.0 as the vertical diffusion was varied. The horizontal diffusion was held at $4645 \text{ cm}^2/\text{sec}$ and the particle density at 1.7 g/cm^3 . As the vertical diffusion was increased, the plume width increased then leveled off for larger values with a certain degree of oscillating phenomena; this was most likely caused by the increasing instability of the model. The width decreased as time increased after 30 min. The width was significantly greater for the deeper integrated depth levels with small values of vertical diffusion. More particles stayed at lower levels below the free surface as the settling processes dominated over the upward diffusion. In other words, this was caused by the fact that with a small diffusion particles were not pushed into the top section of the Eulerian grid. For intermediate and large values for the vertical diffusion the width was slightly greater for greater depth integrated plume depths as were the cases mentioned above. Figures 21 to 23 show the plume width at the equal concentration of 1.0 as the particle density was varied. The times and integrated depths are as specified above. The horizontal diffusion was held at $4645 \text{ cm}^2/\text{sec}$ and the vertical at $46.45 \text{ cm}^2/\text{sec}$. For small particle densities the plume width increased with time. As the density increased, the width increase slowed with time. For large values of particle density, the width of the plume decreased with time. This was caused by the changing balance between vertical diffusion and particle density. If particles were lighter than the ambient seawater, more particles were pushed upward toward the free surface due to the combined physical processes of buoyant force and upward diffusion. The concentration near the surface as well as the width of the plume increased as time increased. For neutrally buoyant particles, upward diffusion was the only driving force responsible for the increases in concentration in levels near the surface. For larger particle densities, the settling process was the dominant factor causing the decrease in plume width as the time increased at a given level. Figures 24 through 29 show, for different vertical diffusions, the change in the plume width with time at a concentration equal to 1.0 at the different integrated depth levels. Horizontal diffusion was

held at $4645 \text{ cm}^2/\text{sec}$ and particle density at 1.7 g/cm^3 . For the smallest vertical diffusion values, figure 24, plume concentrations were only found at integrated levels one through four, and as a result the plume width decreased with time. Obviously, particle settling was a dominant process in this case. For the larger diffusion values, figures 25 through 29, the plume width increased until time equal to about 30 min then decreased. For small vertical diffusion coefficients, the concentration values were the smallest for level one, larger for integrated levels one through two, and the largest for integrated levels one through four. The values of concentrations at the different integrated depth levels were closer together as the vertical diffusion increased. This was caused by the larger vertical diffusion pushing the plume up to the top of the Eulerian grid or the surface of the water more quickly. The concentration distribution over the water column of the top four levels was uniform. The number of levels used for integration to obtain average concentration was no longer an important factor. Figure 30 shows the averaged settling velocity as the particle density was varied. There was a fairly linear increase in the particle settling velocity as the particle density was increased above the ambient density. This was because the density and the settling were linearly related in the Watson-Rubey settling equation in this model.

Figures 31 to 33 show the plume width with equiconcentration contours from a top view at 15, 30, 45, 60, and 75 min. The horizontal diffusion coefficient was held at $4645 \text{ cm}^2/\text{sec}$, the vertical diffusion coefficient at $46.45 \text{ cm}^2/\text{sec}$, and the particle density at 1.7 g/cm^3 . The plume could be seen advecting at a constant rate. As time increased, the maximum concentration decreased and the equal concentration lines spread out. This was caused by diffusion and settling. At an equal concentration line of 1.0, the width increased until time equal to 30 min then decreased as the settling brought more of the plume to deeper layers in the Eulerian grid or water column. At a concentration of 0.1, the width kept increasing through 75 min. The settling had not removed enough material to reduce this level of concentration by 75 min. As before, the plume width was slightly greater for greater integrated depth levels. Figures 34 to 36 show the plume width for different equal concentrations at all levels at time equal to 15, 45, and 75 min. The horizontal diffusion constant was held at $4645 \text{ cm}^2/\text{sec}$, the vertical diffusion constant at 46.45

cm²/sec, and the particle density at 1.7 g/cm³. At 15 min, figure 34, the maximum concentration was at level 7 below the water surface. At 45 min, figure 35, it was at level 6 below the surface and, at 75 min, figure 36, at level 9 below the surface. The plume center was between levels four and five originally and spread out as the center slowly dropped with some fluctuation in the water column. This was a combined result of diffusion and settling as had been studied and presented in previous figures.

Results throughout the parametric study showed general trends. Concentrations were always lower for the level one depth than for the levels one through two depth. These both had lower concentrations than the levels one through four depth. This difference was more pronounced for smaller vertical diffusion values. This was due to the fact that the initial center of the plume was placed below level four, and that the vertical diffusion at this level and above was in an upward direction due to the existence of a concentration gradient. For all the parameters under investigation, concentration of the plume decreased with time because of diffusion and settling. The concentration also decreased when horizontal diffusion and density gravity increased.

3.2. NASA Remote Sensing Data

NASA supplied remotely sensed data of a metropolitan New York sewage sludge plume dumped in the New York Bight. This data was taken from an aircraft with Modular Multispectral Scanner onboard flying at about 3,048 m (10,000 ft) on July 15, 1976 of a spot dump from a stationary barge. Multiple passes and in situ monitoring were made over the plumes at about 15-min intervals for 2 hr after the dump. When plume radiance values were normalized to ocean water in the area, characteristic responses were found. Applying multiple regression analysis techniques, R. W. Johnson et al. (ref. 9), developed a single regression equation that could be used to determine suspended solid concentrations in the plume for each of the aircraft passes. In this way it was possible to determine and map the concentration distribution for each of the passes even though sea truth measurements were not made for each one. Equiconcentration contours of the spot dump were determined for the surface concentration distributions at time equal to 15, 30, 45, 60, and 75 min. These are shown in figures 37 through 41. This data set was used in this

study for qualitative comparison with the model results in terms of diffusion and settling. Advective studies could not be made since precise coordinates were not determined.

While NASA was taking remotely sensed data, NOAA was taking ground truth data of the sewage plumes. An attempt was made to correlate the wind data with the current data. Unfortunately, wind velocity but not direction was recorded on the day that NASA took its data. Wind directions were taken with velocity on the day before and the day after, but these were in opposite directions, so no information could be gained from that. Drogues at 2 m and 18 m were also deployed the day before and the day after, but again not on the day that NASA took its data. Classical Eckman spiral calculations were carried out with the wind and current data that was provided, but they did not show good correlation. NOAA's data indicated that wind speed was less than 15 kn (7.7 m/sec). Pycnocline was between 9 and 16 m. Temperature was 16° to 20°C at surface and 10° to 11°C at bottom. Water depth was 25 m, and salinity was 30 ‰ at surface and 32 ‰ at bottom. Current speed varied from 13 to 60 cm/sec at a depth of 2 m, and 15 to 50 cm/sec at a depth of 18 m. These data were only for references in this study. They were not synoptic measurements made during the remote sensing flights.

With the exception of NASA data for 15 min, which was quite irregular in shape, there was a general agreement with some of the computer-generated data. NASA's equiconcentration lines showed that the plume width increased to 45 min then decreased.

In figures 31 through 33, it is seen that the plume width increased until time equaled 30 min, and then decreased for the equiconcentration line of 1.0. However, when the 2.0 and higher concentration lines were considered, the width of the plume decreased with time. The plume width also increased with time for the equiconcentration line of 0.1. This trend was the same for all three figures in which the integrated depth from the surface was varied.

This trend did not change much as vertical diffusion was varied (as shown in figures 24 through 29). As the particle specific gravity was varied, as shown in figures 21 through 23, the plume width, which was only calculated for the 1.0 equiconcentration line, changed with time. For slightly negatively buoyant particles of the specific gravity 1.7 g/cm³ chosen in this study, the width increased until 30 min, then decreased. As shown in figures 12

through 14, this trend was generally the same as horizontal diffusion was varied. A typical averaged horizontal diffusion coefficient as studied by Ketchum (cited by Yudelson, ref. 38) in the New York Bight was 4645 cm²/sec. Figures 25 through 29 indicate also that the plume width increased up to a time 30 min after the initial release and decreased thereafter. A report by Falk, Myers, and Thomann indicated that initial mixing was completed 10 to 30 min after the release of waste from a barge (ref. 26). The Pavish-Spaulding model used for this study did not consider the initial mixing phase since long-term and far-field processes were of primary interest. If this initial mixing time were considered in the model used, the sewage sludge plume width would reach maximum at 45 to 50 min after the release. The result would match very well with the remote sensing data.

There was a partial agreement between NASA's maximum concentration data and computer-generated data. In NASA's data, the maximum concentration was low at 15 min (no data was supplied for time equal to zero), increased to 45 min, then decreased for larger time.

In figure 33, which shows integrated depth levels one through four, the concentration was maximum at time equal to zero then decreased with time. In figures 31 and 32, showing level one and depth integrated levels one through two, the concentration was maximum at time equal to 15 min then decreased with time. This trend was unchanged with a change in horizontal diffusion (figs. 3, 4, and 5), vertical diffusion (figs. 6 to 8), or particle specific density (figs. 9 to 11). In order to have a more precise one-to-one comparison between the remote sensing data and the model results, fairly accurate in situ determinations of horizontal and vertical diffusion, particle density and size distribution were necessary. To achieve the type of comparison desired, a well-calibrated mathematical model was needed. For this reason, only qualitative comparisons and the parametric study for the general behavior of the sewage sludge plume were included.

3.3. Results of Parametric Studies for Continuous Release

In order to simulate a continuous rather than an instantaneous release, several changes had to be made to the WAPIC algorithm. There were two major changes that had to be made. The first was that the Lagrangian marker particles, representing the sludge plume, had to be released at each time step to simulate

the continuous release of materials. The second change was that the Eulerian grid system, representing the ocean, could not be allowed to expand or translate with the movement of the Lagrangian marker particles. This was a consequence of the way in which the algorithm was written.

There were several adjustments that had to be made to the program. The number of marker particles had to be adjusted; there had to be enough to give a reasonable distribution at each time step, and this distribution was only available at certain incremental steps: 4, 12, 16, etc. However, due to large computer storage requirements and calculation time, the total sum of the number of particles had to be kept below reasonable limits. This sum, of course, depended on how long a data record was required.

The subroutine which added particles at every time step to the grid system was not written to allow for an array of particle diameters. Since the particle distribution added was much smaller than the distribution used for the instantaneous routine, this was an appropriate simplification. The average size diameter of the previously used array was selected as the single size specified.

Another adjustment that had to be made was in the amount of mass which represented the total mass of the particle array added at each time step. This was a relative number with unspecified units chosen for the best display of output concentrations or for comparison with other data.

The number of Eulerian grid spaces or boxes that was used also had to be adjusted. Since the grid system could not expand or translate, enough grid boxes had to be provided to allow for the movement of the Lagrangian marker particles. However, this had to be balanced against computer storage requirements and computing time. Adding grid boxes increased both of these significantly.

A parametric study of the horizontal diffusion constants and the advective longitudinal or X-direction velocity was then carried out and the results studied. These parameters, however, had to be balanced between showing a significant change in the output and keeping the marker particles within in fixed Eulerian grid system. Due to the excessive computer time required for each run, the study was limited.

The data from two computer runs were selected for detailed analysis. For both runs, 36 particles of equal diameter and mass were added at each time step. The vertical diffusion coefficient was held at $46.45 \text{ cm}^2/\text{sec}$ and the particle specific density at 1.7 g/cm^3 for both runs. For the first run, the horizontal diffusion constant was $929 \text{ cm}^2/\text{sec}$ and the advective longitudinal velocity was 3 cm/sec . For the second run, a larger diffusion constant of $4645 \text{ cm}^2/\text{sec}$ and a larger velocity of 6 cm/sec were used. The data was analyzed until either the plume reached a point on the horizontal edge of the grid system or 75 min had elapsed. For the first run, no part of the plume had reached the boundary at time equal to 75 min, but during the second run the plume reached the boundary after 35 min.

Figures 42 through 45 show the maximum relative concentration horizontally averaged over nine grid cells at five-min intervals at various depth levels. For both sets of data the concentration increased rapidly at first then leveled off to an almost constant value. This was a result of mass or particles being added continuously into the grid system, being advected and diffused, and eventually settling out at the bottom boundary of the grid. At first, particles were being added at every time step, were advecting and diffusing, but none had reached the bottom to be removed from the calculations. As particles started reaching the bottom, the rate of concentration increase started slowing down. After a period of time the particles added essentially equaled those settling out at the bottom, approaching a steady-state condition, clearly seen in the longer run, figures 42 and 43.

For both data runs, figures 42 and 44, the concentration was highest for integrated levels one through four, next highest for integrated levels one through two, and lowest for level one. Comparing individual levels in figures 43 and 45, we see that level five had the highest concentrations, then level three, and levels one and eight had the lowest concentrations. The differences were caused by the fact that the particles were continuously released between levels four and five, then diffused away from that point both in the upwards and the downwards direction. Ten levels were considered in the study.

The first run, figures 42 and 43, with its smaller diffusion coefficient and advection rate, had higher relative concentrations at all levels and times, other than zero, than the second run, figures 44 and 45. The greater the diffusion and advection of the plume, the more quickly the plume was spread out and, hence, the lower the relative concentration achieved.

Figures 46 and 47 show the maximum relative concentration horizontally averaged as before, plotted with depth at different times. For the first run with smaller advection and diffusion values, figure 46 shows the concentrations at time equal to 0, 15, 30, 45, and 60 min. For the second run with larger advection and diffusion values, figure 47 shows the concentrations at time equal to 0, 10, 20, and 30 min.

For both runs the concentrations were highest at levels four and five. The concentrations decreased at approximately equal rates in both the upward and downward directions from these levels. As mentioned before, the particles were added between levels four and five and diffused upward and downward from that area. The center of the added particle distribution is slightly closer to level four, and at time equal to zero the concentrations are slightly higher at level four. At all subsequent times the effects of settling are seen and the concentrations are definitely higher at level five.

As seen before in both runs, the concentrations increased with time, rapidly at first, then more slowly, and finally for the longer run almost not at all. This showed the time lag involved in the process of a particle being added into the top half of the grid system, diffusing, and eventually settling out at the bottom of the grid.

Figure 46, showing data from the first run with its lower advection and diffusion values, had higher relative concentrations at all levels and all times, after time equal to zero, than figure 47. Figure 47 shows data from the second run which had higher advection and diffusion values, causing the plume to spread out more and have lower concentration values. This was also seen in figures 42 through 45.

Figures 48 through 55 are of the plume at integrated levels one through four plotted in the horizontal plane at a range of equiconcentrations. Figures 48 through 52 are from the run with lower advection and diffusion values at time equal to 15, 30, 45, 60, and 75 min respectively. Figures 53 through 55 are for the second run and at time equal to 10, 20, and 30 min respectively. All of the equiconcentration lines in these graphs are egg shaped, shortened in the negative longitudinal or X direction and elongated in the positive X direction. The origin point is considered to be the center of the area in

which the particle distribution was added at each time step. This distortion of the plume in the longitudinal direction was caused by the longitudinal advective velocity pushing the particles toward the positive X direction while new particles were being added near the origin and were diffusing in all directions from the origin. The continuous release and diffusion processes also caused the relative concentrations to be highest near the origin and to decrease at a decreasing rate away from the origin.

As time increased for the first run, the concentration increased near the origin between 15 and 30 min and the equiconcentration line of 50.0 was added. At the same time, the equiconcentration lines were constant in the negative X direction except near the origin, moved slightly outward in the lateral or Y direction, and moved significantly away from the origin in the positive X direction. After 30 min the equiconcentration lines continued to move away from the origin in the positive X direction with the advective current, but remained in the same position in the other three Cartesian directions.

In view of the continuous release of mass, diffusion, and a horizontal advective current, it is quite understandable that the relative concentration increased in the positive X direction with time. In the negative X direction, the horizontal diffusive velocity of the continuously released mass and the advective velocity were in opposite directions, and by time equal to 15 min they seemed to balance each other. In the Y direction the advection was moving at right angles to the diffusion. In the first 30 min the diffusion of the continuously released mass seemed to be the dominant factor since the concentration of the plume was increasing, but after that the concentration was constant. Because diffusive velocity was dependent on the concentration gradient present, this changed with a changing gradient. The new particles diffusing outward also had a settling velocity acting on them, so a balance was achieved between the outward decreasing diffusion velocity of the added mass and the settling velocity which removed the particles to lower layers of the grid system. The entire plume was subjected to this advection, horizontal and vertical diffusion, and settling. The combination of factors determined whether a balance would be achieved and, if so, at what distance from the origin and in what length of time.

For figures 53 through 55, the same trend was seen. Between 10 and 20 min, there was no change in the position of the equiconcentration lines in negative X direction, a slight increase in the positive and negative Y directions, and a large increase in the positive X direction. Between 20 and 30 min, the concentration increased near the origin and the equiconcentration line of 30.0 was added. There was no change in the negative X direction and in the outer equiconcentration lines in the Y directions. The inner lines in the Y direction moved slightly outwards with the increase of concentration at the origin. The lines moved significantly in the positive X direction with the horizontal advective velocity.

Figures 56 through 61 show the equiconcentration lines of the plume on the vertical plane for the two data runs at different times. The figures indicate the locations of maximum relative concentration, which were near the center of the area in which the marker particles representing the plume were added at each time step. The change in concentration was less in the vertical direction due to smaller specified diffusion velocities.

Figures 56, 57, and 58 show the run with the smaller diffusion coefficient of $929 \text{ cm}^2/\text{sec}$ and smaller advective current of $3 \text{ cm}/\text{sec}$ at time equal to 15, 45, and 75 min, respectively. Between 15 and 45 min the equal concentration lines moved outwards in all directions from the origin, especially in the positive X or down current direction. Near the origin the equiconcentration line of 70 was added since the maximum concentration increased due to continuous release. Between 45 and 75 min, there was a slight increase in the maximum concentration. The equiconcentration lines changed primarily with a marked move in the positive X direction due to the advective current.

Figures 59, 60, and 61 show the run with the larger diffusion of $4645 \text{ cm}^2/\text{sec}$ and larger advective current of $6 \text{ cm}/\text{sec}$ at time equal to 10, 20, and 30 min, respectively. The same trend is seen as in figures 56 through 58. The overall concentrations were lower due to the increased advection and diffusion.

4. LABORATORY STUDIES OF SLUDGE DUMPING IN VARIOUS AMBIENT DENSITY CONDITIONS

4.1 Laboratory Setup

Four sets of different quiescent density structures were created in a glass tank in which the behavior of dumped sludge was studied. The first density structure was freshwater. This was used as a control environment to compare with the other cases. Salt water of either 15‰ or 25‰ was the second structure studied. This represented a temperate, well-mixed, coastal ocean or sea in the late fall through early spring.

The third density structure was a two-layer system with an upper layer of freshwater and a saltwater lower layer of 15 ‰ or 25 ‰. This represented a strong thermocline in a temperate ocean or sea which occurs from late spring through fall. The last structure was a linearly varying density system. The relationship between water depth and salinity for this case is shown in figure 62. This system was representative of a thermocline region. The same laboratory setup was used by Kuo to create a linear density stratification (ref. 35). The rectangular glass tank used, tank C in figure 63, was 107-cm high and 43.4 cm by 43.9 cm wide. During experiments the tank was filled with water to a depth of 100 cm. The volume of water was 0.193 m³, and the weight was 192.7 kg, assuming the density of the water to be 1.0 g/cm.

The experimental setup shown in figure 63 was used to create a linearly varying density system. Two identical plastic tanks, tanks A and B, were connected by a siphon. Tank B was filled with salt water of concentration C_0 , salinity 25 ‰, and tank A was filled with freshwater. Tank B was connected to the glass tank, tank C, by a flexible rubber tube. Water entered the glass tank through this tube. A round, wooden plate which floated on the surface of the water in the glass tank was used to minimize the turbulence of the downward momentum of the water when it entered the tank. As the water level in tank B was lowered, water entered the tank from tank A through the siphon. By this method, the concentration of the water, C_s , filling the glass tank was linearly changing and equal to $(C_0 H)/H_0$. Figure 62 is a typical variation for the case of linear density stratification. The same setup was used to create the two-layer density systems, except the siphon did not connect

tanks A and B. For this case the glass tank, tank C, was filled halfway from the saltwater tank, tank B. Then, the salt water was overlaid with freshwater from tank A to fill the remainder of the glass tank.

4.2. Sludge

A typical wastewater treatment process is illustrated in figure 64. Contaminants in wastewater are removed by physical, chemical and biological means. The means of treatment in which the application of physical forces predominate are known as "unit operations"; thus, screening, mixing, flocculation, sedimentation, flotation, elutriation, vacuum filtration, heat transfer, and drying are unit operations. The means of treatment in which the removal of contaminants is brought about by the addition of chemicals or by biological activity are known as "unit processes." Precipitation, combustion, and biological oxidation are examples of unit processes.

We can obtain sludge from point A, point B or point C. Sludge which comes from point A is called primary sludge. It is separated from fresh municipal sewage in primary settling tanks, and is mostly grey to dark grey. It contains small or larger pieces of fecal matter and other readily recognizable particulate matter. Such sludge has characteristically objectionable odors, does not filter readily, and has a high moisture (water) content, usually 94 to 97 percent. Sludge which comes from point C is called activated digested sludge. It is more homogeneous and has a moisture content which is usually appreciably less than that of the fresh sludges. It is commonly jet black (due to iron sulphide) and has a tar-like odor which is not unpleasant. Contrary to most raw (fresh) sludge, it may be drained or filtered readily because the particles are distinctly granular. Digestion alters the fundamental character of the organic matter present in the primary sludge. In general, the characteristics of sludges are as varied as the wastes from which they originate. A general characteristic which is fairly common to most sludges, especially the troublesome ones, is that they are comprised of light, flocculent, hydrophilic solids and hence tend to be voluminous. They may contain a great deal of water, the amount of which depends on the nature of the sludge solids. This water is often removed from sludges by sludge treatment processes, such as thickening, digestion, chemical conditioning, etc. Some of the most important characteristics of sludges are the rheological properties.

The final purpose of the various sludge treatment processes is to facilitate dispersal of the solids (contained in the sludges) to obviate public nuisances of odor, dust, etc. Treatment also ensures that natural waters and soils are not polluted or harmfully contaminated in any way by organisms or toxic substances derived from the sludges.

In this experiment, the primary sludges were obtained from the Army Base treatment plant, and the digested sludges were from the Elizabeth-Chesapeake treatment plant. The digested sludge is called the secondary sludge. Both treatment plants are branches of the Hampton Roads Sanitation District.

In summary, differences between these two sludges are

1. Primary sludge: Oily, thick, objectionably odorous, colloidal, greyish black, of bigger particle size and uneven particle distribution.
2. Secondary sludge: less odorous, of smaller particle size and uniform particle distribution, black, and thinner.

4.3. Experimental Results

Two different types of sludge were dumped into the four different ambient conditions with three different release methods. These methods were continuous release at the water surface, instantaneous release just below the water surface, and instantaneous release at the water surface.

The results were as follows: for a continuous release at the water surface in freshwater of primary sludge (see photo in Appendix, A-1), a thin oil layer floated on the water surface. There was a good plume shape and almost all particles went down together, except for a few larger particles which settled at a faster rate.

For a continuous release at the water surface in freshwater of secondary sludge (figures A-2a and A-2b), there was a well-formed cloud at first. After a few moments after the initial momentum was gone, it started to disperse quickly.

For the instantaneous release just below the water surface in freshwater of primary sludge (figure A-3), an incomplete dispersion formed in the upper part of the tank, opposed to the continuous release case. Some larger particles

settled quickly; other particles of different sizes had different fall velocities. A small quantity of primary sludge was released under the same conditions as before (figure A-4), and there was no dispersion. A large and some small particles sank rapidly, and another particle floated to the water surface.

For the instantaneous release just below the water surface in freshwater of secondary sludge (figure A-5), there was good dispersion and a uniform distribution of the plume in the upper part of the tank. Some of the larger particles separated from the cloud and settled at faster rates than the cloud.

For the instantaneous release at the water surface in freshwater of primary sludge (figure A-6), a thick cloud was formed. The cloud started to disperse at the midlevel of the tank, but there was no dispersion in the upper level. In a second release of primary sludge under the same conditions, (figures A-7a and A-7b), the sludge separated into two parts. One part consisted of uniformly distributed finer particles that were well dispersed, and the other part consisted of larger particles which settled more rapidly than the cloud.

For the instantaneous release at the water surface of secondary sludge in freshwater (figure A-8), the sludge dispersed quickly in the upper level of the tank. Fine particles were distributed uniformly within the cloud, which settled slowly.

Primary sludge was instantaneously released at the water surface of salt water ($15^{\circ}/\text{oo}$) (figure A-9). There were some large particles which settled rapidly. The remaining small and medium particles started to spread in the upper section of the tank. (This should be compared with figure A-6.)

Secondary sludge was instantaneously released at the water surface of salt water ($15^{\circ}/\text{oo}$) (figure A-10). It dispersed quickly in the upper section of the tank due to the higher density of the ambient fluid as compared with the freshwater case. Fine particles were uniformly distributed within the cloud.

Primary sludge was released instantaneously at the water surface in a two-layered system (figures A-11a, A-11b, and A-11c). The upper layer was freshwater, and the lower layer was salt water ($15^{\circ}/\text{oo}$). Large particles oscillated at the interface between the two layers at first, then passed across and

settled towards the bottom of the tank. The finer, lighter particles dispersed above the interface horizontally. Compared to the one-layer, freshwater case the dispersion was more rapid.

Secondary sludge was released instantaneously at the water surface into a two-layered system. The upper layer was freshwater and the lower layer salt water (15⁰/oo) (figures A-12a and A-12b). There was a good dispersion and uniform distribution of particles within the cloud. When the cloud reached the interface, it oscillated a moment, then started to disperse quickly in the horizontal direction. Due to the higher density in the lower layer, the cloud remained in the upper layer without further penetration for a long time.

Secondary sludge was again instantaneously released at the water surface into a different two-layer system (figures A-13a and A-13b). The upper layer was again freshwater, but the lower layer was salt water of greater salinity (25⁰/oo). Due to the initial momentum, the sludge which was composed of fine particles settled quickly with no dispersion in the upper quarter of the tank. When it hit the interface, it started to disperse in the horizontal direction quickly and uniformly. Due to the higher density in the lower layer, the cloud could not penetrate the interface.

Primary sludge was instantaneously released at the water surface of the linearly varying density system (figures A-14a to A-14d). Larger, heavier particles were separated from the cloud since they settled more rapidly. The cloud, because of its lighter specific gravity, stayed in the upper one quarter of the tank. It was well dispersed in the horizontal direction with a uniform distribution. Of the larger particles, the very largest settled more rapidly at first and the smaller of these particles settled at a slower rate while the liquid cloud remained hanging at the top layer.

Secondary sludge was instantaneously released at the water surface of the same linearly varying density system (figures A-15a and A-15b). At first the sludge formed a very good cloud in the upper one-sixth of the tank. Then, due to the increasing density with the increase in depth, the fall velocity decreased to zero. It started to disperse smoothly in the horizontal direction, staying in the upper one-fifth of the tank.

4.4. Discussion

During these experiments, the primary and secondary sludge always settled rapidly for a short distance. The initial momentum was dissipated by resistance of the ambient fluid, and its velocity decreased. For all secondary sludges and most primary sludges, as the initial velocity decreased, dispersion began.

Secondary sludge had a faster, more uniform dispersion than primary sludge. Because the viscosity of secondary sludge is smaller than primary and its cohesive force is not as strong, secondary sludge consisted of very fine particles which dispersed uniformly.

In contrast, some of the primary sludge was bound together to form large particles which did not break up. These large particles would separate from the cloud of smaller particles, settling at a faster rate. The fall velocity of these particles was calculated by:

$$V_t = \frac{g}{18\nu} (\rho_s - \rho) D^2$$

where: V_t = terminal fall velocity,

g = force of gravity,

ν = kinematic viscosity,

ρ, ρ_s = densities of ambient fluid and particle, respectively,

and

D = diameter of particle.

Assuming the densities of the particles were uniform and greater than that of the ambient fluid, larger particles resulted in higher fall velocities. Sometimes particles would entrap air or consist of less dense material and ascend to the water surface.

The settling rate of a sludge cloud as a whole was dependent on its concentration, the type of sludge, its water content before dumping, and environmental conditions. Significant differences existed between sludges from different sources and also from the same source taken at different times. As a result a wide variation of settling phenomena was expected. For these reasons, reproductive laboratory experiment was difficult to carry out.

In salt water, dispersion was faster than in freshwater in the horizontal direction. The higher the ambient density, the less negatively buoyant was sludge, hence decreasing the downward vertical settling velocity so the sludge would disperse more in the horizontal direction.

Instantaneous release at the water surface produced the fastest dispersion of the three release methods. This method of dumping produced a higher initial downward momentum.

The higher downward initial momentum of this release method also entrained more ambient water, which diluted and, therefore, broke the sludge cloud more. Secondary sludge entrained more water than primary due to its finer particles and uniform distribution.

5. CONCLUSIONS

The Pavish-Spaulling, three-dimensional, Eulerian-Lagrangian, marker particle model shows great potential in describing the long-term, far-field transport processes of ocean-dumped sewage sludge. It provides information on the effect of the magnitude of the horizontal and vertical diffusion coefficients, particle density and size distribution on the sludge plume as it changes with time. Based upon the results of this study, the behavior of the plume can be best illustrated by the following ways: locating the maximum concentration within the plume, the size of the plume, equiconcentration lines on selected vertical planes and horizontal planes at various depths. All of these indicators vary as a function of time after the dumping. A big limitation of this model is model calibration and verification, specifically for ocean dumping of sludge.

The Koh-Chang model is another well-known model to predict ocean dumping of wastes. The calibration and verification work are in progress. Much of the effort has been directed toward the study of dredged material, not sewage sludge. Characteristics of sewage sludge before dumping and of that dumped in an ocean environment are more complex than those of the dredged material. Some of the problems that are not fully understood are the inhomogeneity of the sludge, sludge cloud break-up and particle flocculation mechanisms involved in various ocean environments.

NASA provided data on equiconcentration lines of the sludge plume after the dumping at the ocean surface by means of remote sensing techniques. The computer model was studied for the plume behavior using the best estimated data inputs from in situ measurement or available information. Comparison between the model outputs and remote sensing data shows that the agreement is fairly good on the trend of plume growth. It demonstrates the capability of remote sensing technique in monitoring the sewage plume at ocean surface. It also indicates that conjunctive use of numerical model and remote sensing may provide the best monitoring strategy. Data obtained through remote sensing can be used to verify and calibrate the numerical model for prediction purposes such as dumping permit evaluation. Direct one-to-one comparison between the numerical model outputs and the remote sensing data can be achieved only if complete and reliable input data to a calibrated model is available.

This study shows that the concentrations obtained from averaging over the top two feet, four feet, and eight feet are significantly different. In general, the integration over the top eight feet indicated higher concentrations than the others. The higher concentrations exhibited in the lower layers are due to the closeness to the source of release. Of course, the settling rates of the particles and the vertical diffusion coefficient have strong influence on the vertical concentration distribution near the ocean surface. It is essential to incorporate this important feature in the development of remote sensing capability to quantify the surface plume of interest. Optical properties such as the penetration depth are important parameters to be considered in order to improve the resolution of the remote sensing technique.

Laboratory studies were made on the plume behavior of the dumped sewage sludge at the water surface. Primary and secondary sludge in four different ambient fluid density structures were investigated. Two types of release, continuous and instantaneous, were also studied. Secondary sludge in general disperses or breaks up faster than the primary sludge due to uniform and smaller particle size. The composition of sludge material was found to vary so much that reproduction of a specific experimental run was difficult. A sludge plume normally settles in a laboratory calm fluid until it reaches a neutrally buoyant position and then spreads horizontally. It was observed that larger particles and unbroken sludge mass separate from the cloud and settle individually with faster descending velocities.

Table 1. Typical data for settling velocity of sewage sludge and dredged material.

Browne and Callaway (EPA - Corvallis) (Ref. 33)	At 24° to 25°C Major Portion of Solids Settles At Less Than 0.015 cm/sec Mean Settling Velocity ~ 6.0(10 ⁻⁴) to 3.7(10 ⁻²) cm/sec		
Callaway (Ref. 16)	Larger Flocculated Sludge Particles (Avg.) ~ 0.5 To 1 cm/sec. Center of Mass of Waste Field ~ 0.01 to 0.3 cm/sec Remainder of Dispersing Sludge Field ≤ 10 ⁻³ cm/sec		
Proni et al. (Ref. 36)	W _s = 0.7 cm/sec (Particle Density 1.5 gm/cm ³)		
Koh and Chang* (Ref. 22)	W _s (Avg.) = 1.58(10 ⁻³) cm/sec		
Pavish and Spaulding* (Ref. 32)	W _s = 3.05(10 ⁻²) To 9.14(10 ⁻¹) cm/sec For Particle Dia. = 0.15 to 0.85 cm		
Rittall (Ref. 28)	Settleable Solids - 0.1524 cm/sec Floating Solids - 1.524 cm/sec		
Deb (Ref. 27)	W _s (Avg) (cm/sec)	% Total Suspended Solids	Special Data
	3.28(10 ⁻³)	30	Wet Density of Waste = 1.1398 g/cm ³
	1.16(10 ⁻²)	20	Dry Density of
	4.40(10 ⁻²)	20	Suspended Solids
	9.51(10 ⁻²)	30	= 1.6387 g/cm ³

* For dredged material.

Table 2. Typical data for horizontal diffusion coefficients.

Broecker et al.
(Ref. 37) $K_x = 1(10^6) \text{ to } 3(10^6) \text{ cm}^2/\text{sec}$

Koh and Chang
(Ref. 22) $K_x = 5(10^2) \text{ to } 4(10^8) \text{ cm}^2/\text{sec}$
Note: $K_x = A_L L^{4/3}$

$$10^{-1} H \leq L \leq 10^8 H$$

$$A_L = 5(10^{-3}) \text{ to } 6.5(10^{-4}) \text{ ft}^{2/3}/\text{sec}^*$$

Falk et al.
(Ref. 26) $E_y = 6.6(10^3) \text{ to } 1.6(10^5) \text{ cm}^2/\text{sec}$ for Depth
From Surface to 140 ft*
 E_y (Best Fit) = $3.3(10^4) \text{ cm}^2/\text{sec}$

Burgess
(Ref. 34) Width From 600 to 1320 ft*; Diffusion Coefficients From
 $1.86 \text{ to } 3.5(10^{+2}) \text{ cm}^2/\text{sec}$

Ketchum (cited by Yudelson, ref. 38)	<u>K(cm²/sec)</u>	<u>L(cm)</u>
	1.9(10 ³)	1.07(10 ⁴)
	2.5(10 ³)	1.65(10 ⁴)
	6.8(10 ³)	2.25(10 ⁴)

Data was for New York Bight

* 1 ft = 0.3048 m

Table 3. Typical data for vertical diffusion coefficients.

Koh and Chang
(Ref. 22)

$K_z = 10^{-2}$ to $3(10^2)$ cm^2/sec (Maximum at Surface)

Falk et al.
(Ref. 26)

E_z (Best Fit) - Above Thermocline ~ 100 cm^2/sec
- Below Thermocline ~ 50 cm^2/sec

Rittall
(Ref. 28)

Summer Conditions:

Depth *	K_z
0-30 ft	$2.04(10^{-2})$ cm^2/sec
30-45 ft	$2.04(10^{-2})$ to $4.65(10^{-3})$ cm^2/sec
45-55 ft	$4.65(10^{-3})$ cm^2/sec
55-65 ft	$4.65(10^{-3})$ to $1.02(10^{-2})$ cm^2/sec
65-100 ⁺ ft	$1.02(10^{-2})$ cm^2/sec

Winter Conditions:

0-100⁺ft; $K_z = 1.02(10^{-2})$ cm^2/sec

Deb
(Ref. 27)

Summer Conditions:

Depth *	K_z
0-45 ft	1.00 cm^2/sec
50-70 ft	0.502 cm^2/sec
75-135 ft	0.595 cm^2/sec

Winter Conditions:

0-150 ft; 1.00 cm^2/sec

* 1 ft = 0.3048 m

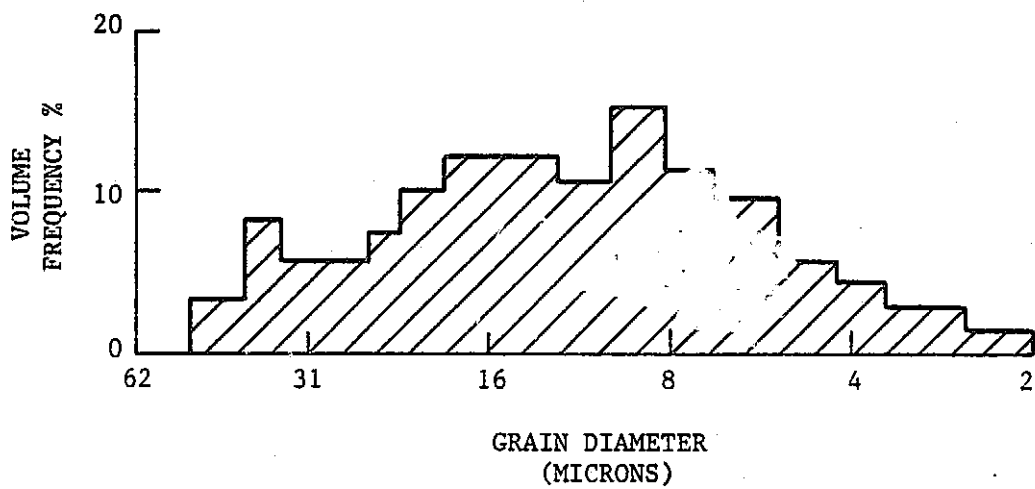


Figure 1. Particle size distribution measured by NOAA.

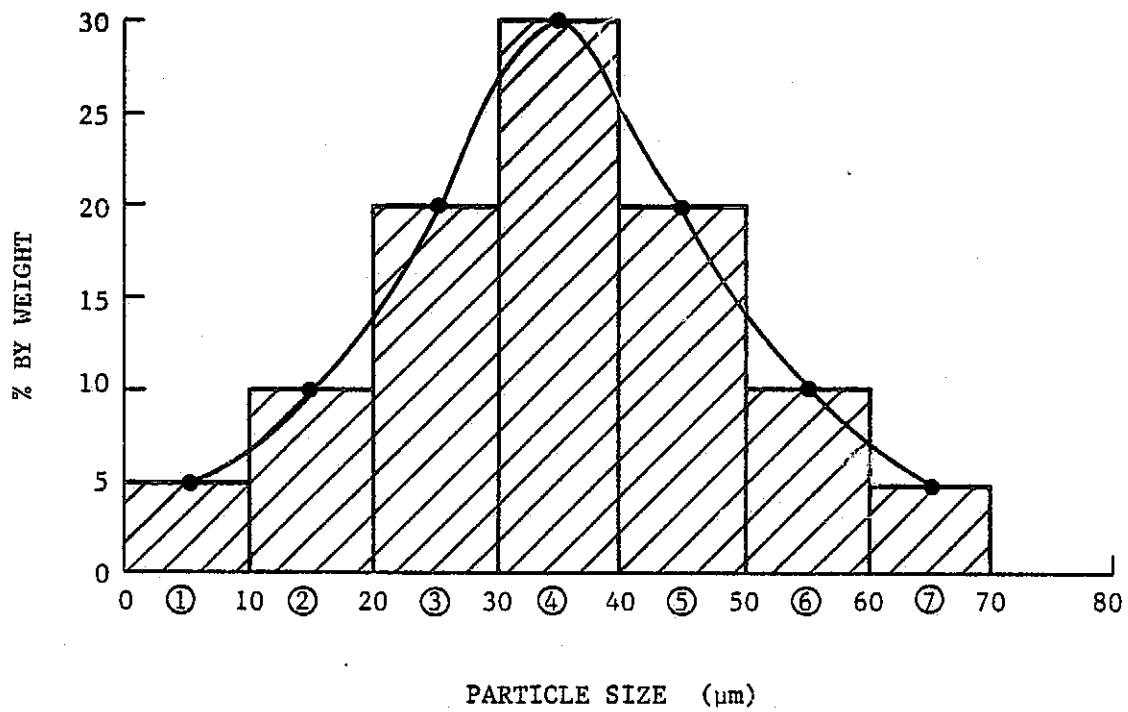


Figure 2. Particle size distribution fitted by a Gaussian curve.

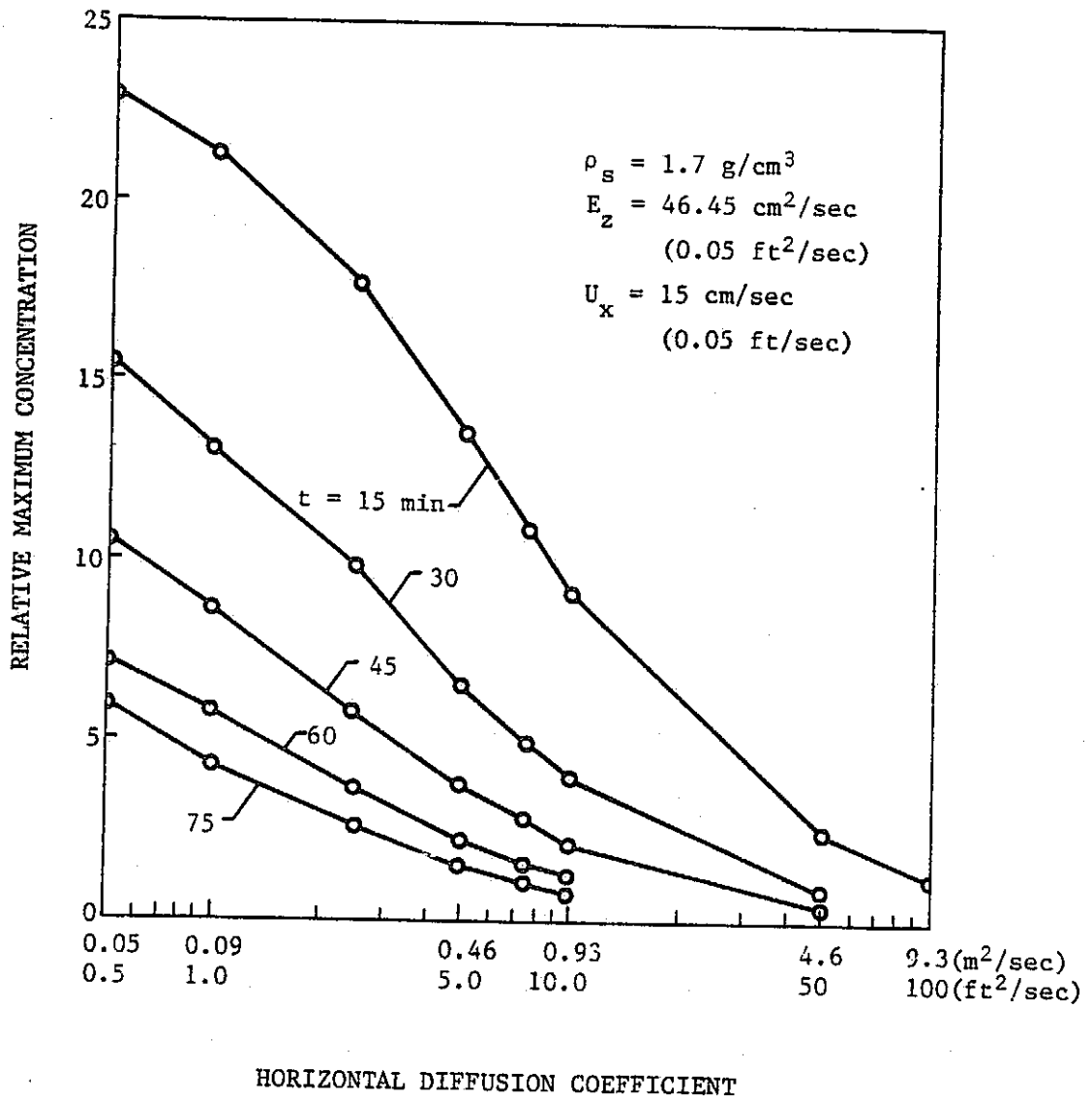


Figure 3. Relative maximum concentration vs. horizontal diffusion coefficient, level 1.

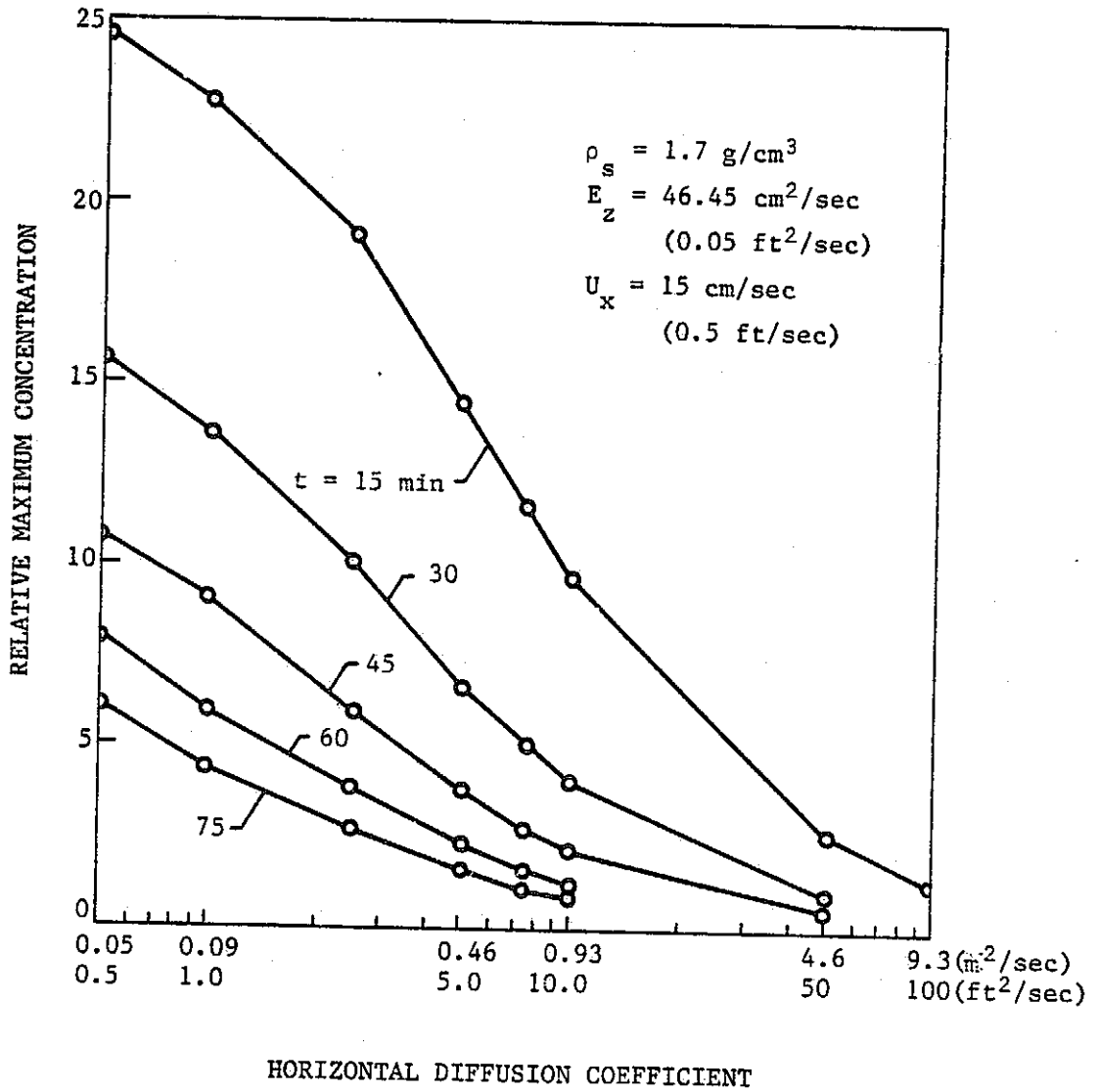


Figure 4. Relative maximum concentration vs. horizontal diffusion coefficient, levels 1 to 2.

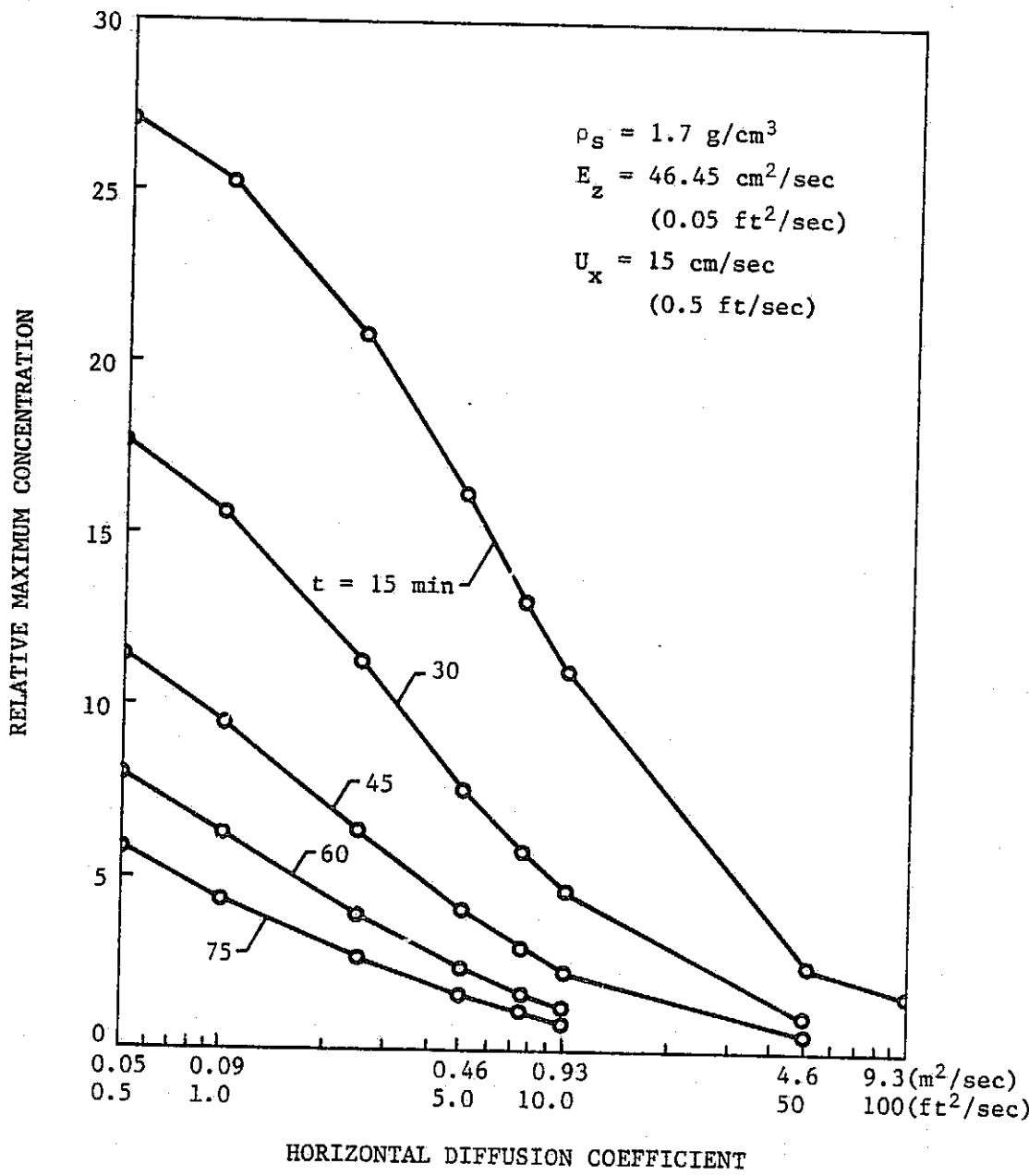


Figure 5. Relative maximum concentration vs. horizontal diffusion coefficient, levels 1 to 4.

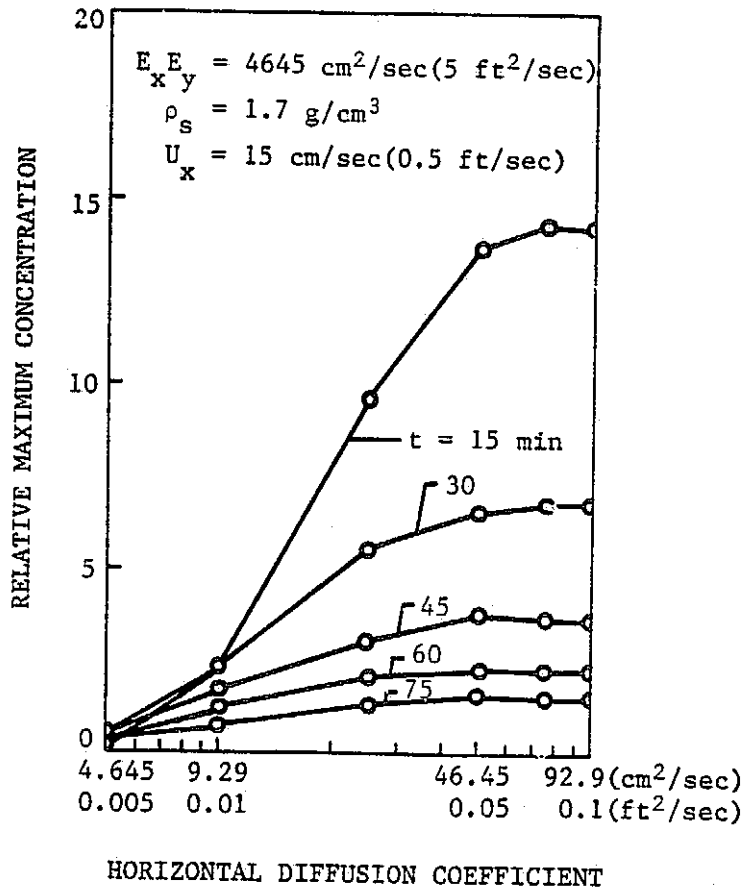


Figure 6. Relative maximum concentration vs. vertical diffusion coefficient, level 1.

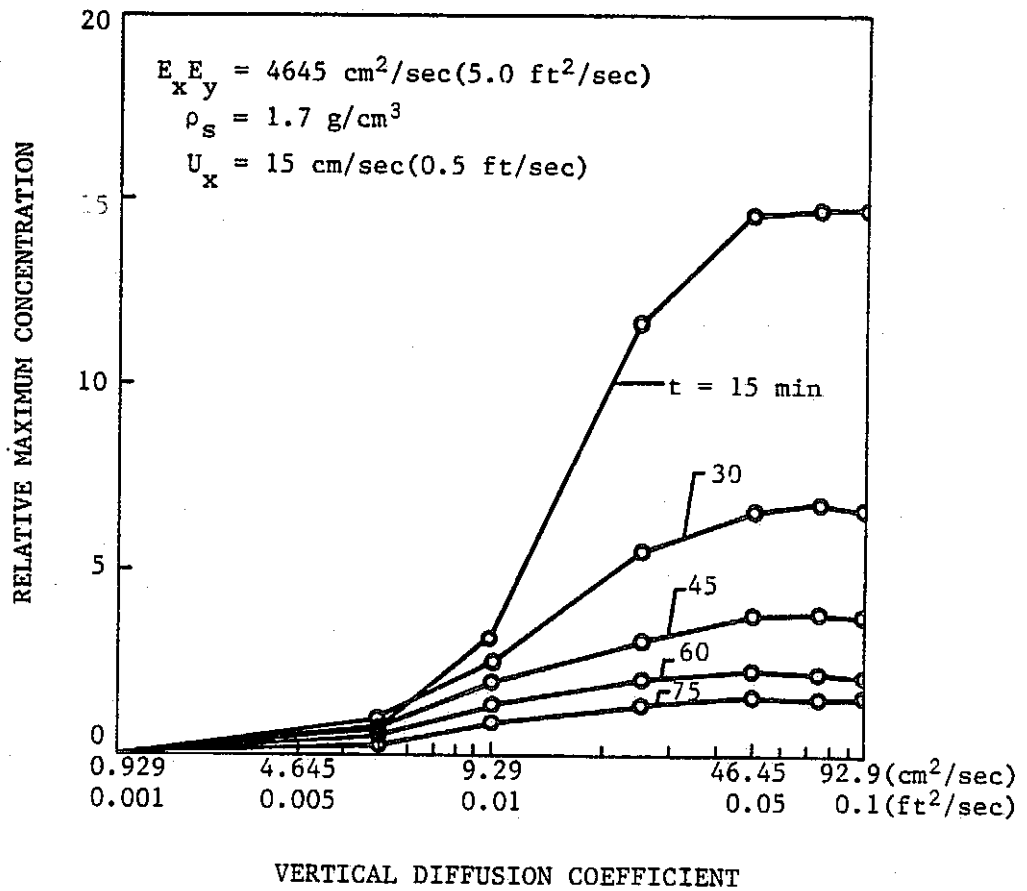


Figure 7. Relative maximum concentration vs. vertical diffusion coefficient, levels 1 to 2.

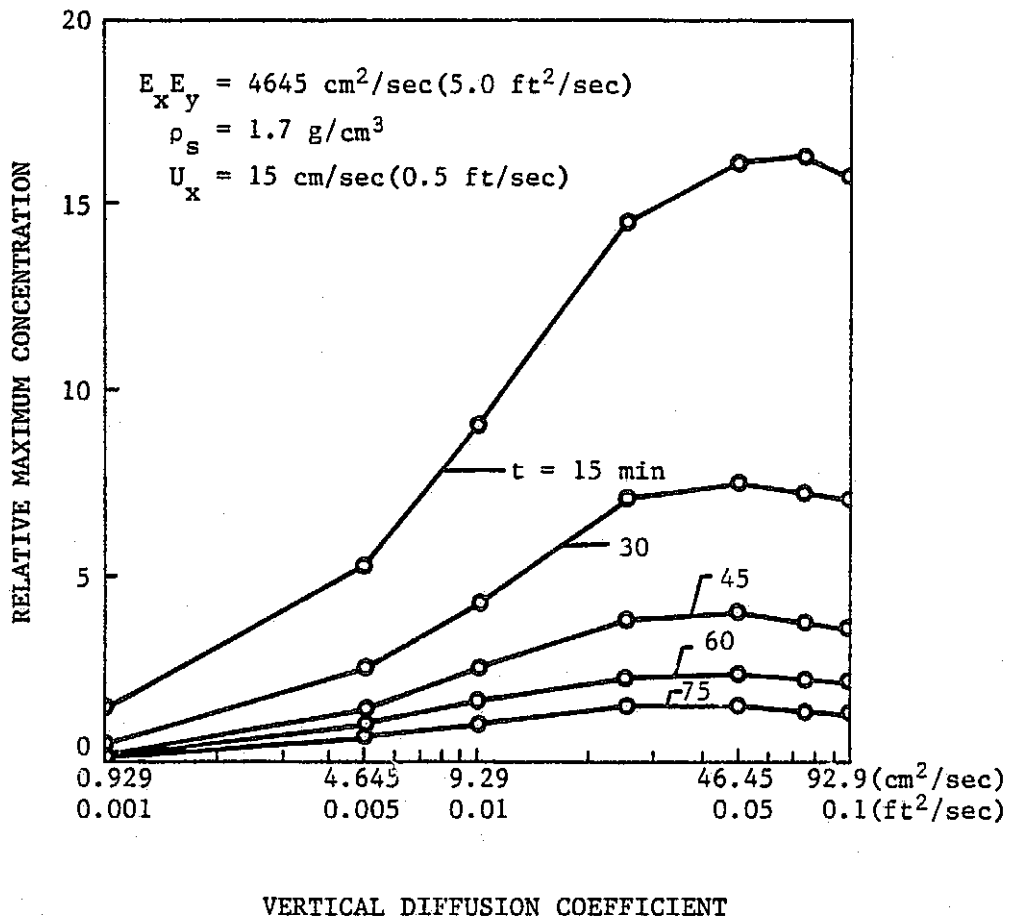


Figure 8. Relative maximum concentration vs. vertical diffusion coefficient, levels 1 to 4.

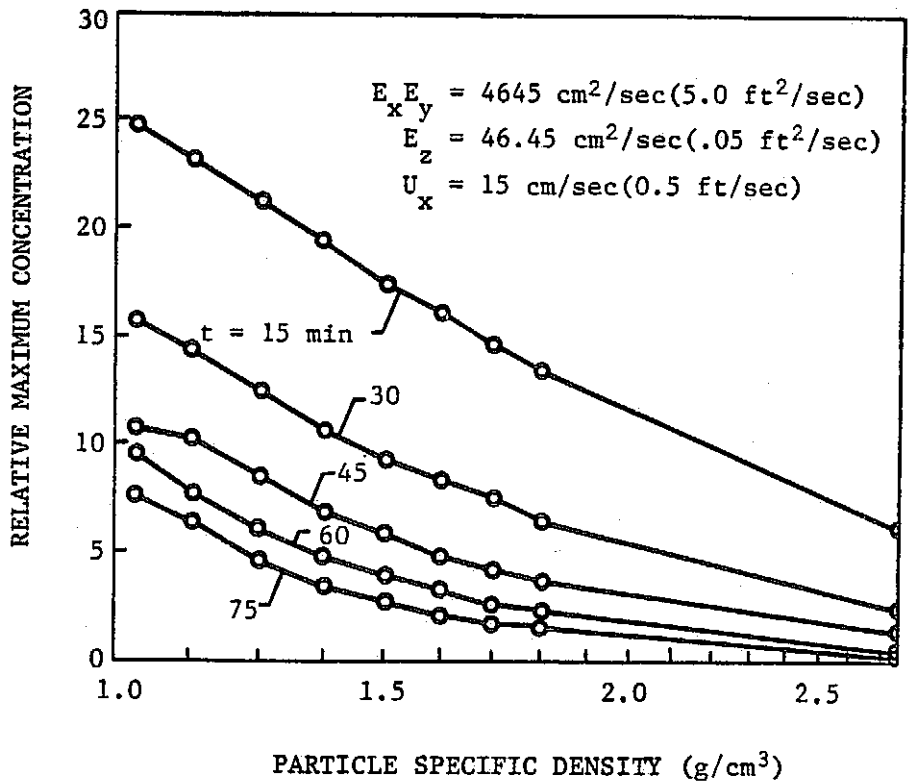


Figure 9. Relative maximum concentration vs. particle specific density, level 1.

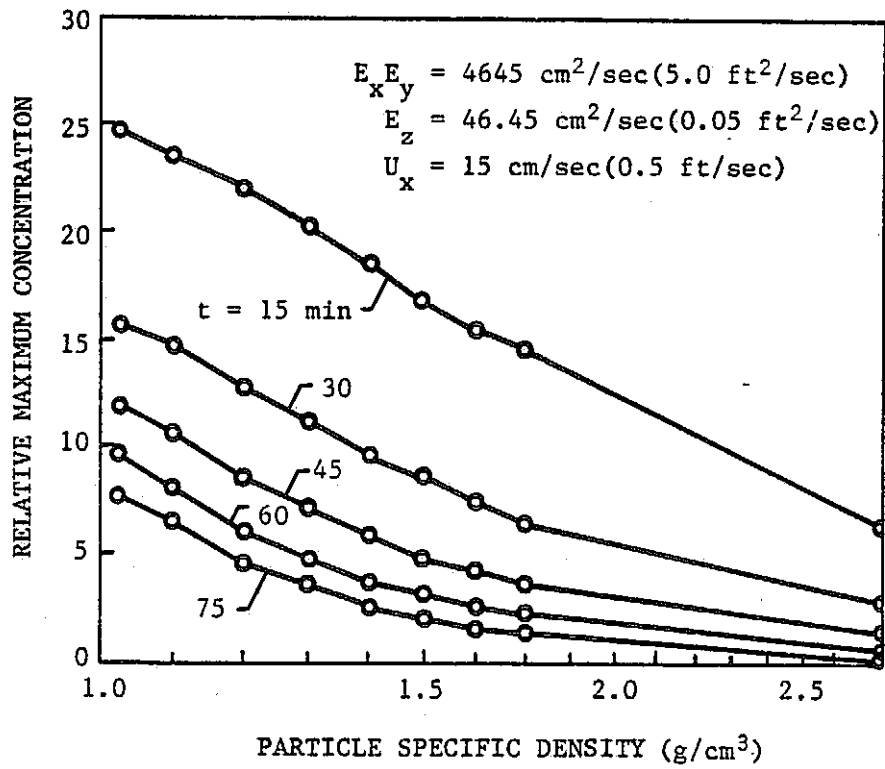


Figure 10. Relative maximum concentration vs. particle specific density, levels 1 to 2.

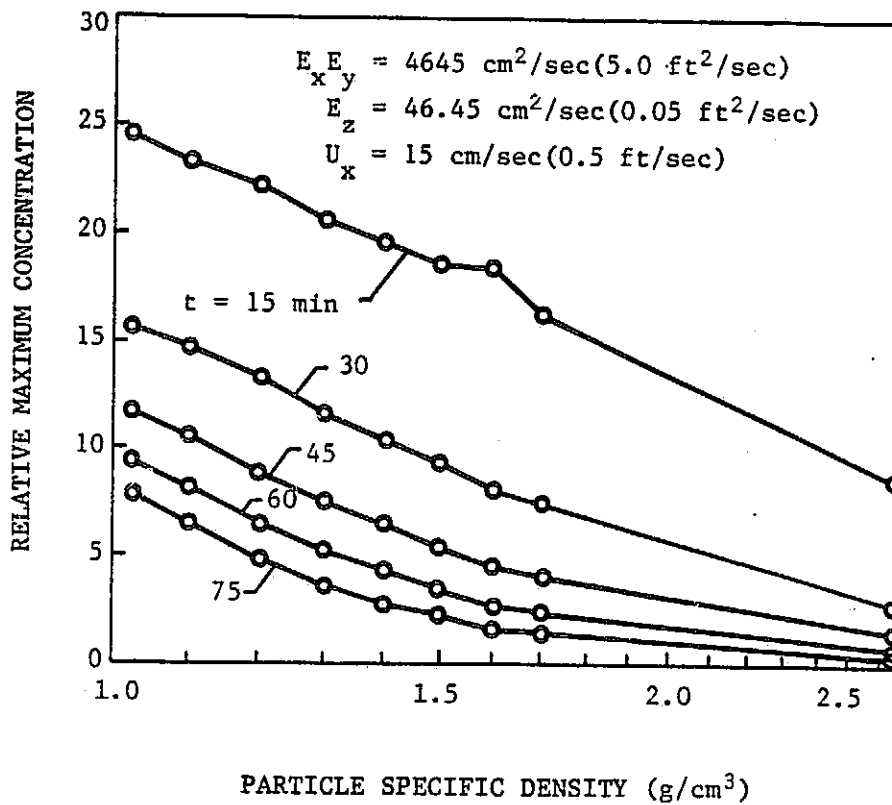


Figure 11. Relative maximum concentration vs. particle specific density, levels 1 to 4.

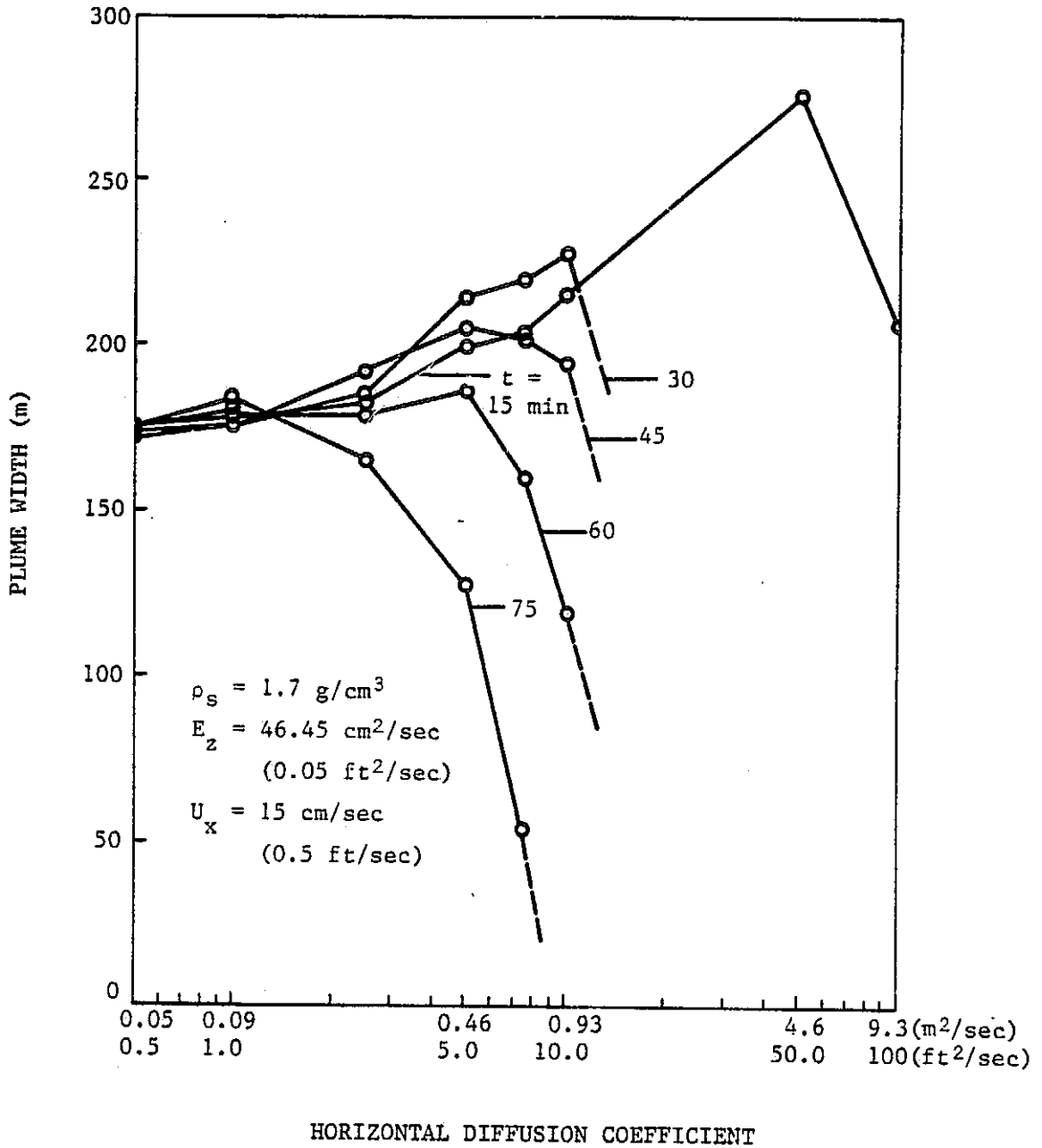


Figure 12. Plume width vs. horizontal diffusion coefficient, level 1 (equal concentration line = 1.0).

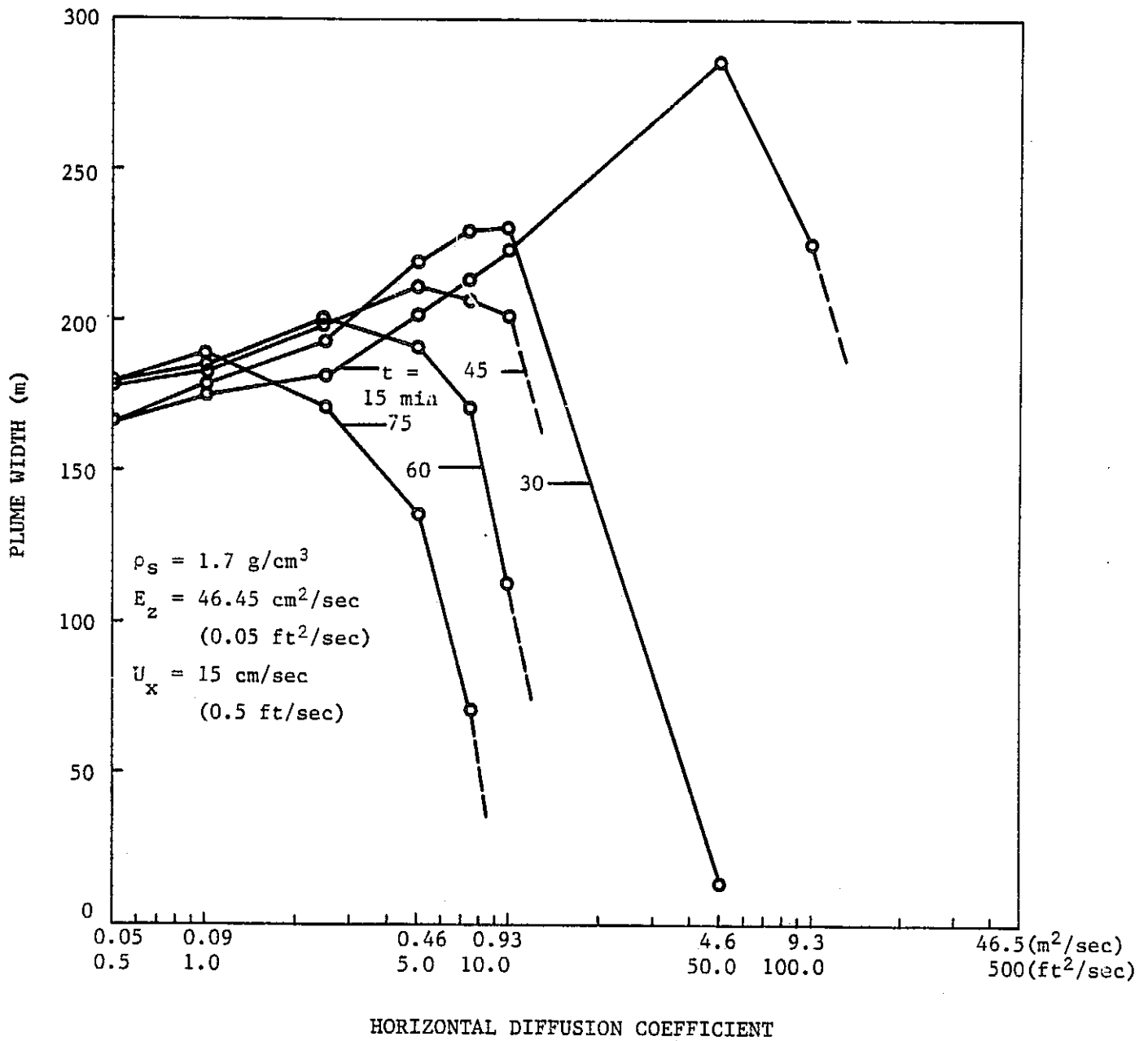


Figure 13. Plume width vs. horizontal diffusion coefficient, levels 1 to 2 (equal concentration line = 1.0).

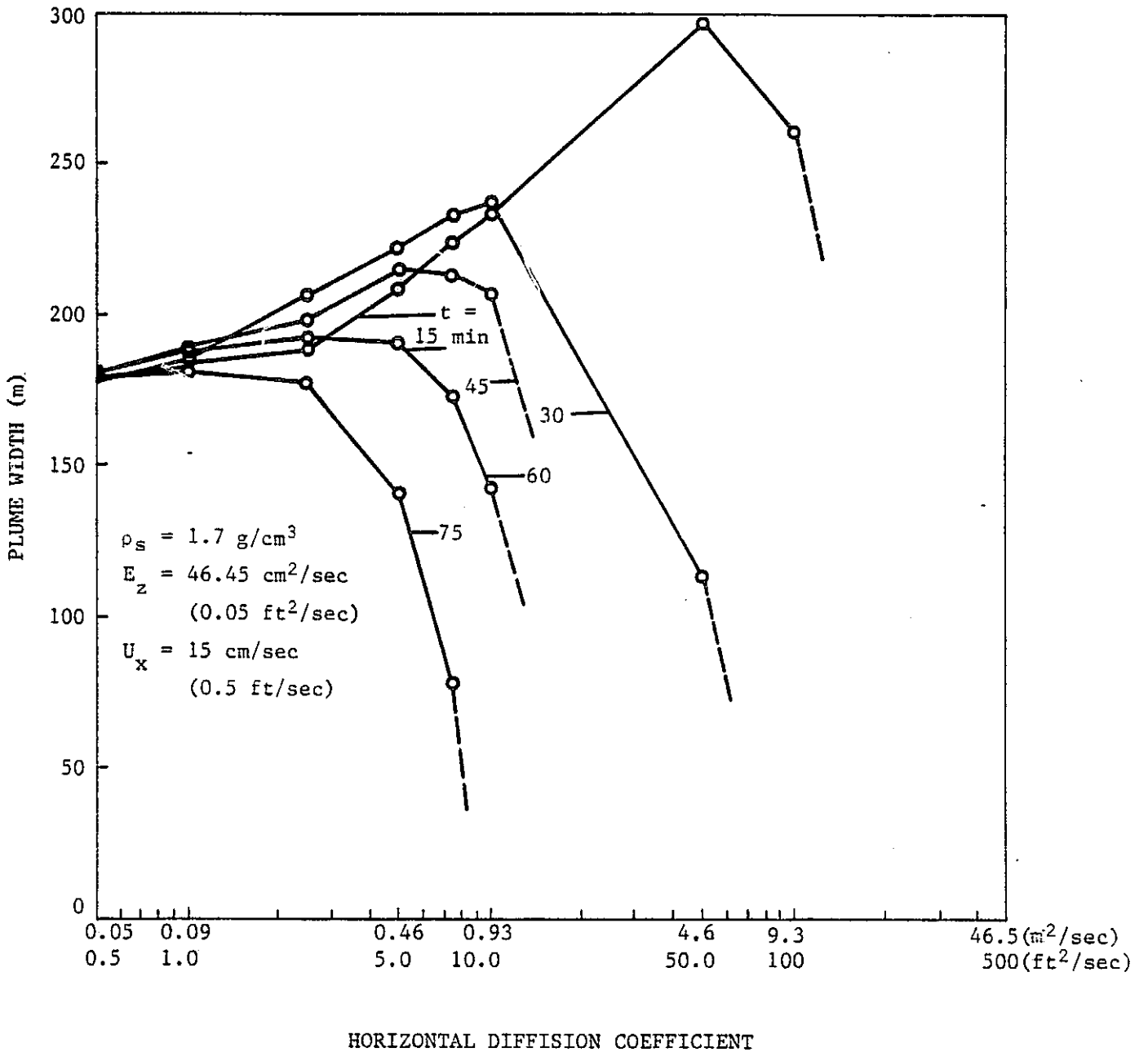


Figure 14. Plume width vs. horizontal diffusion coefficient, levels 1 to 4 (equal concentration line = 1.0).

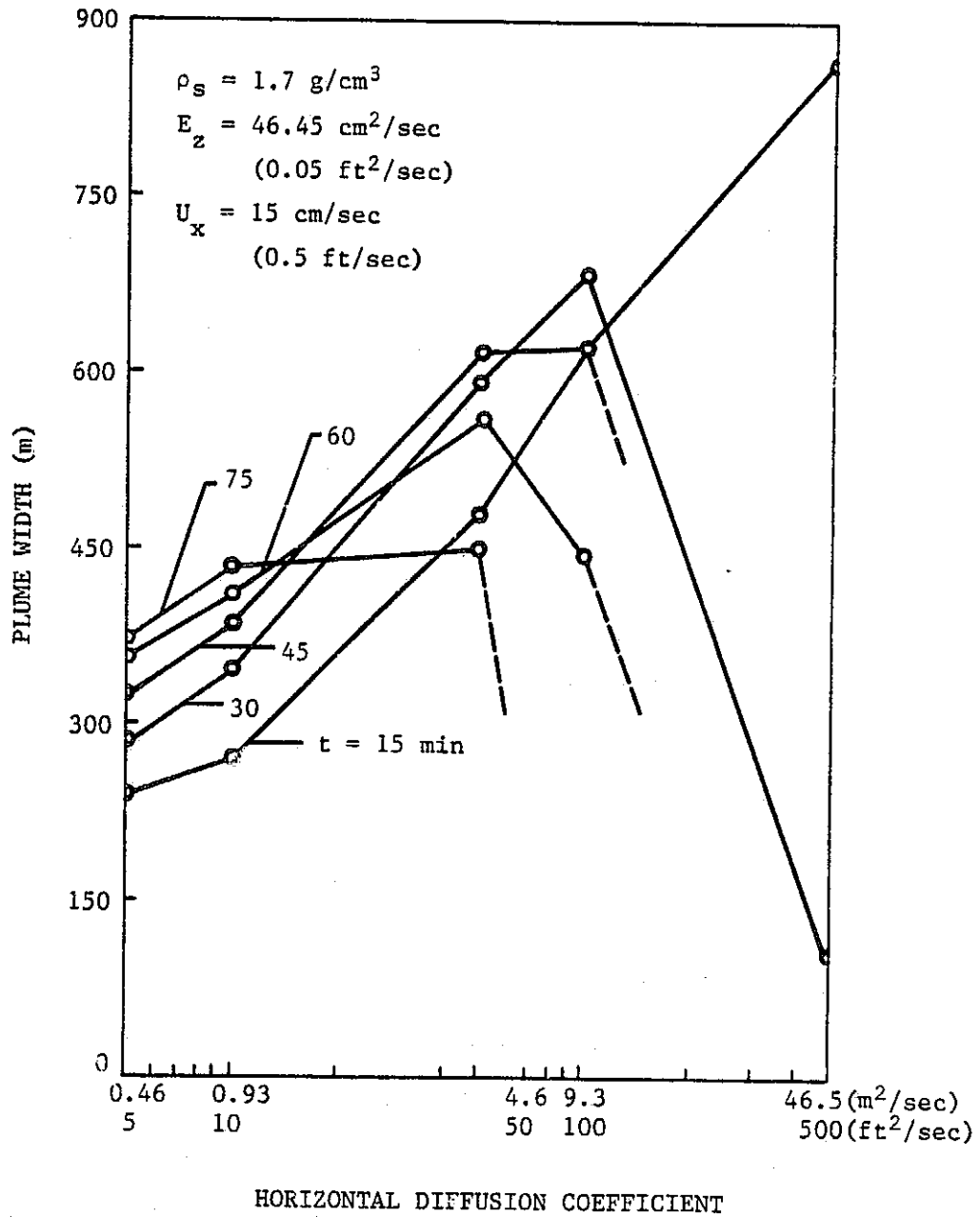


Figure 15. Plume width vs. horizontal diffusion coefficient, level 1 (equal concentration line = 0.1).

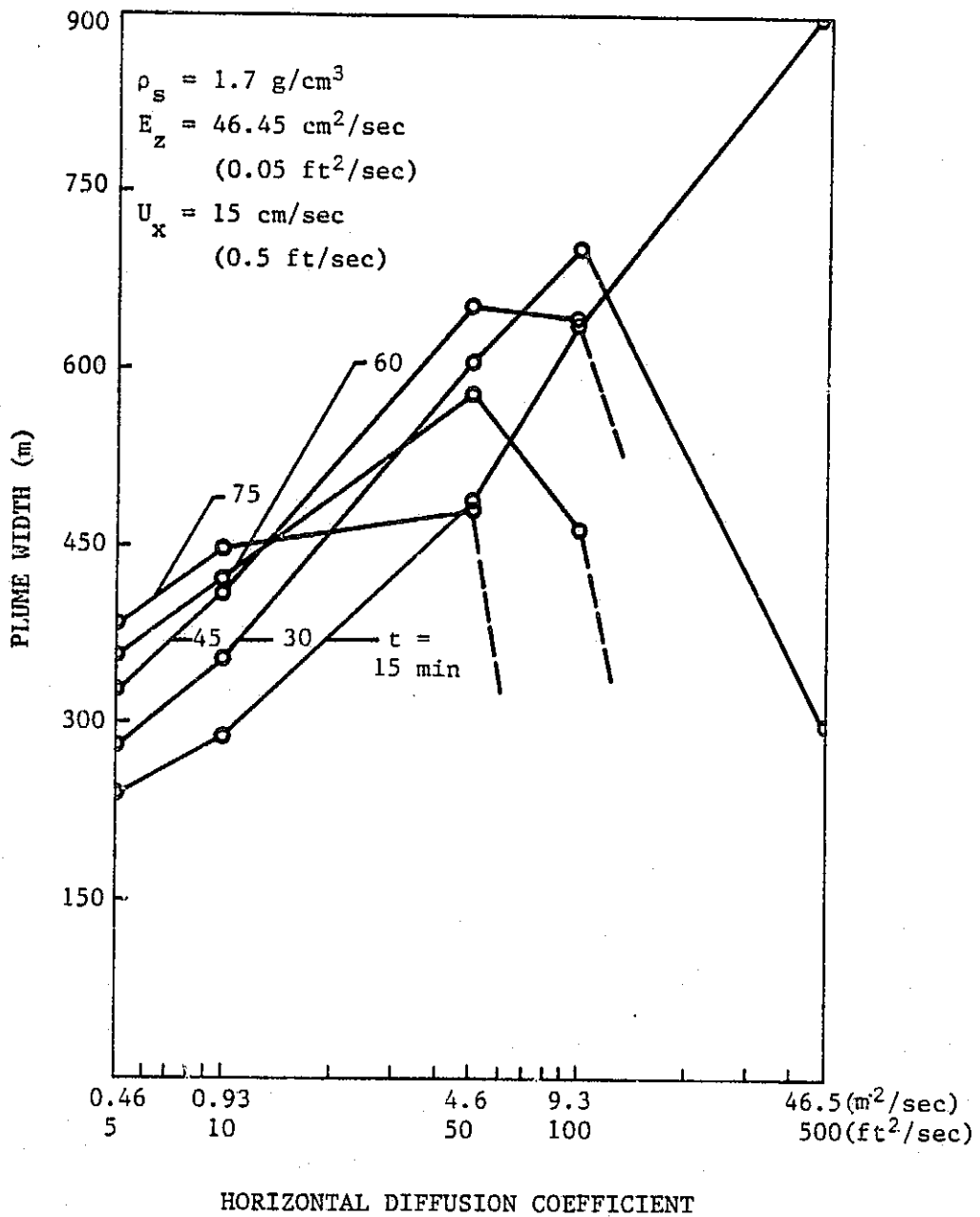


Figure 16. Plume width vs. horizontal diffusion coefficient, levels 1 to 2 (equal concentration line = 0.1).

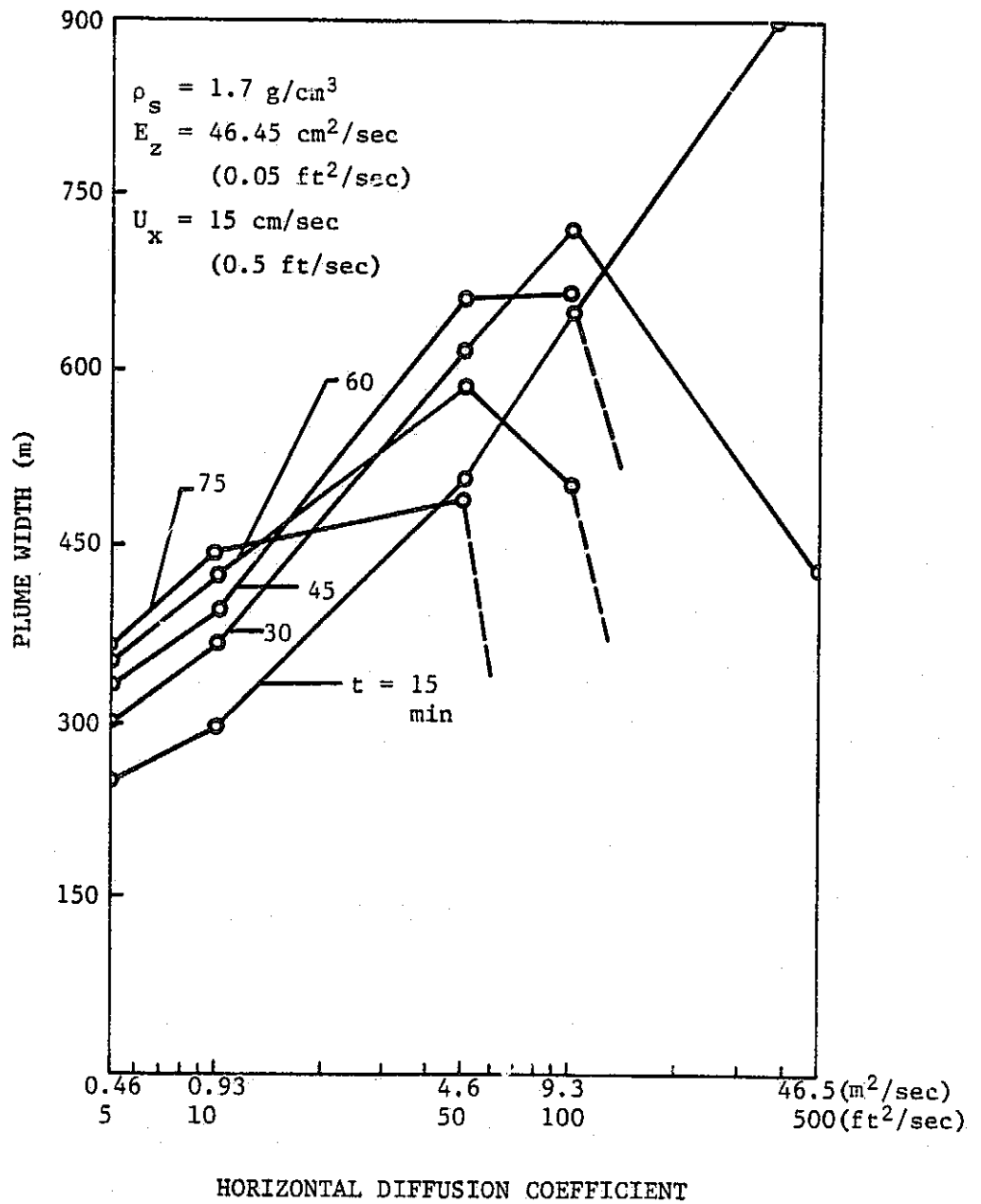


Figure 17. Plume width vs. horizontal diffusion coefficient, levels 1 to 4 (equal concentration line = 0.1).

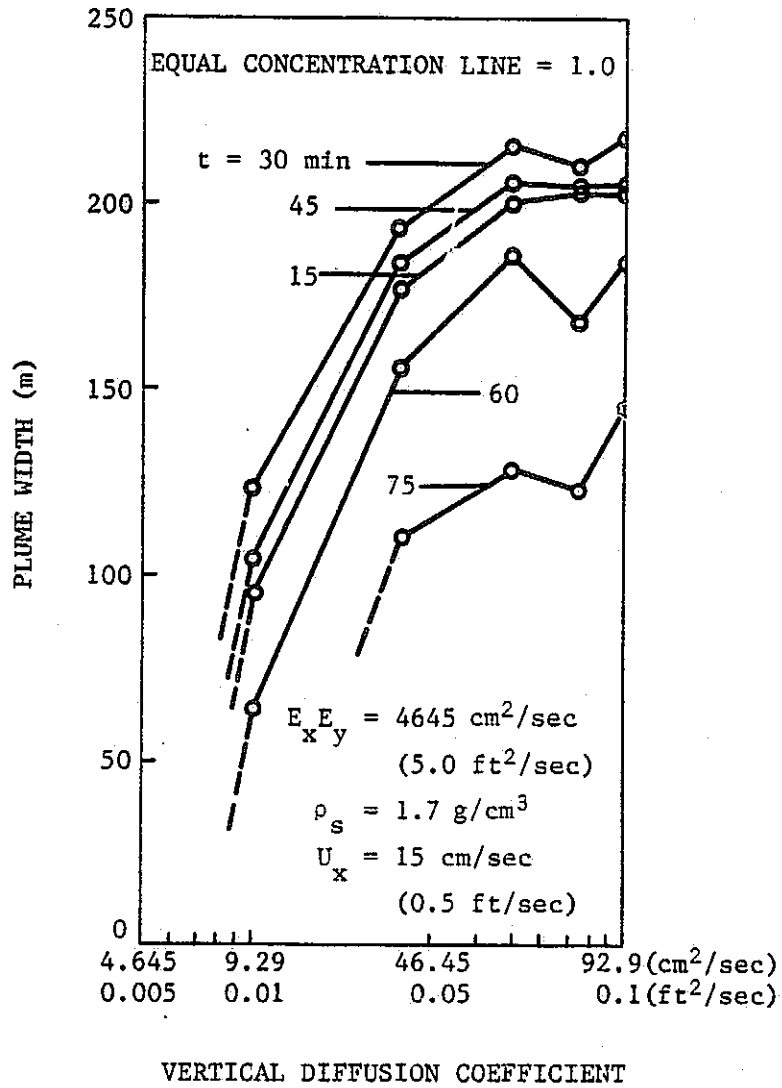


Figure 18. Plume width vs. vertical diffusion coefficient, level 1.

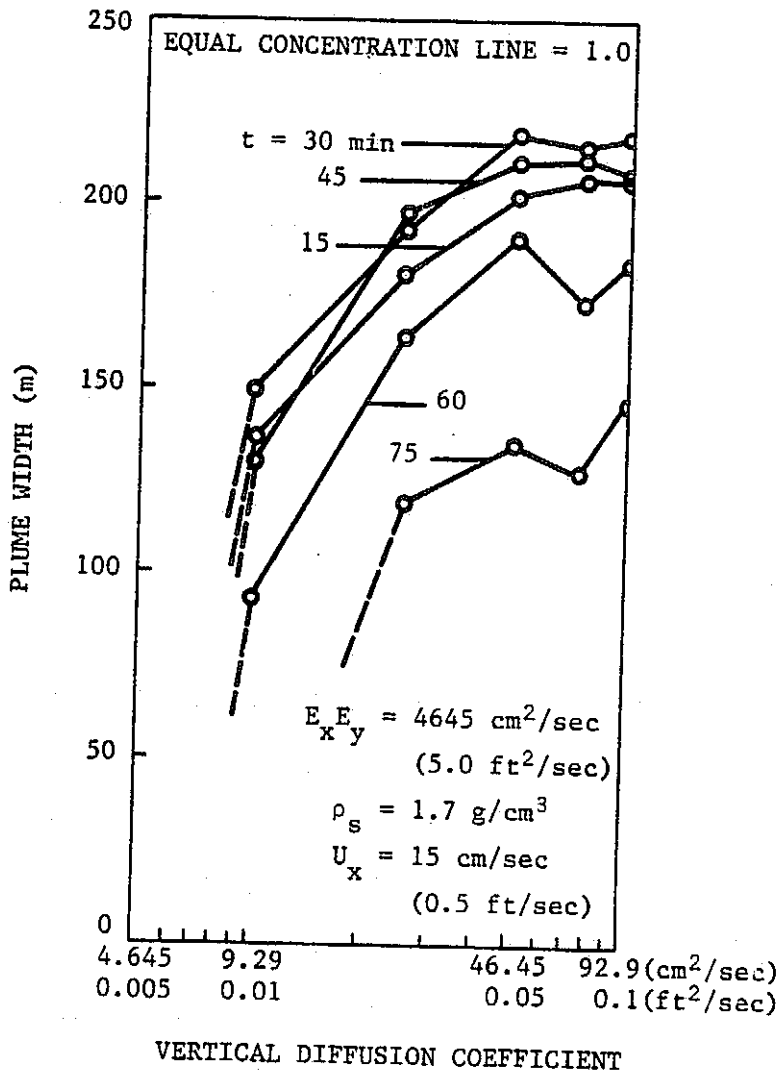


Figure 19. Plume width vs. vertical diffusion coefficient, levels 1 to 2.

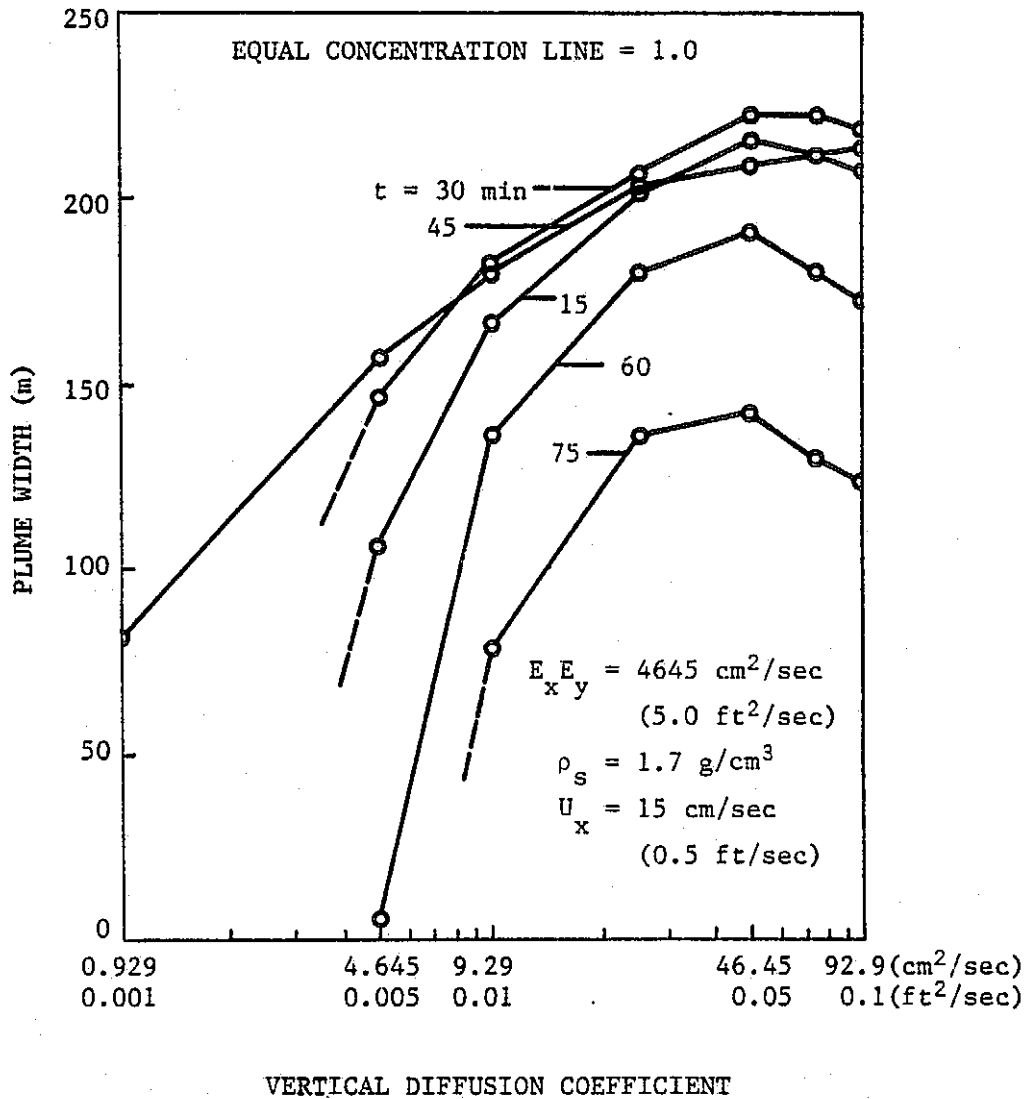


Figure 20. Plume width vs. vertical diffusion coefficient, levels 1 to 4.

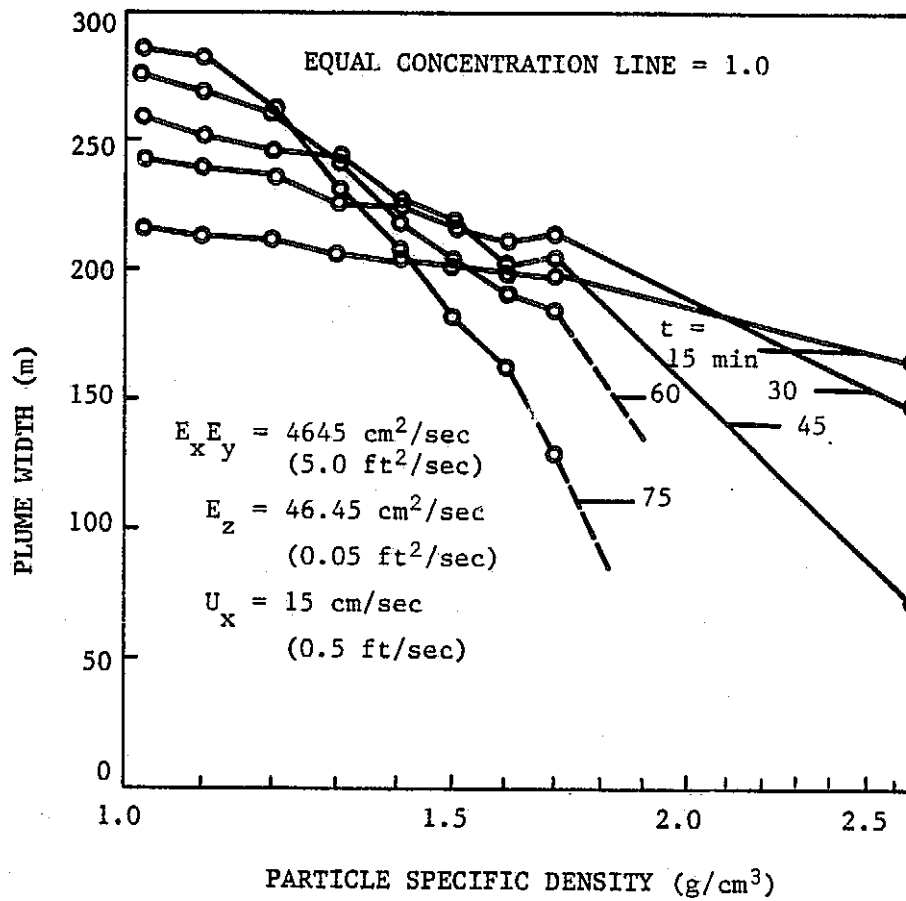


Figure 21. Plume width vs. particle specific density, level 1.

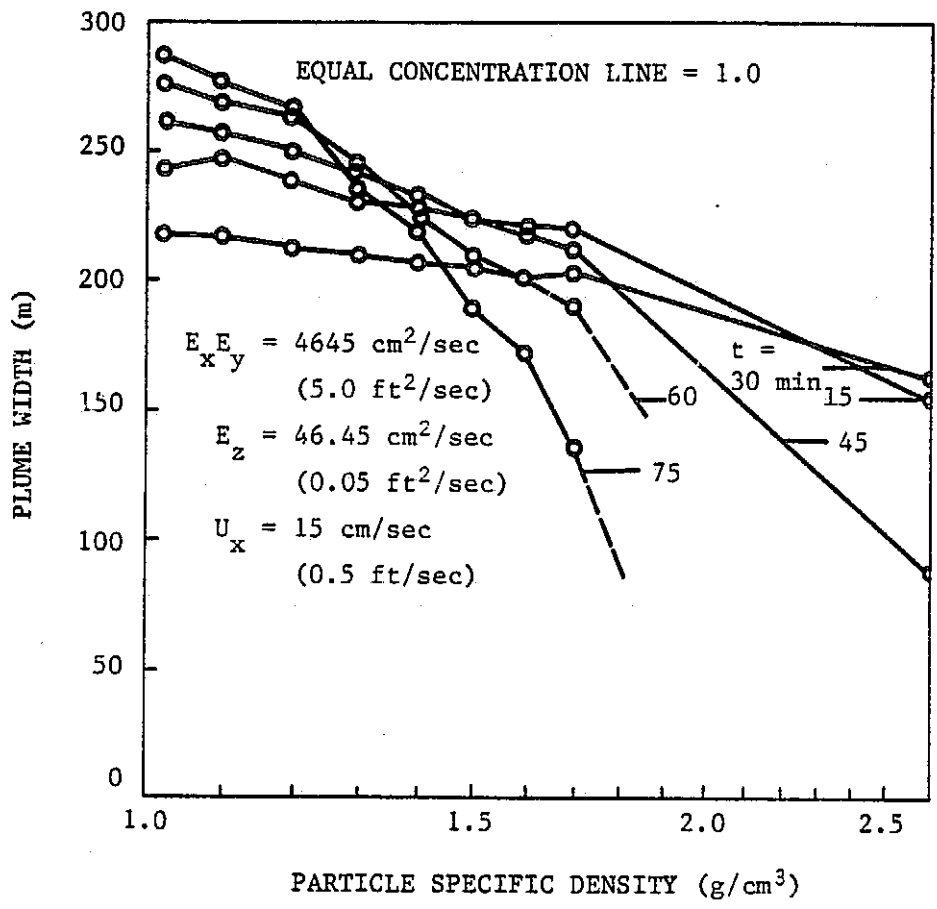


Figure 22. Plume width vs. particle specific density, levels 1 to 2.

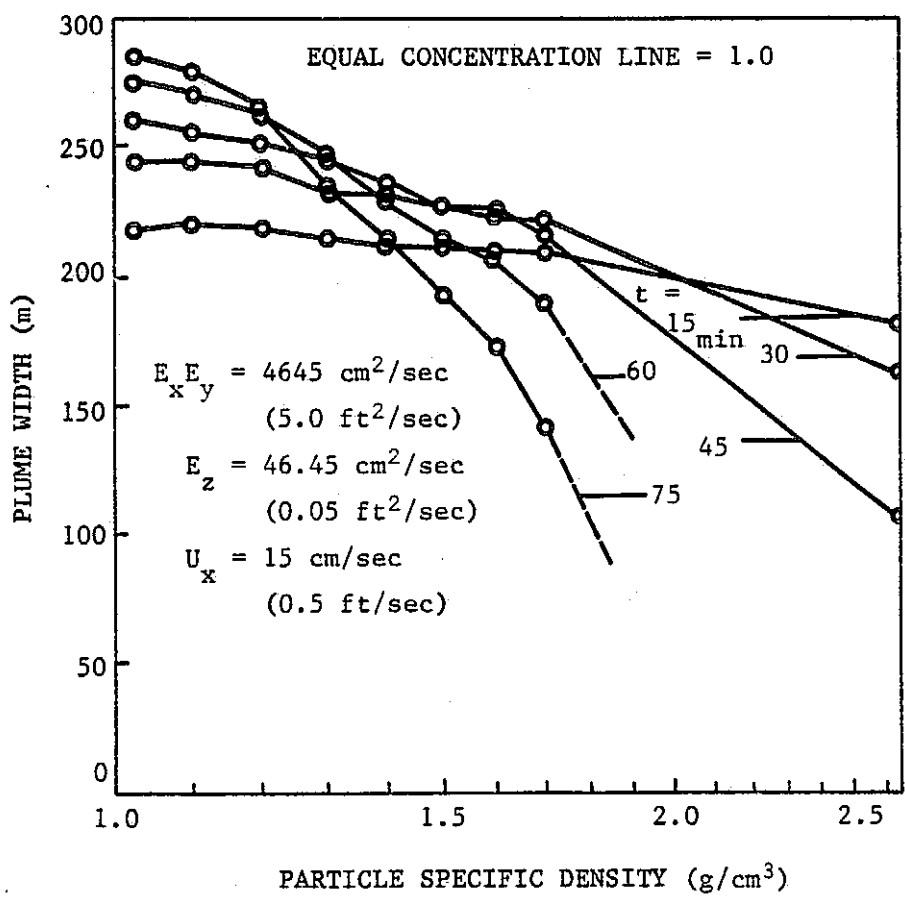


Figure 23. Plume width vs. particle specific density, levels 1 to 4.

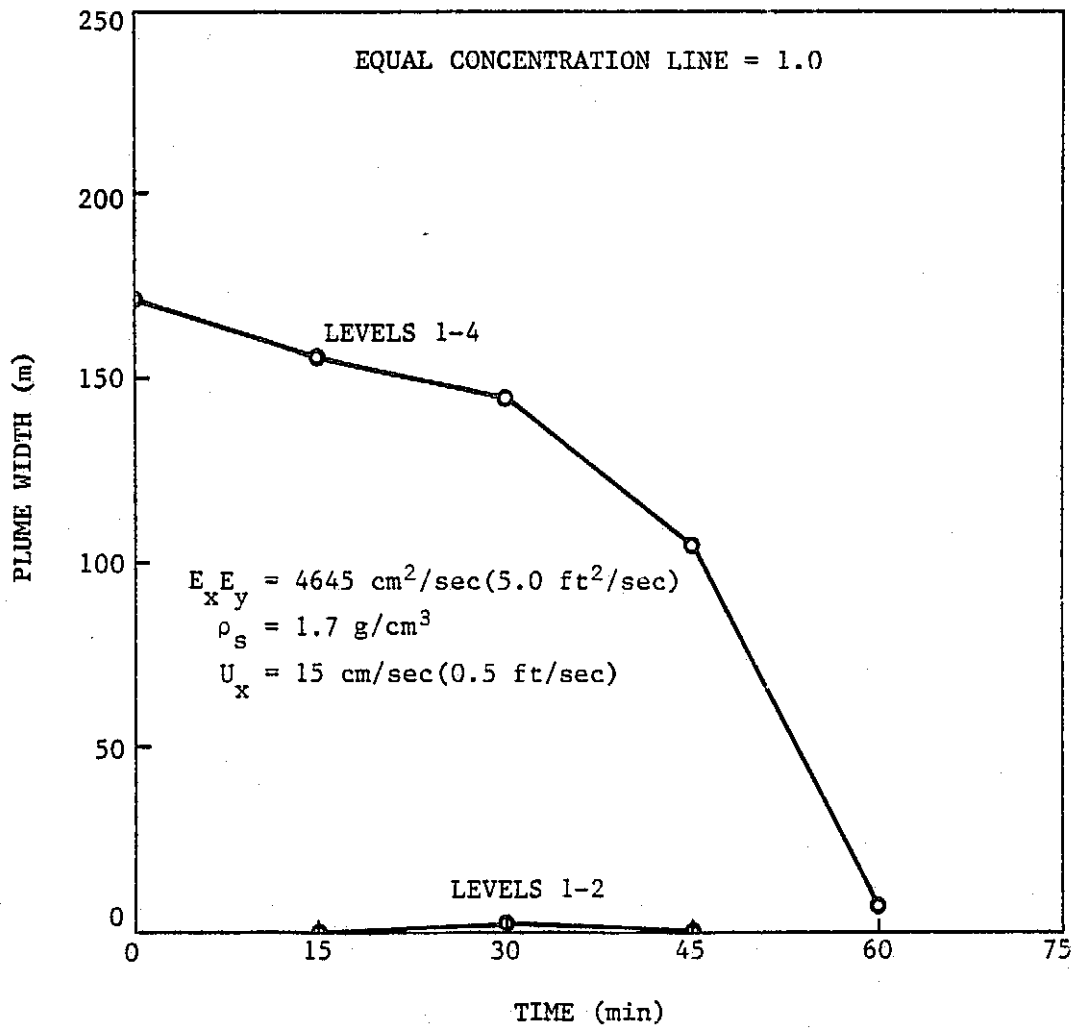


Figure 24. Plume width vs. time, $E_z = 4.645 \text{ cm}^2/\text{sec} (0.005 \text{ ft}^2/\text{sec})$.

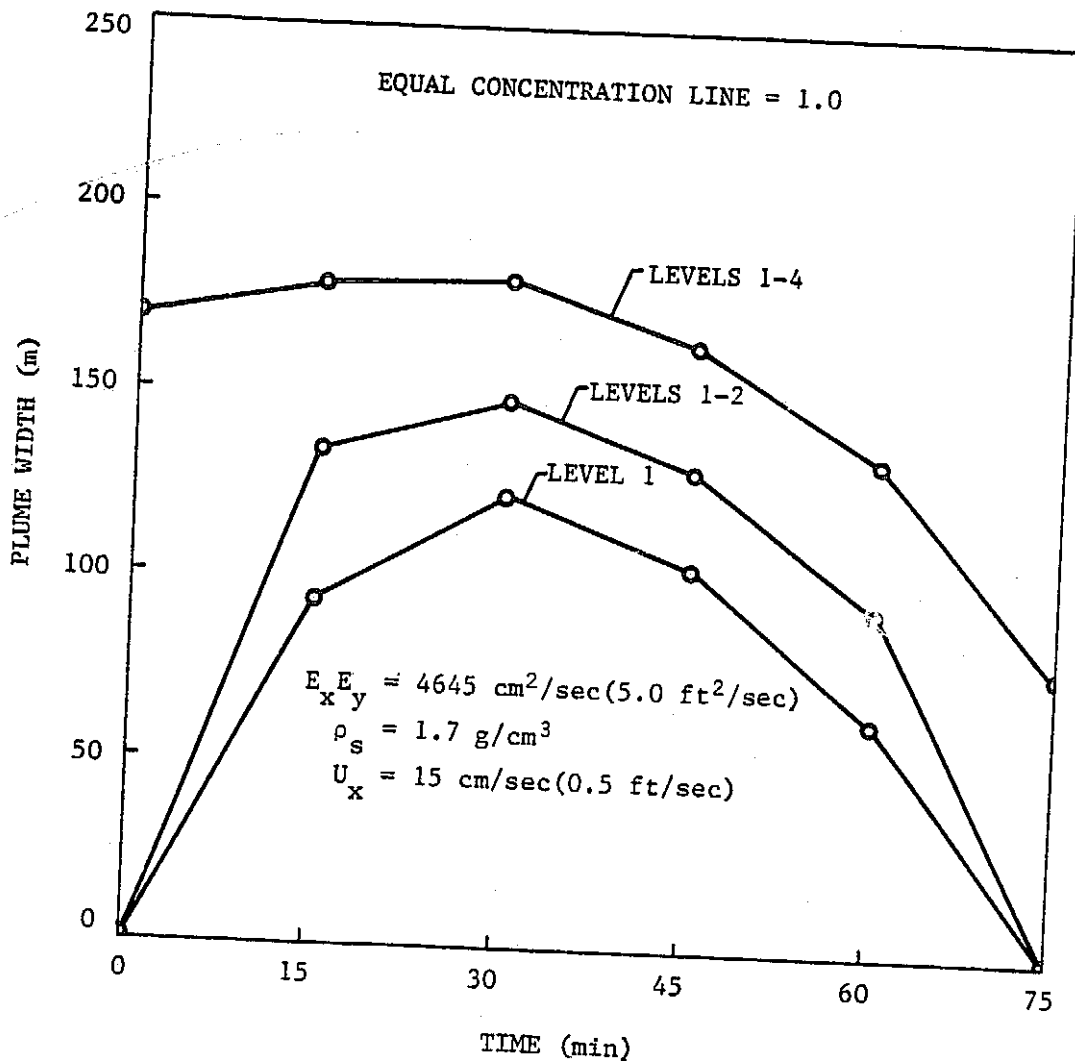


Figure 25. Plume width vs. time, $E_z = 9.29 \text{ cm}^2/\text{sec} (0.01 \text{ ft}^2/\text{sec})$.

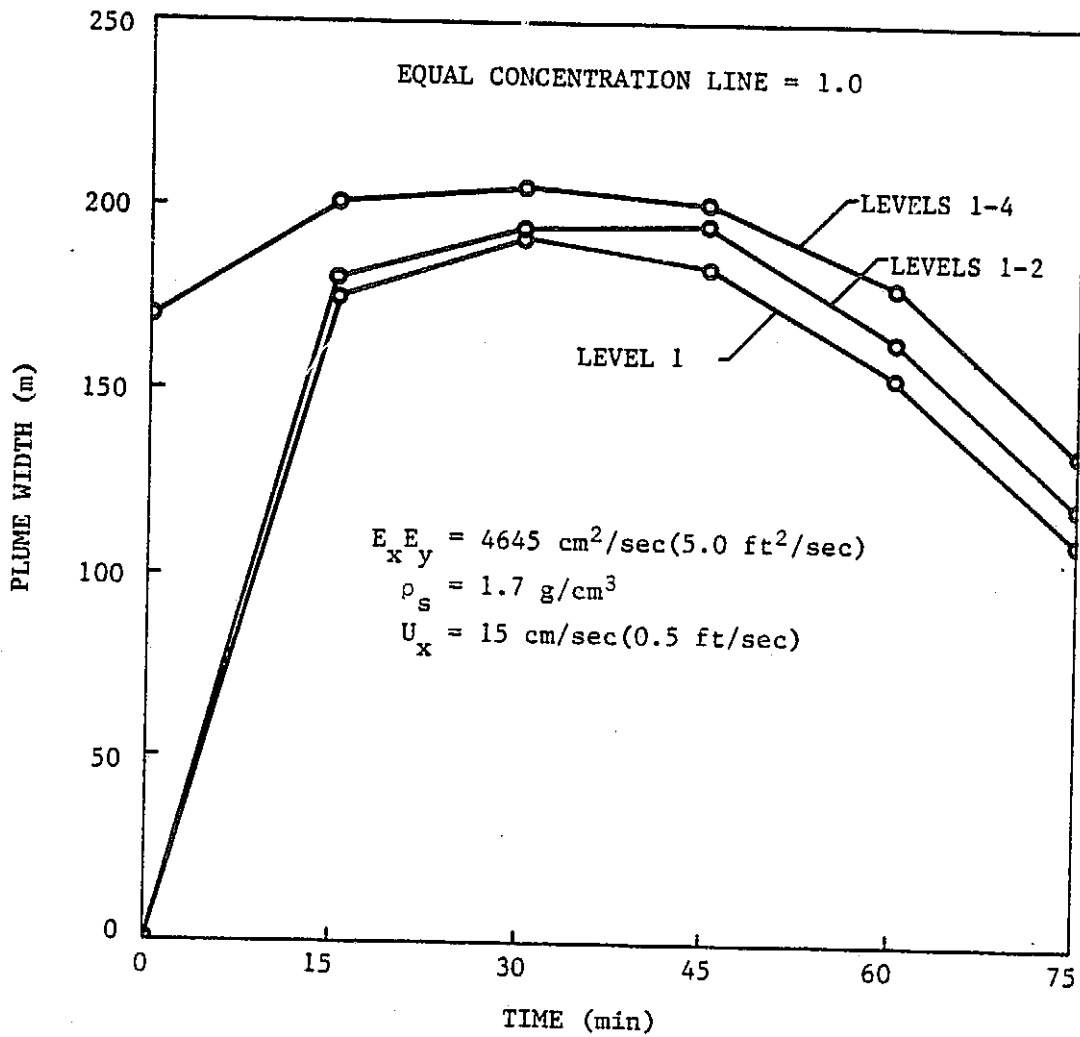


Figure 26. Plume width vs. time, $E_z = 23.23 \text{ cm}^2/\text{sec} (0.025 \text{ ft}^2/\text{sec})$.

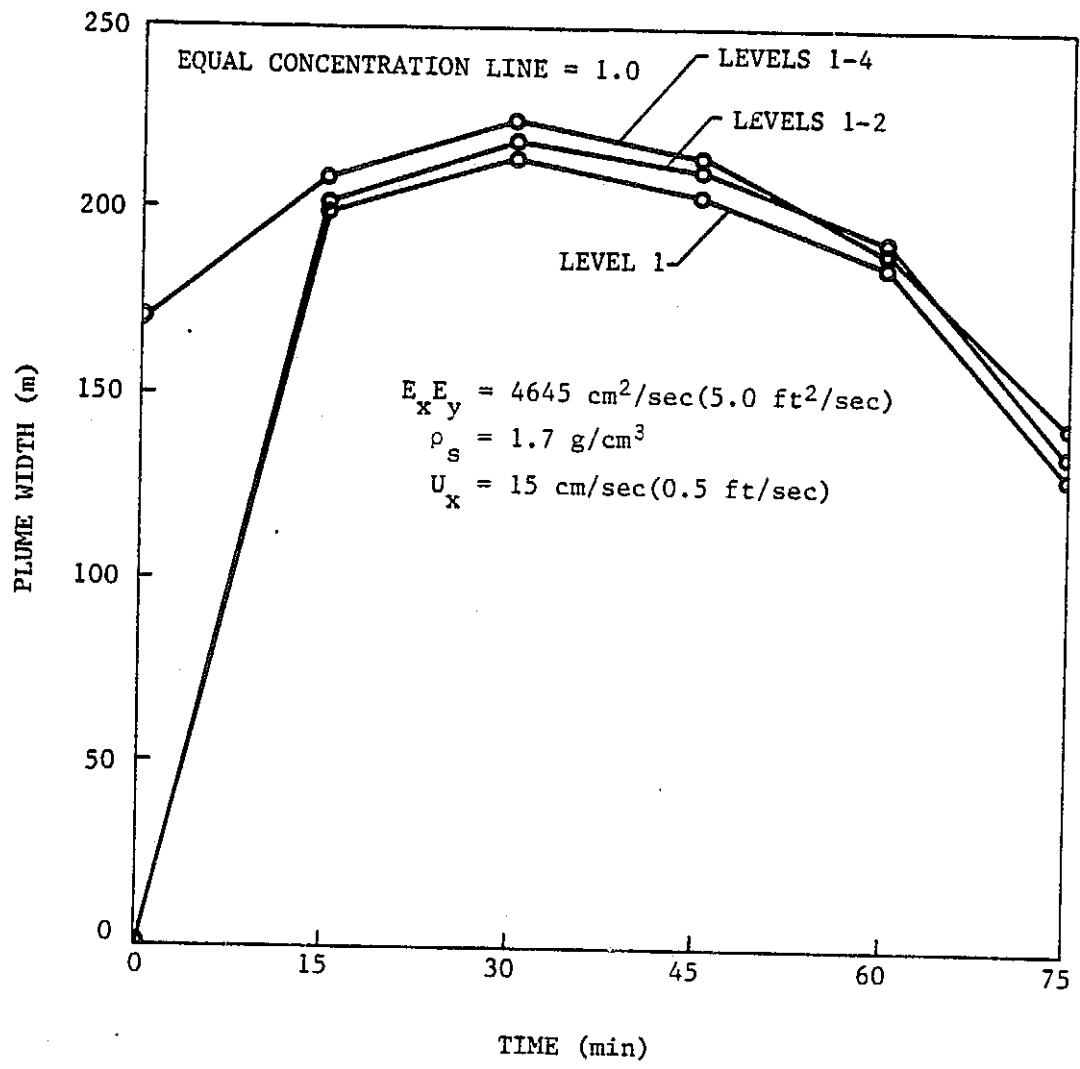


Figure 27. Plume width vs. time, $E_z = 46.45 \text{ cm}^2/\text{sec} (0.05 \text{ ft}^2/\text{sec})$.

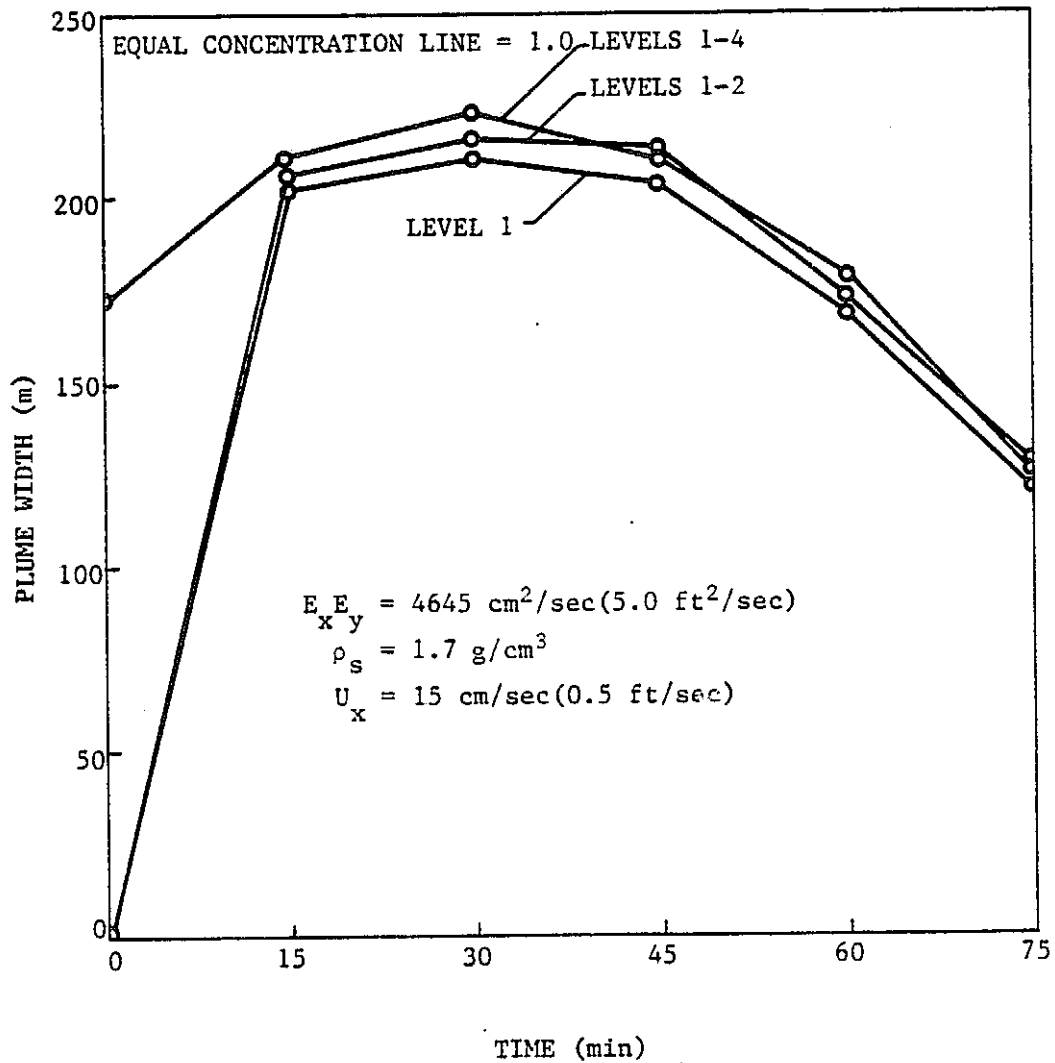


Figure 28. Plume width vs. time, $E_z = 69.68 \text{ cm}^2/\text{sec} (0.075 \text{ ft}^2/\text{sec})$.

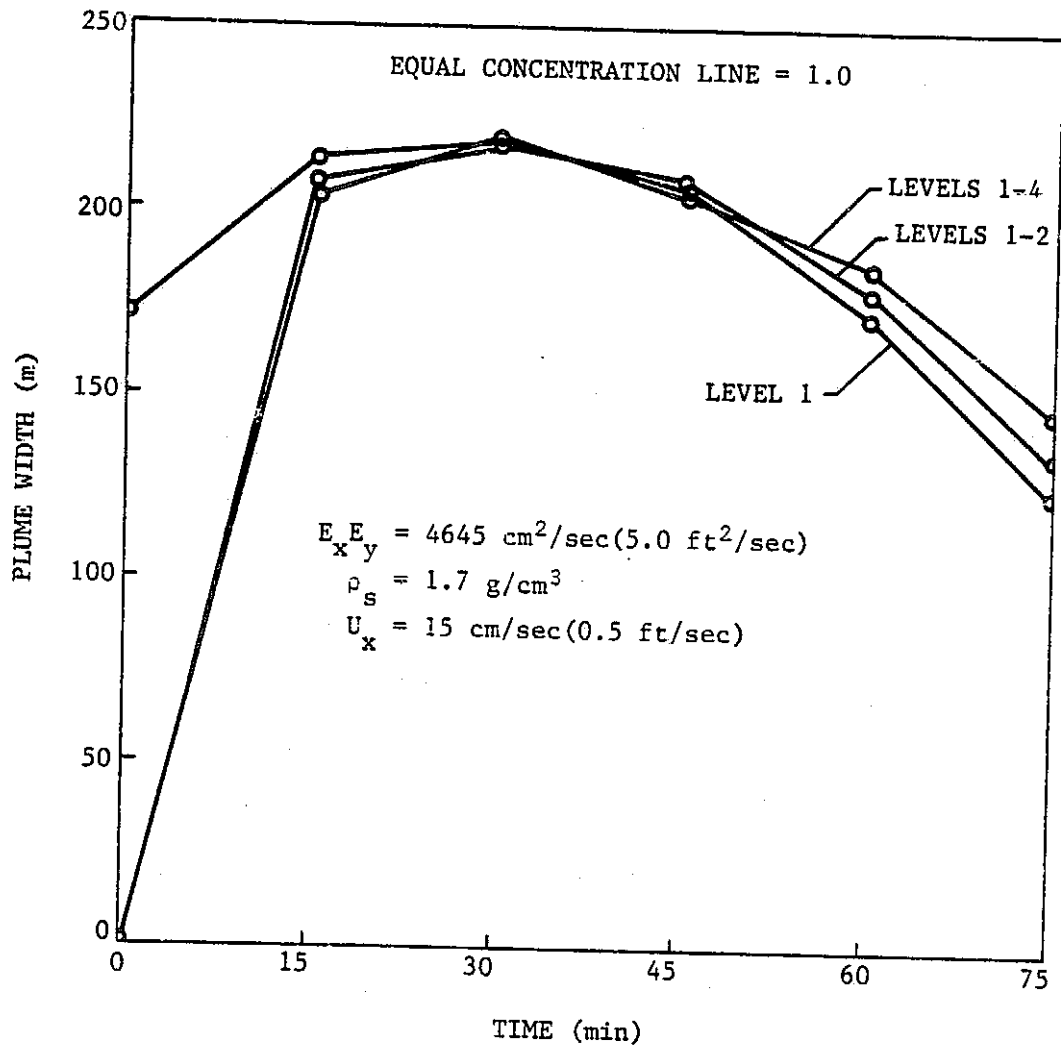


Figure 29. Plume width vs. time, $E_z = 92.90 \text{ cm}^2/\text{sec} (0.1 \text{ ft}^2/\text{sec})$.

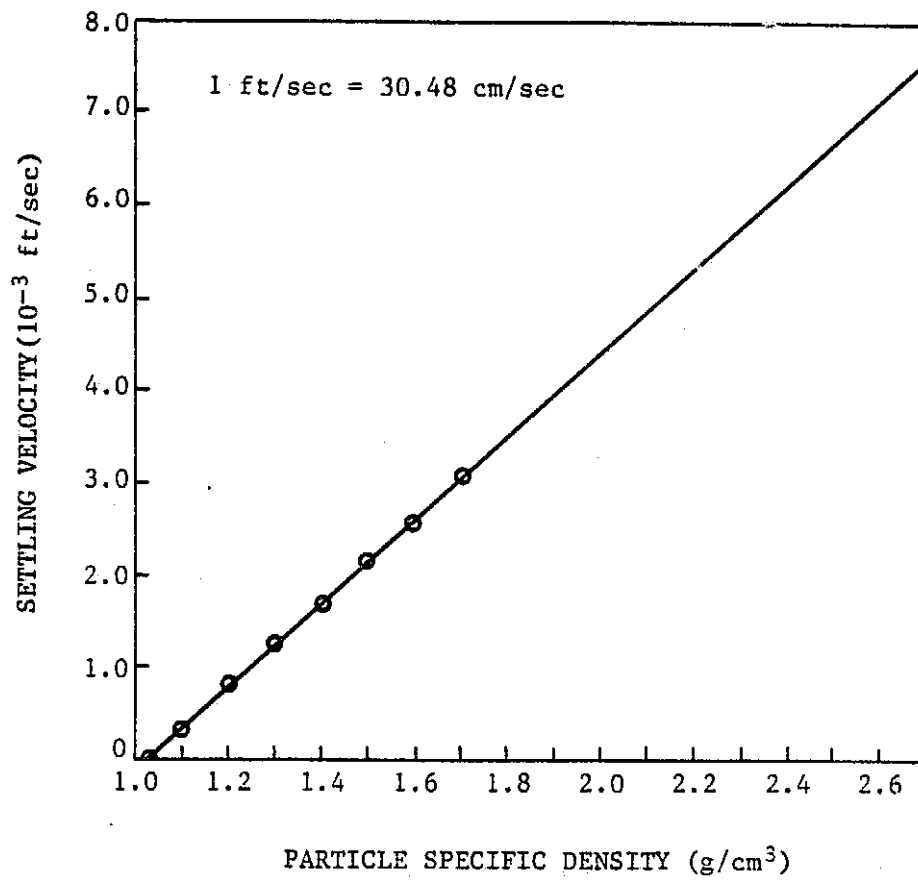


Figure 30. Settling velocity vs. particle specific density.

$E_{xy} = 4645 \text{ cm}^2/\text{sec} (5.0 \text{ ft}^2/\text{sec})$
 $E_z = 46.45 \text{ cm}^2/\text{sec} (0.05 \text{ ft}^2/\text{sec})$
 $\rho_s = 1.7 \text{ g/cm}^3$
 $U_x = 15 \text{ cm/sec} (0.5 \text{ ft/sec})$

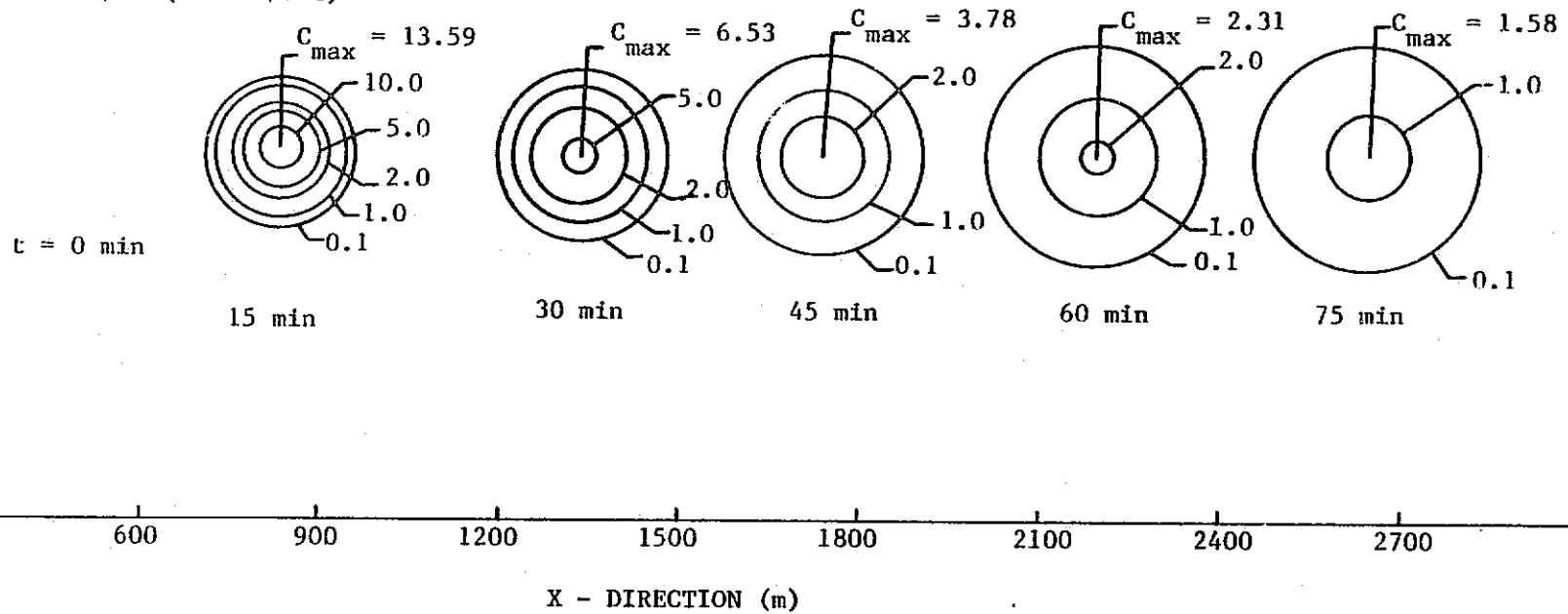


Figure 31. Advection and diffusion of plume, level 1.

$$E_{x,y} = 4645 \text{ cm}^2/\text{sec} (5.0 \text{ ft}^2/\text{sec})$$

$$E_z = 46.45 \text{ cm}^2/\text{sec} (0.05 \text{ ft}^2/\text{sec})$$

$$\rho_s = 1.7 \text{ g/cm}^3$$

$$U_x = 15 \text{ cm/sec} (0.5 \text{ ft/sec})$$

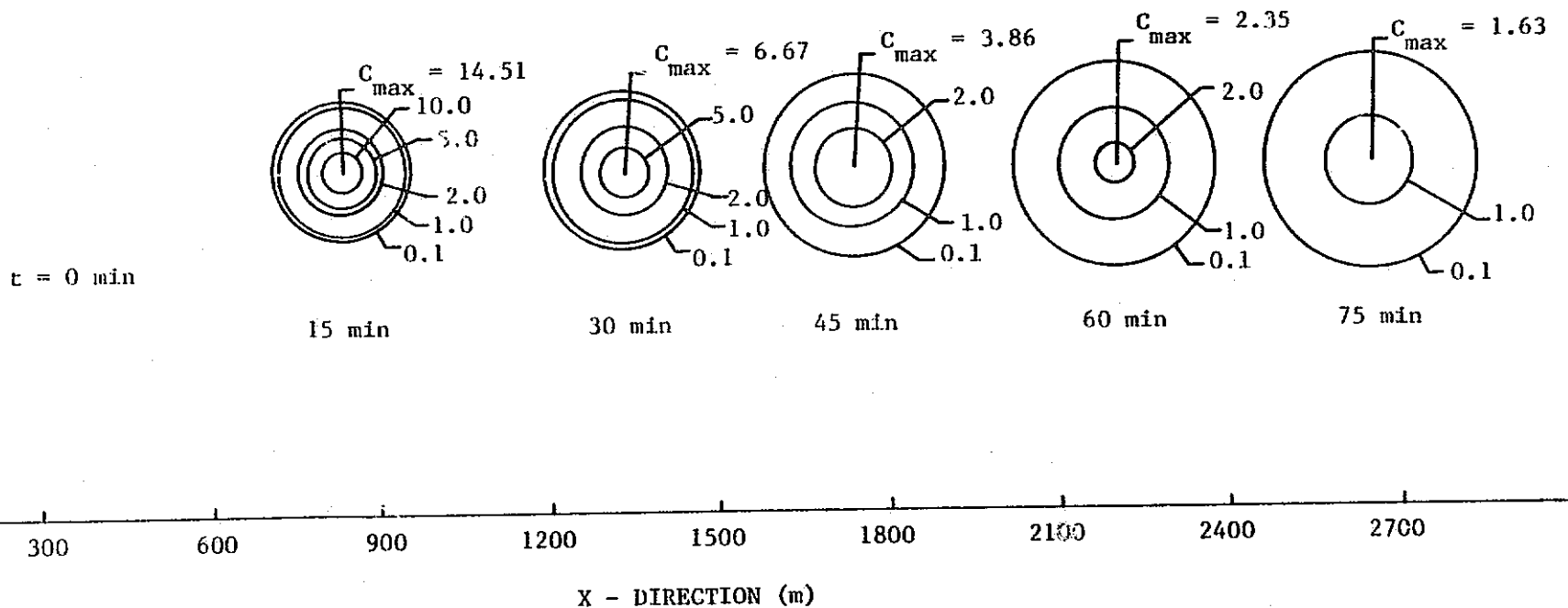


Figure 32. Advection and diffusion of plume, levels 1 to 2.

$$E_{x y} = 4645 \text{ cm}^2/\text{sec} (5.0 \text{ ft}^2/\text{sec})$$

$$E_z = 46.45 \text{ cm}^2/\text{sec} (0.05 \text{ ft}^2/\text{sec})$$

$$\rho_s = 1.7 \text{ g/cm}^3$$

$$U_x = 15 \text{ cm/sec} (0.5 \text{ ft/sec})$$

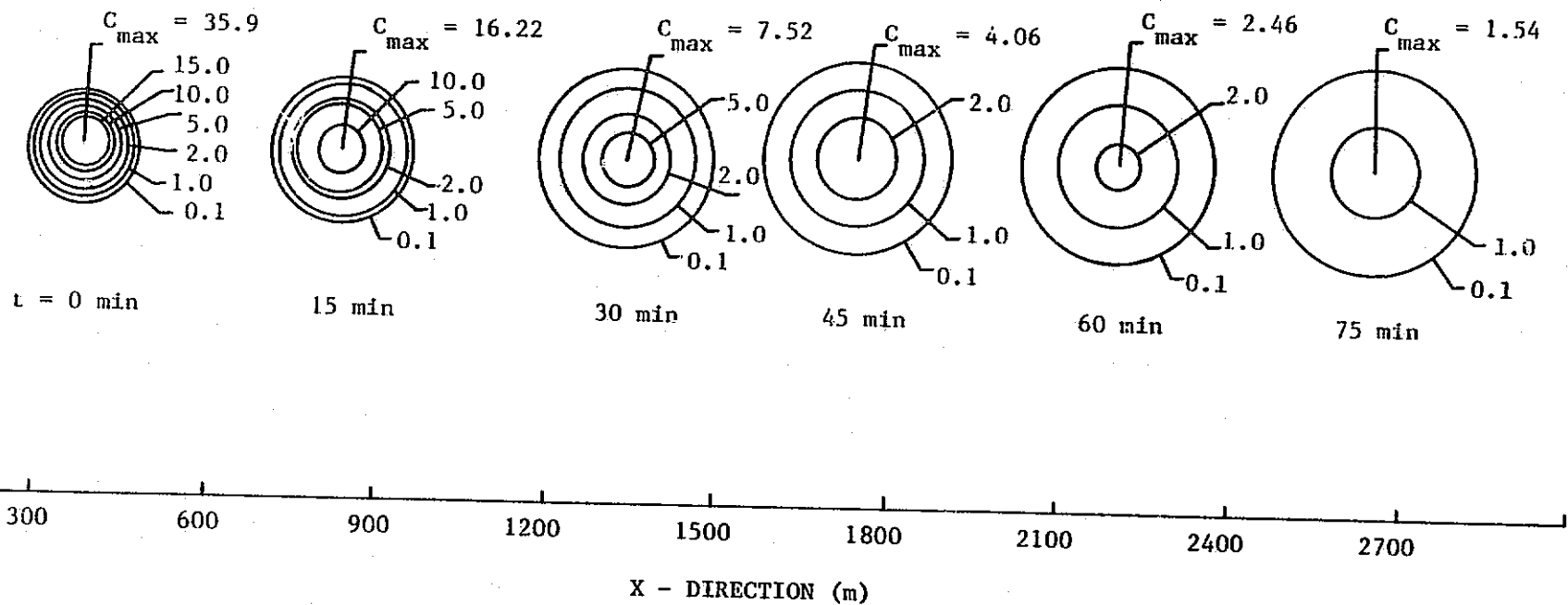


Figure 33. Advection and diffusion of plume, levels 1 to 4.

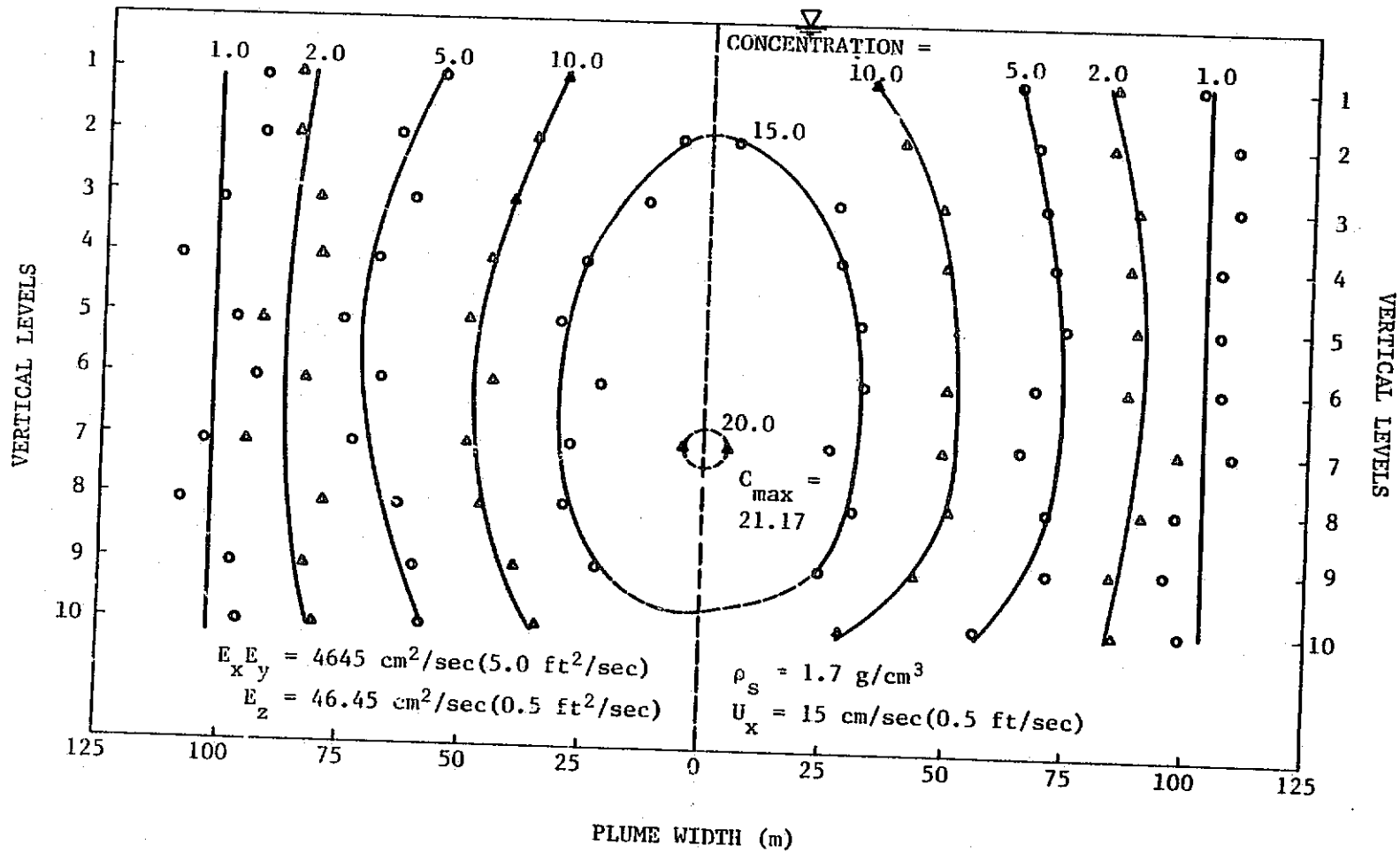


Figure 34. Vertical profile of plume for instantaneous release (time = 15 min).

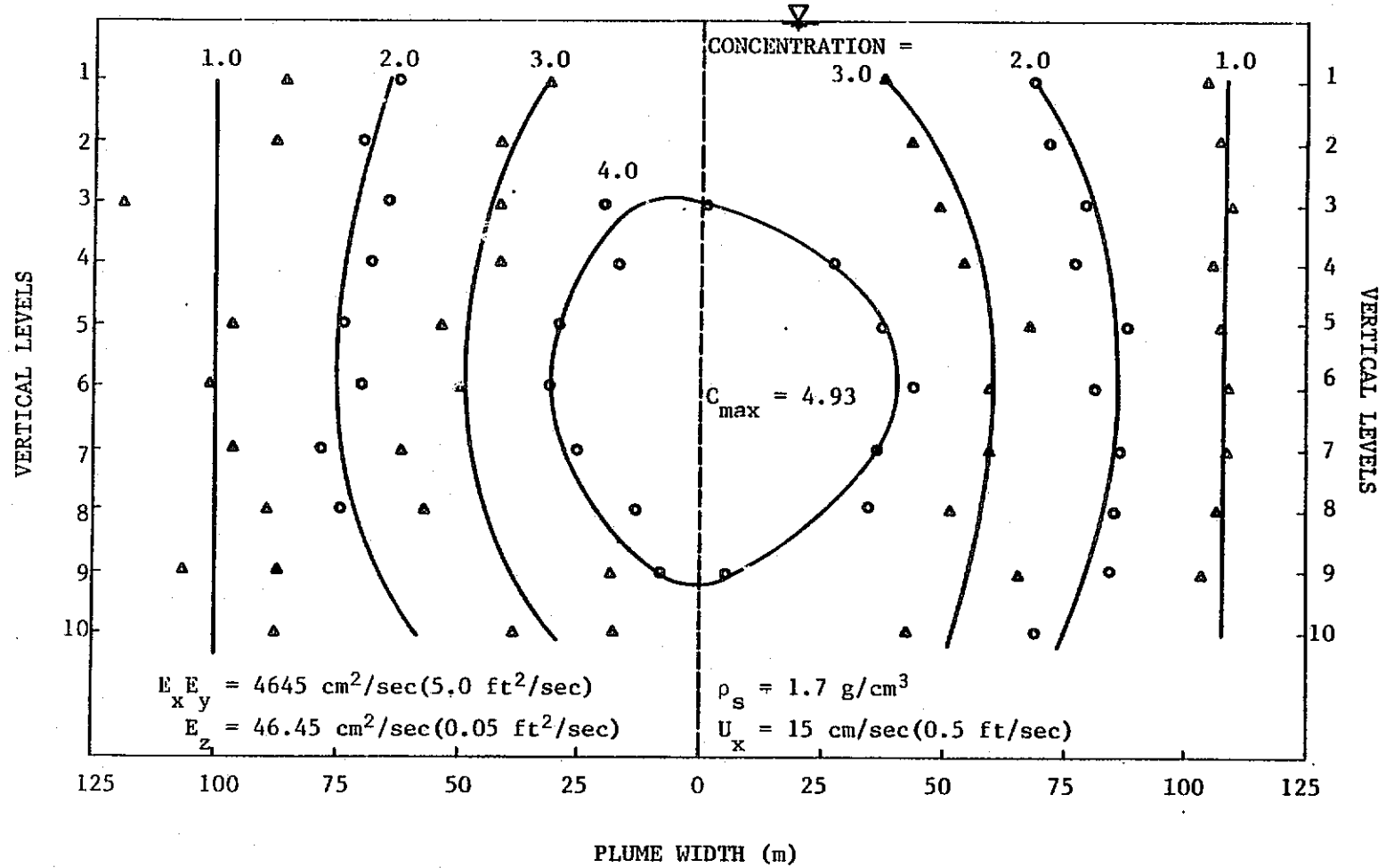


Figure 35. Vertical profile of plume for instantaneous release (time = 45 min).

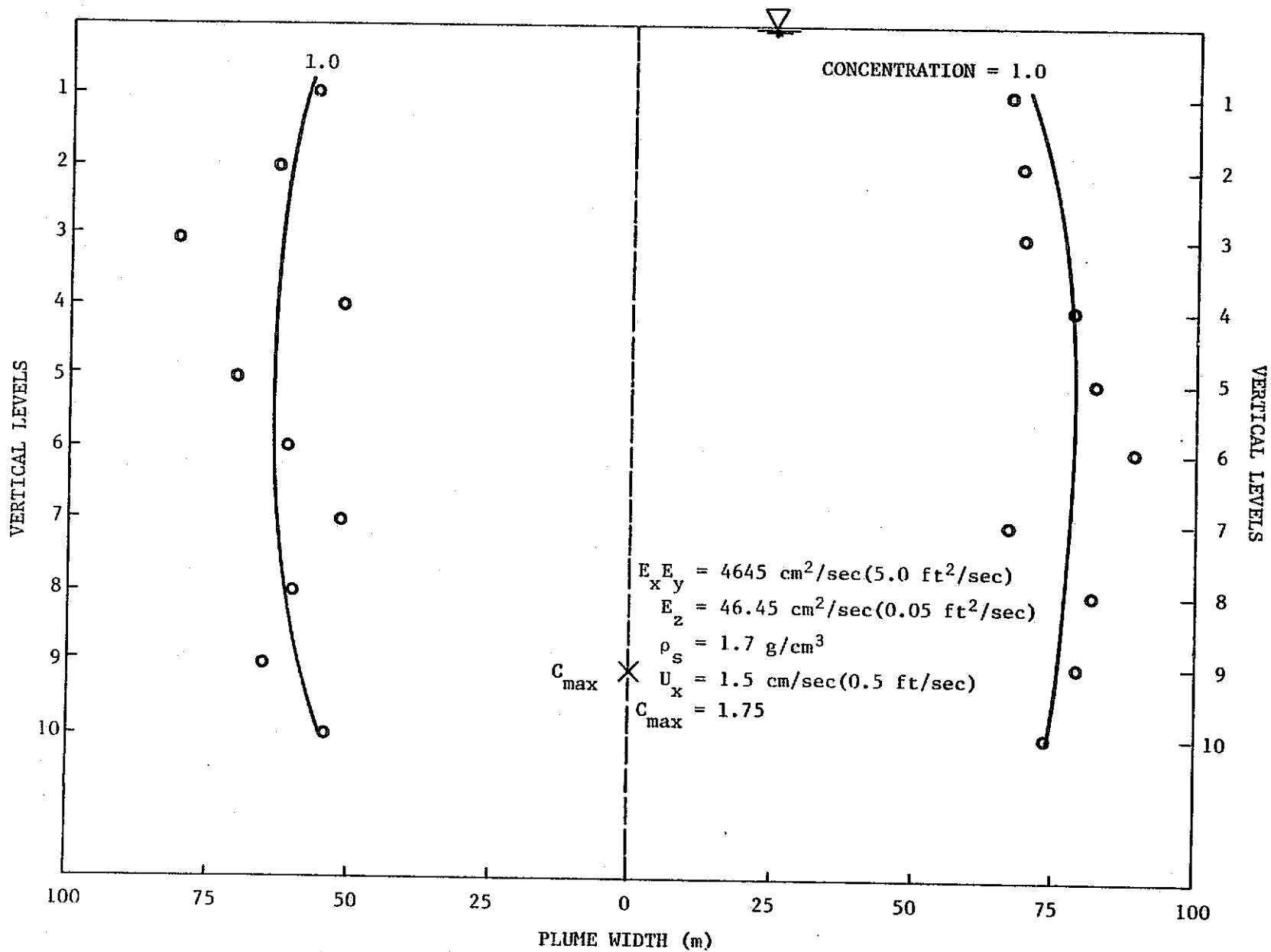


Figure 36. Vertical profile of plume for instantaneous release (time = 75 min).

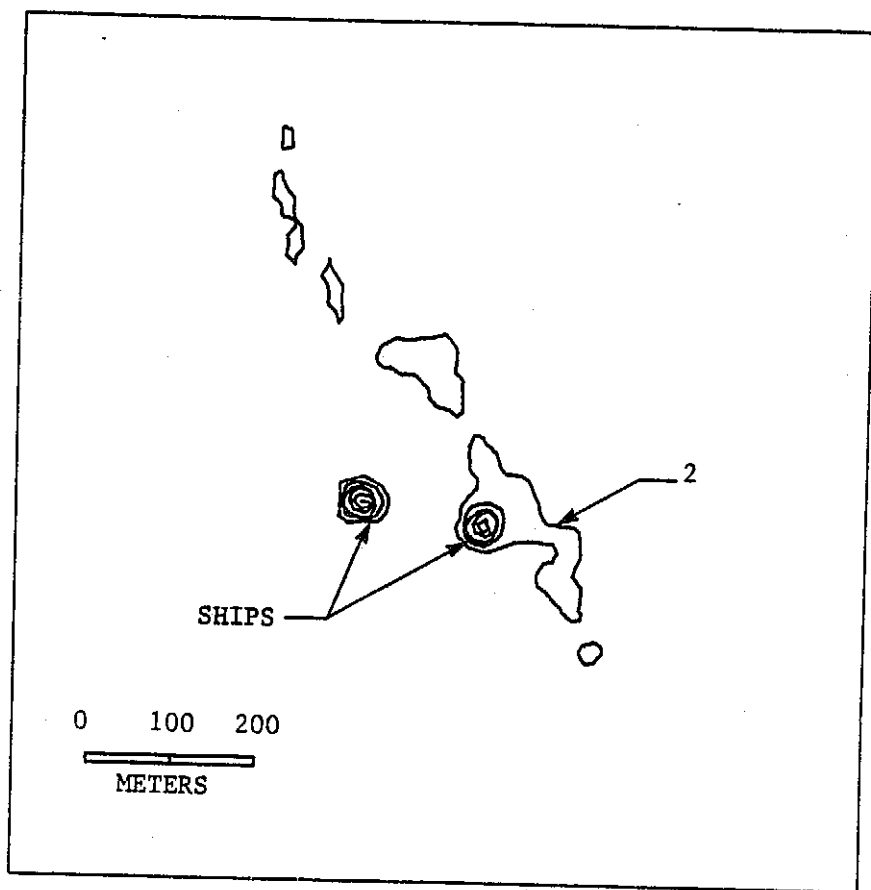


Figure 37. Quantitative distribution of suspended solids concentrations, mg/l, in a "spot" sewage sludge dump in the NY Bight on July 15, 1976, 15 minutes after dump. (Remote sensing data obtained by NASA.)

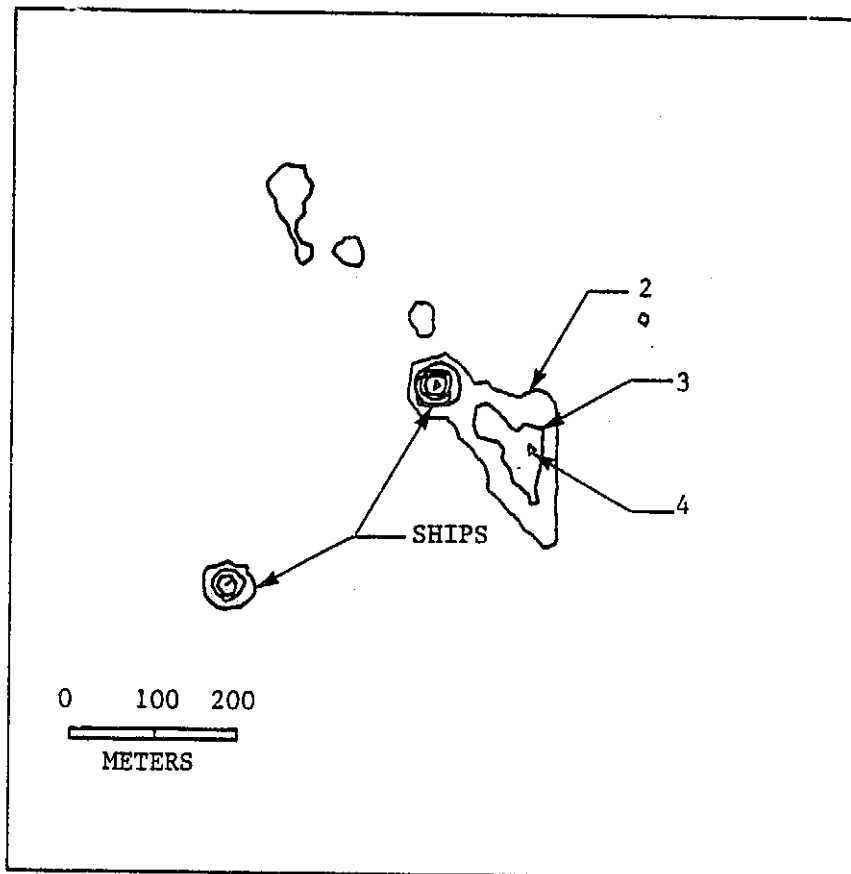


Figure 38. Quantitative distribution of suspended solids concentrations, mg/l, in a "spot" sewage sludge dump in the NY Bight on July 15, 1976, 30 minutes after dump. (Remote sensing data obtained by NASA.)

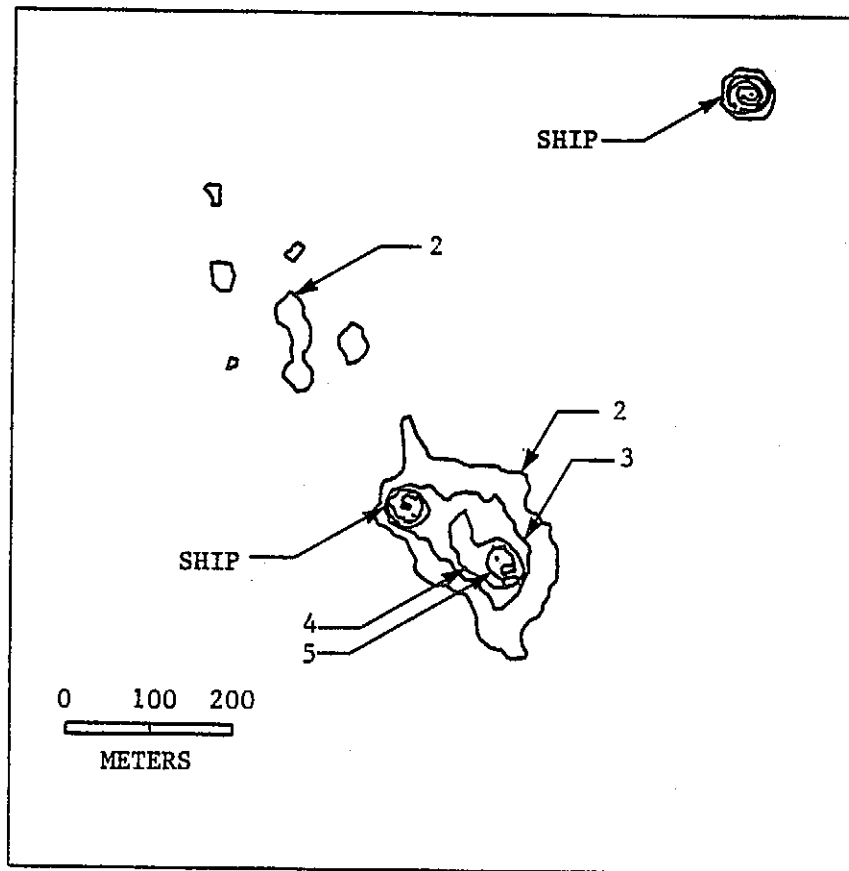


Figure 39. Quantitative distribution of suspended solids concentrations, mg/l, in a "spot" sewage sludge dump in the NY Bight on July 15, 1976, 45 minutes after dump. (Remote sensing data obtained by NASA.)

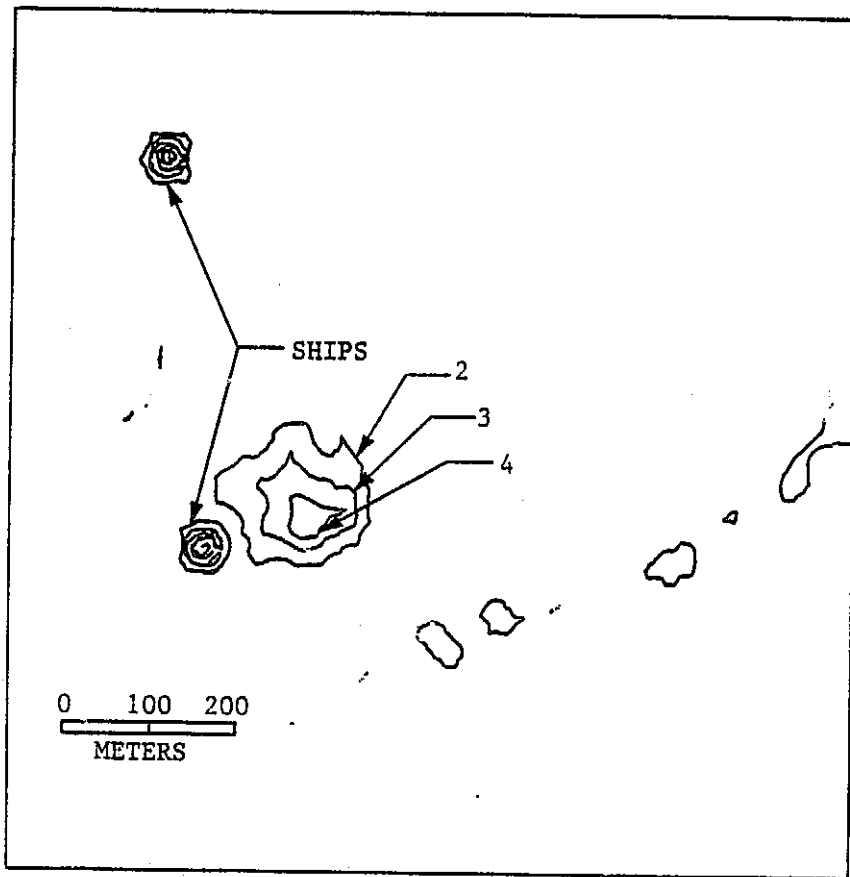


Figure 40. Quantitative distribution of suspended solids concentrations, mg/l, in a "spot" sewage sludge dump in the NY Bight on July 15, 1976, 60 minutes after dump. (Remote sensing data obtained by NASA.)

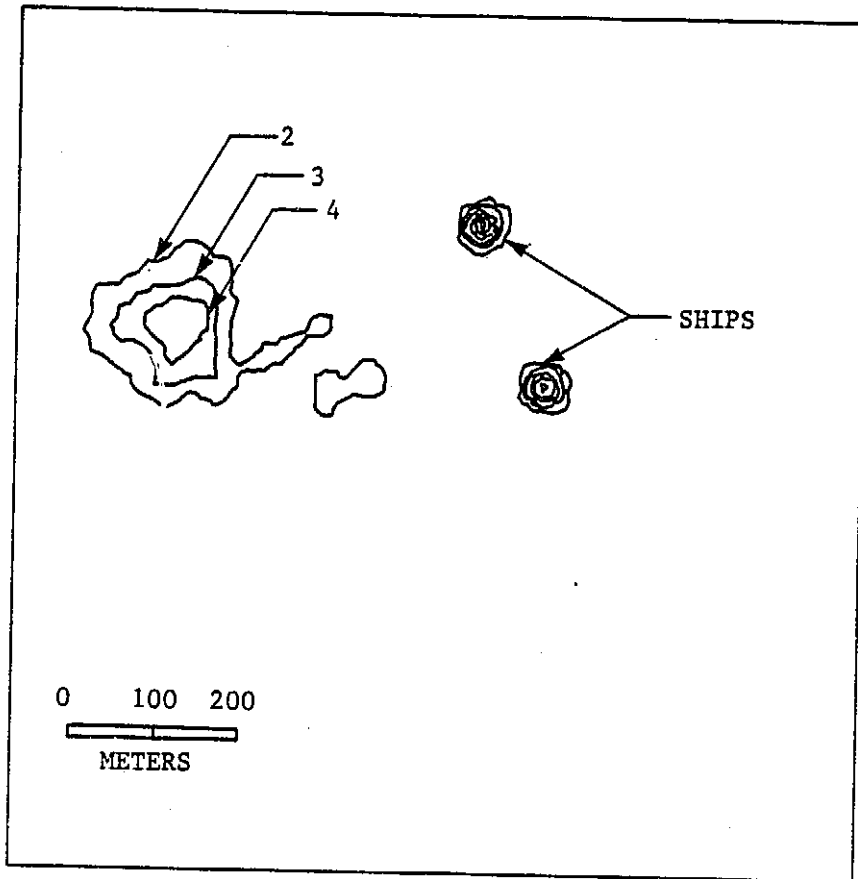


Figure 41. Quantitative distribution of suspended solids concentrations, mg/l, in a "spot" sewage sludge dump in the NY Bight on July 15, 1976, 75 minutes after dump. (Remote sensing data obtained by NASA.)

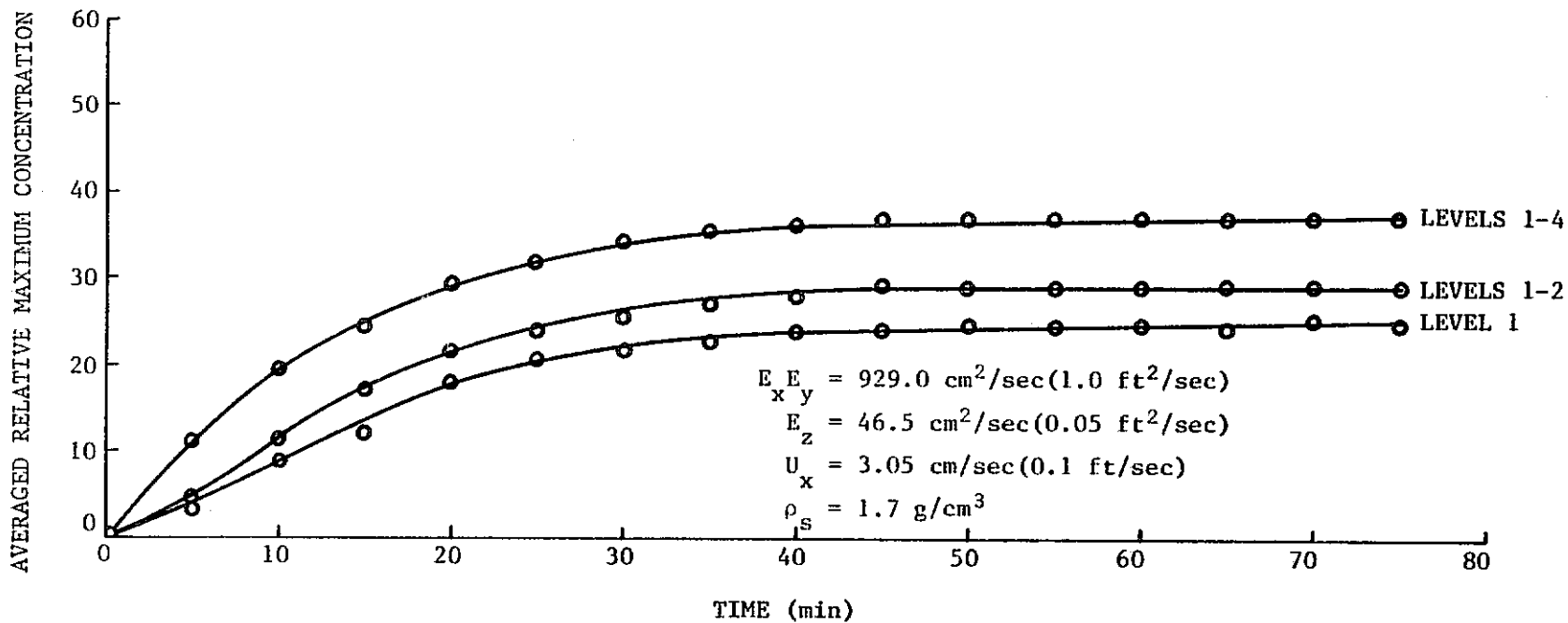
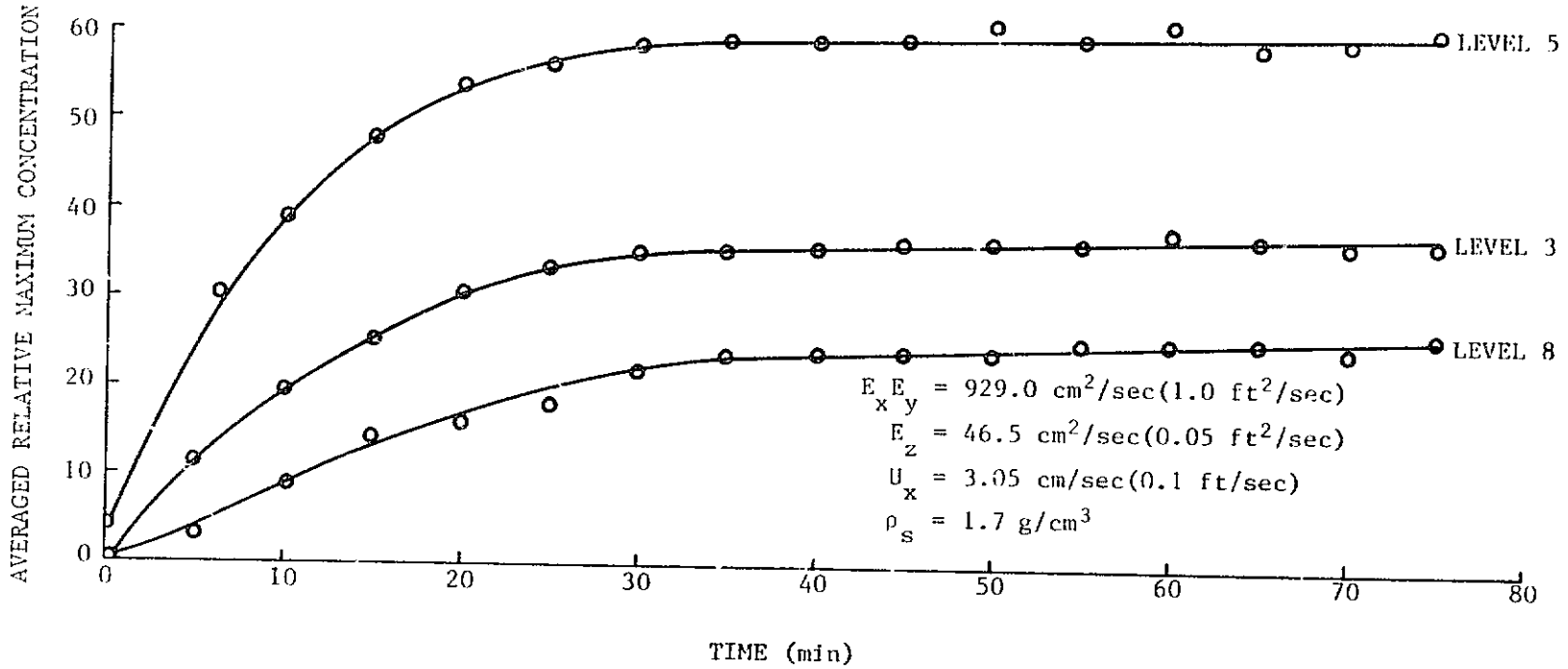


Figure 42. Variation of averaged relative maximum concentration with time ($U_x = 3 \text{ cm/sec}$, $E_x = E_y = 929 \text{ cm}^2/\text{sec}$).



C-2

Figure 43. Variation of averaged relative maximum concentration with time ($U_x = 3 \text{ cm/sec}$, $E_x = E_y = 929 \text{ cm}^2/\text{sec}$).

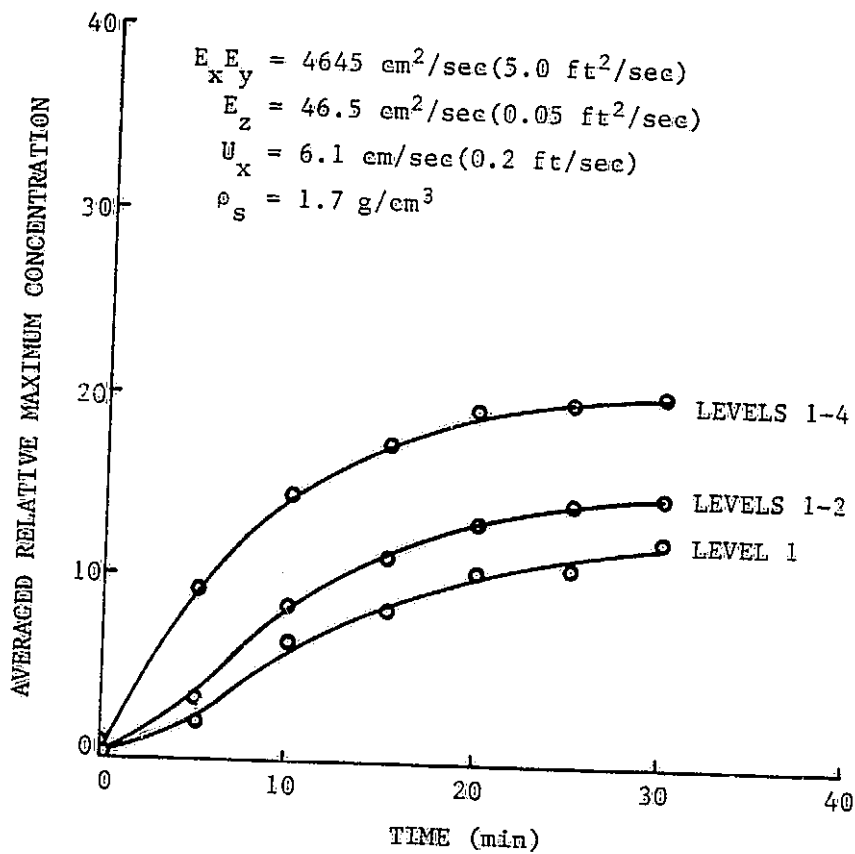


Figure 44. Variation of averaged relative maximum concentration with time ($U_x = 6 \text{ cm/sec}$, $E_x = E_y = 4645 \text{ cm}^2/\text{sec}$).

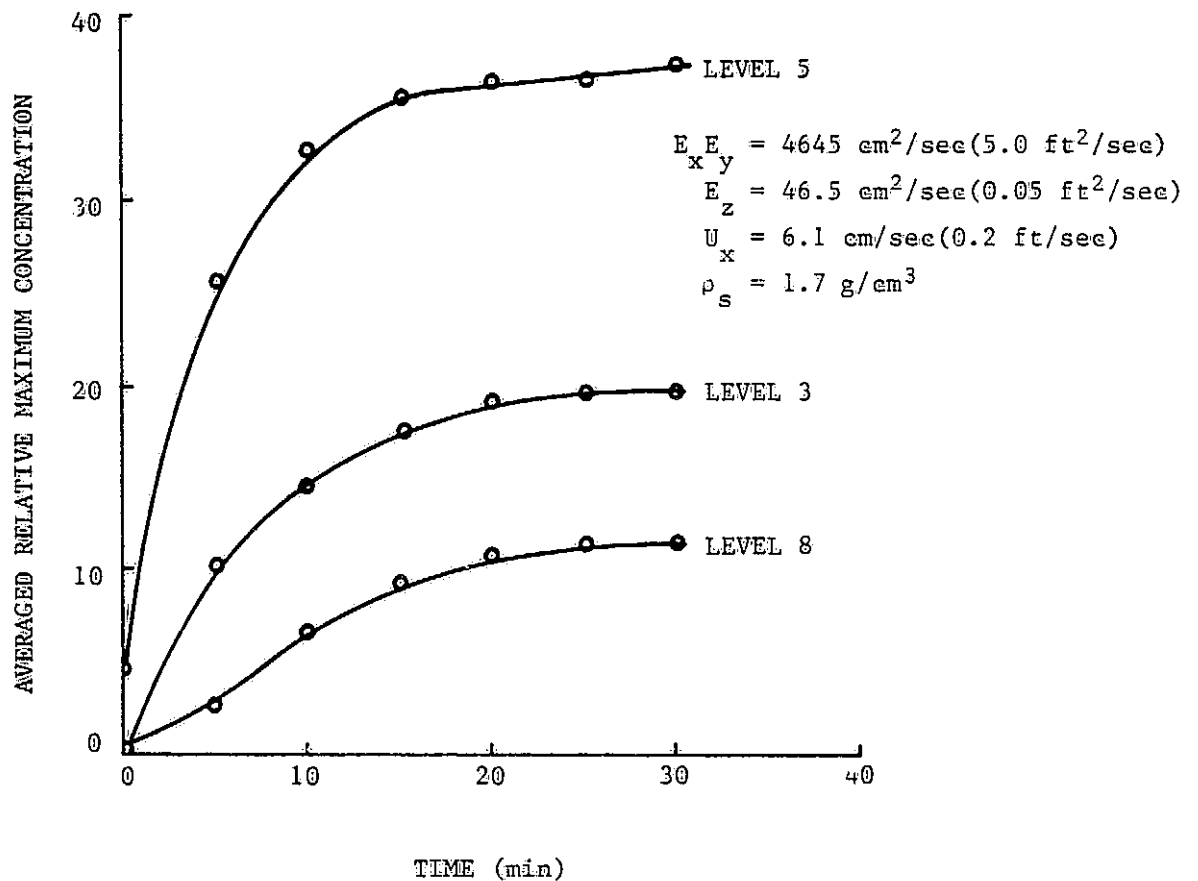


Figure 45. Variation of averaged relative maximum concentration with time ($U_x = 6 \text{ cm/sec}$, $E_x = E_y = 4645 \text{ cm}^2/\text{sec}$).

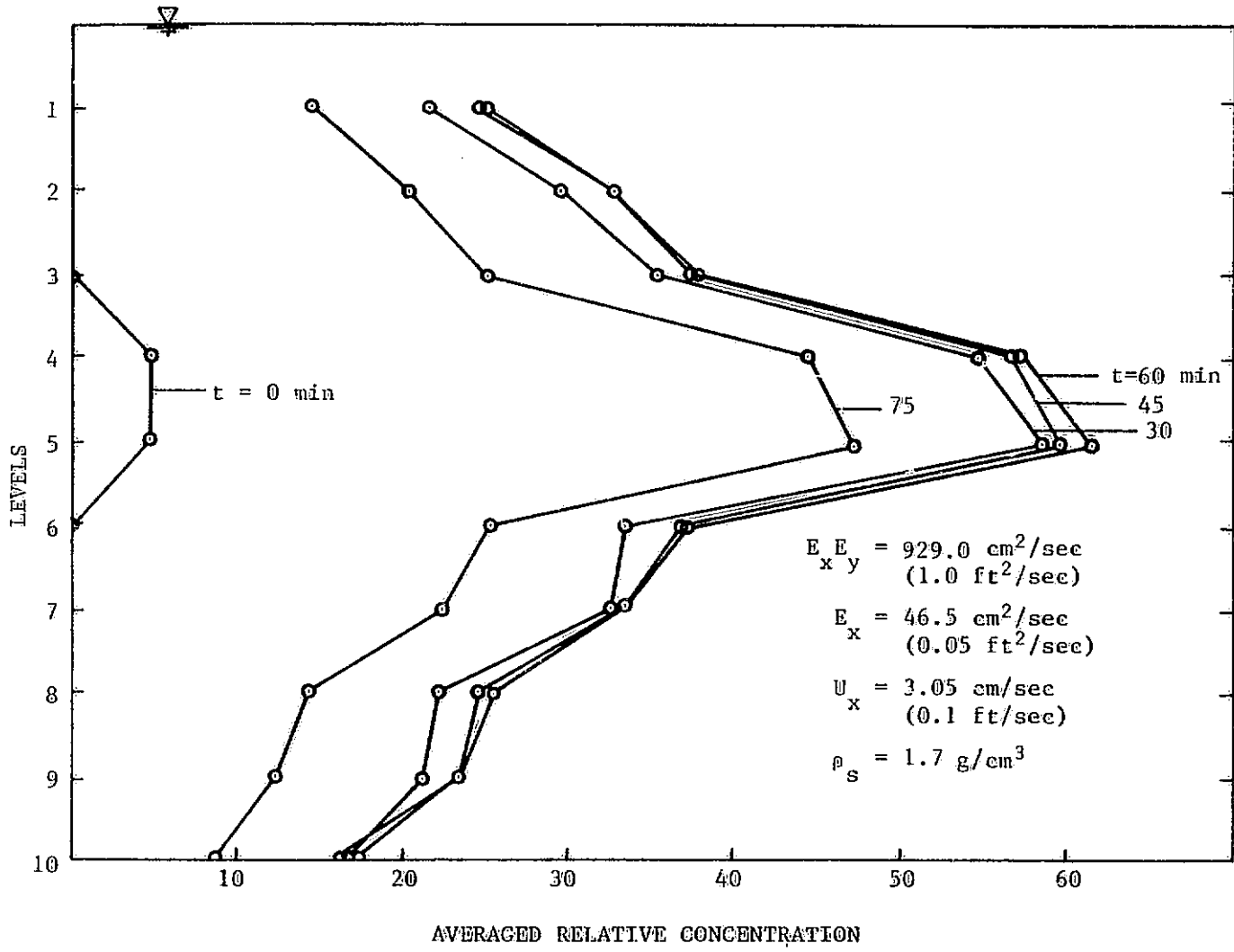


Figure 46. Variation of averaged relative concentration with depth ($U_x = 3 \text{ cm/sec}$, $E_x = E_y = 929 \text{ cm}^2/\text{sec}$).

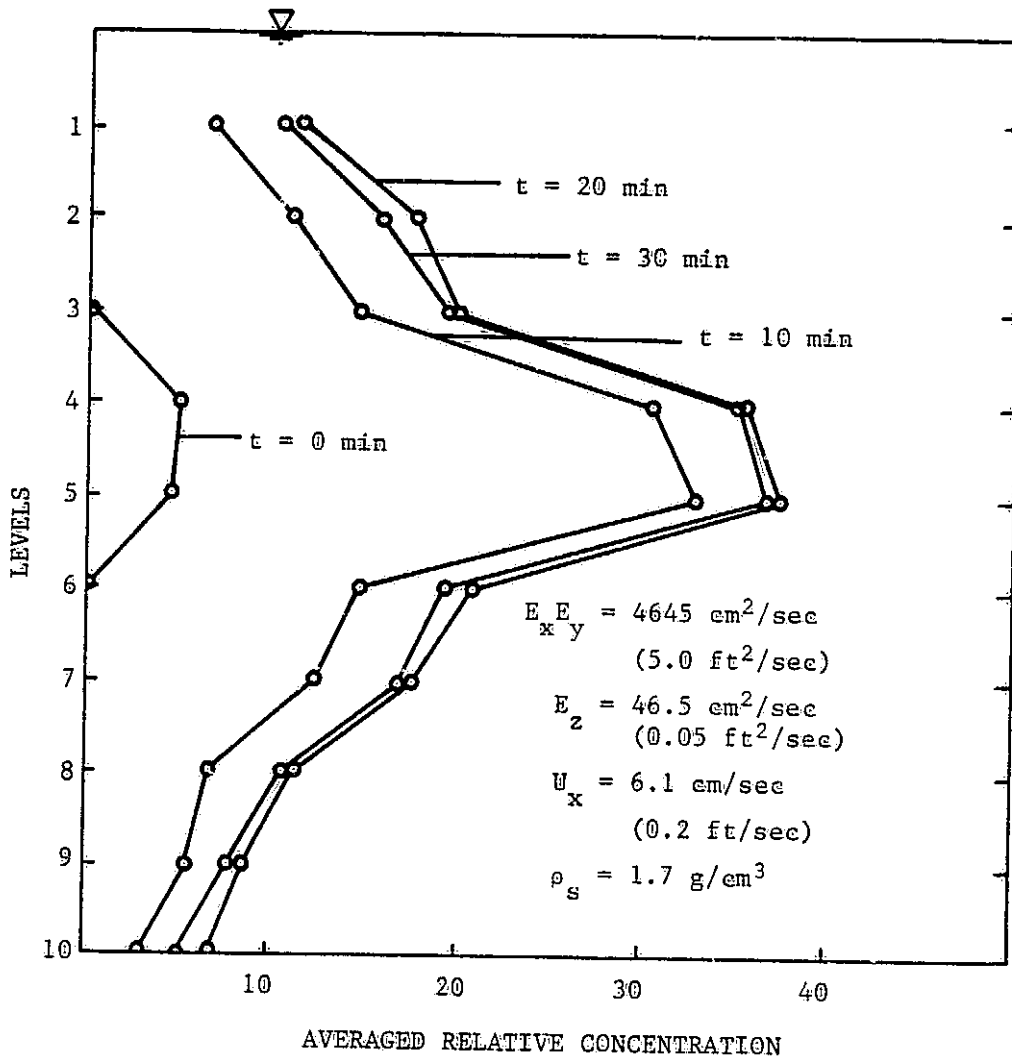


Figure 47. Variation of averaged relative concentration with depth ($U_x = 6 \text{ cm/sec}$, $E_x = E_y = 4645 \text{ cm}^2/\text{sec}$).

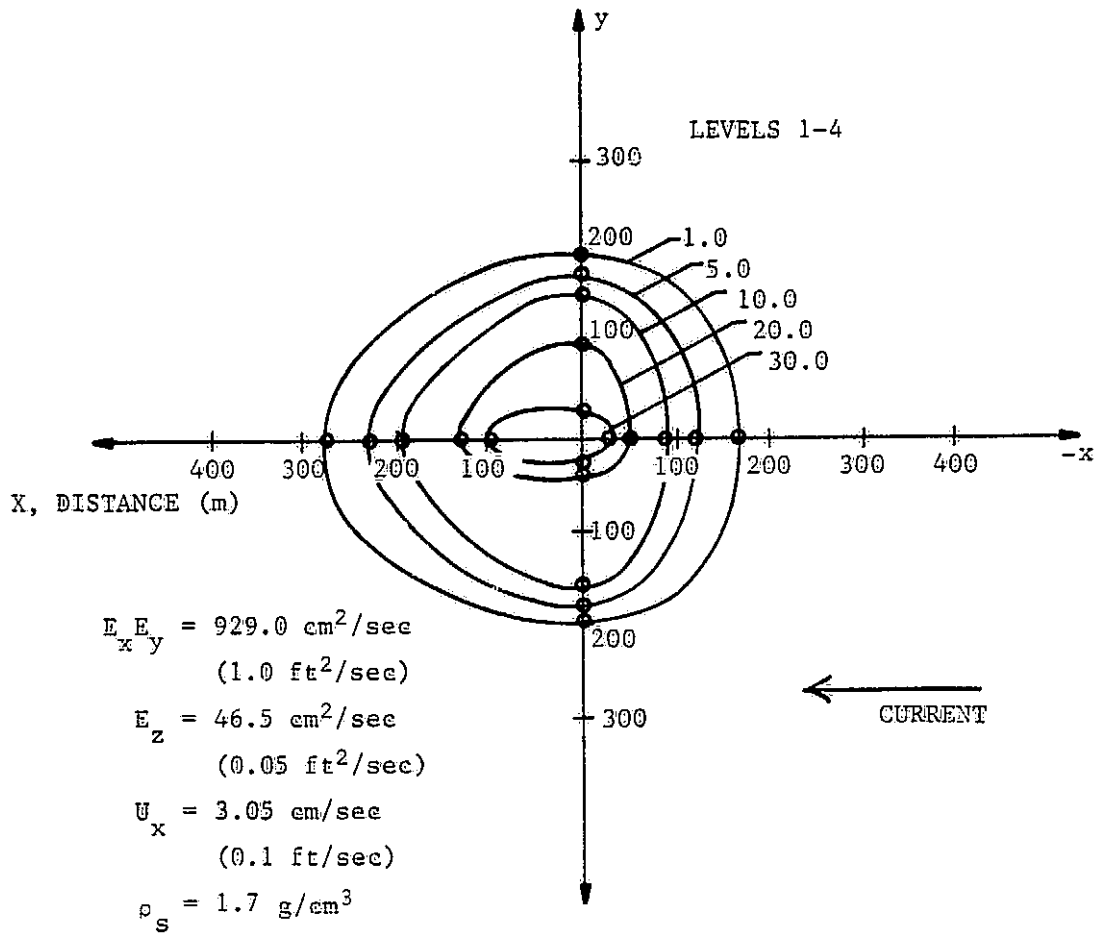


Figure 48. Equiconcentration lines for a continuous release, first case (time = 15 min).

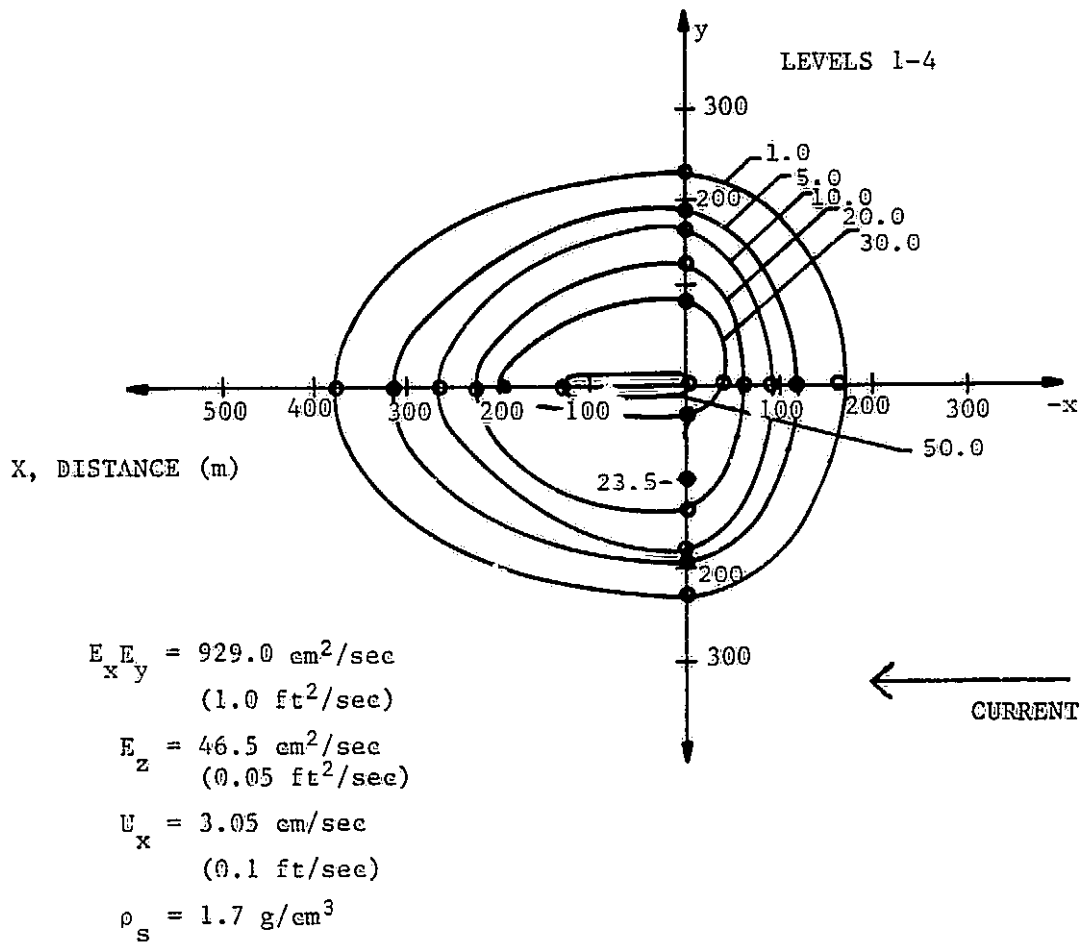


Figure 49. Equiconcentration lines for a continuous release, first case (time = 30 min).

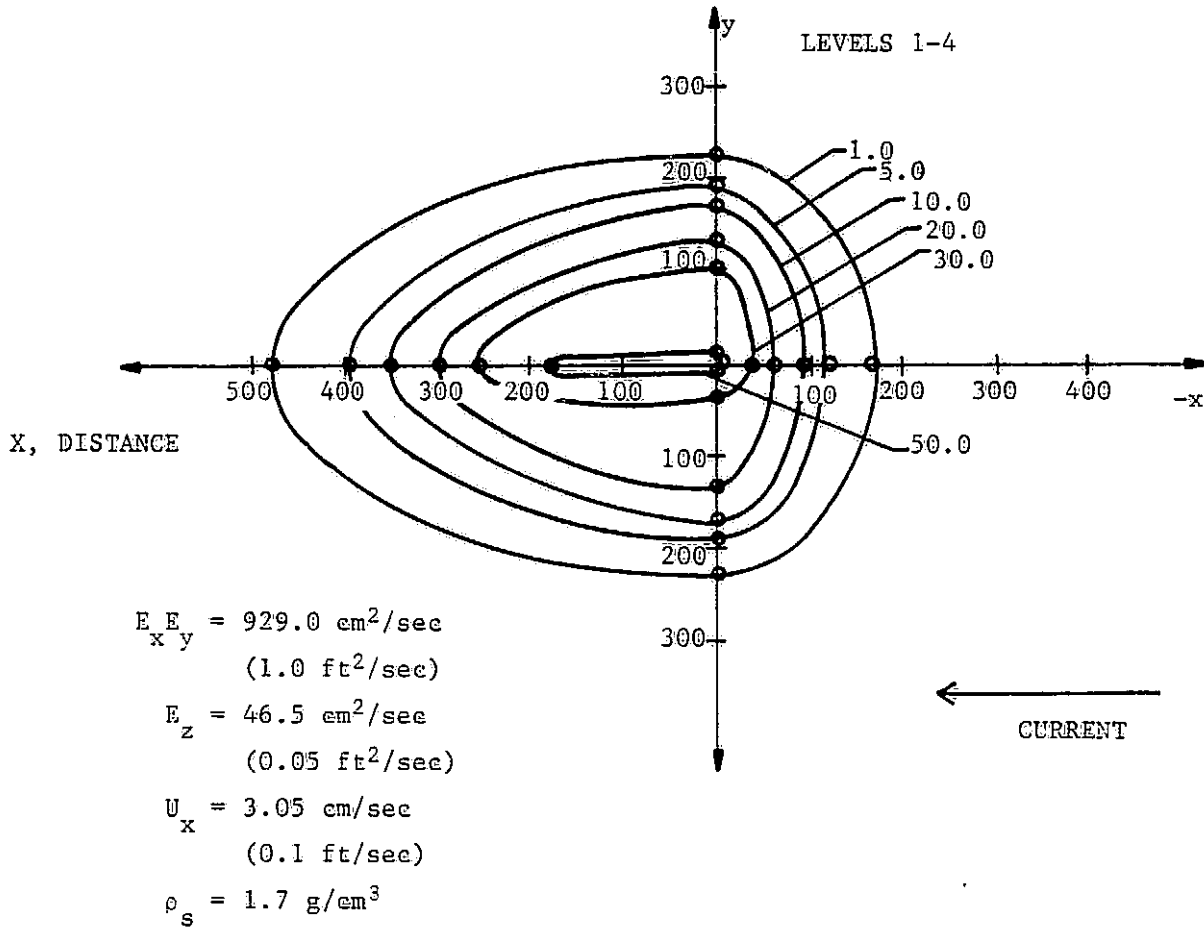


Figure 50. Equiconcentration lines for a continuous release, first case (time = 45 min).

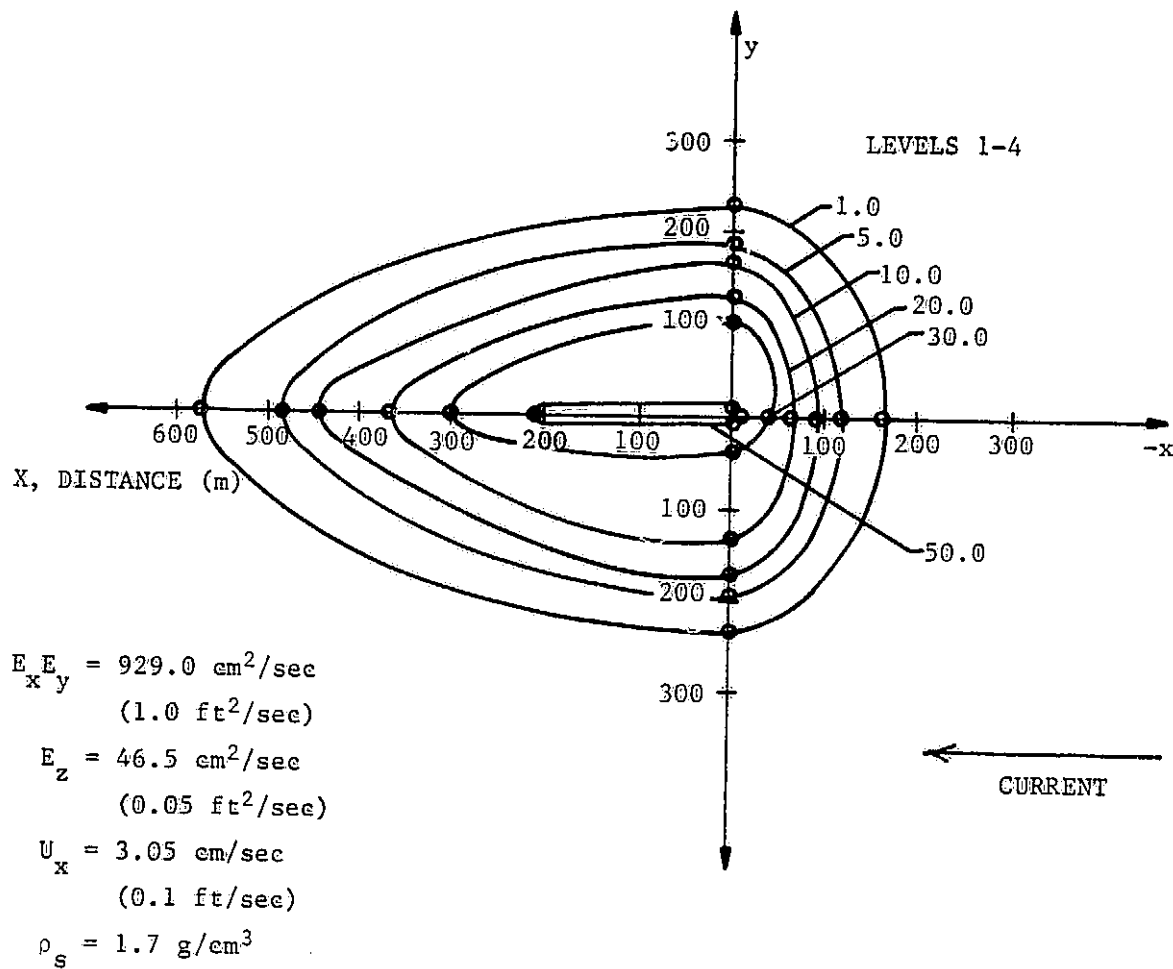


Figure 51. Equiconcentration lines for a continuous release, first case (time = 60 min).

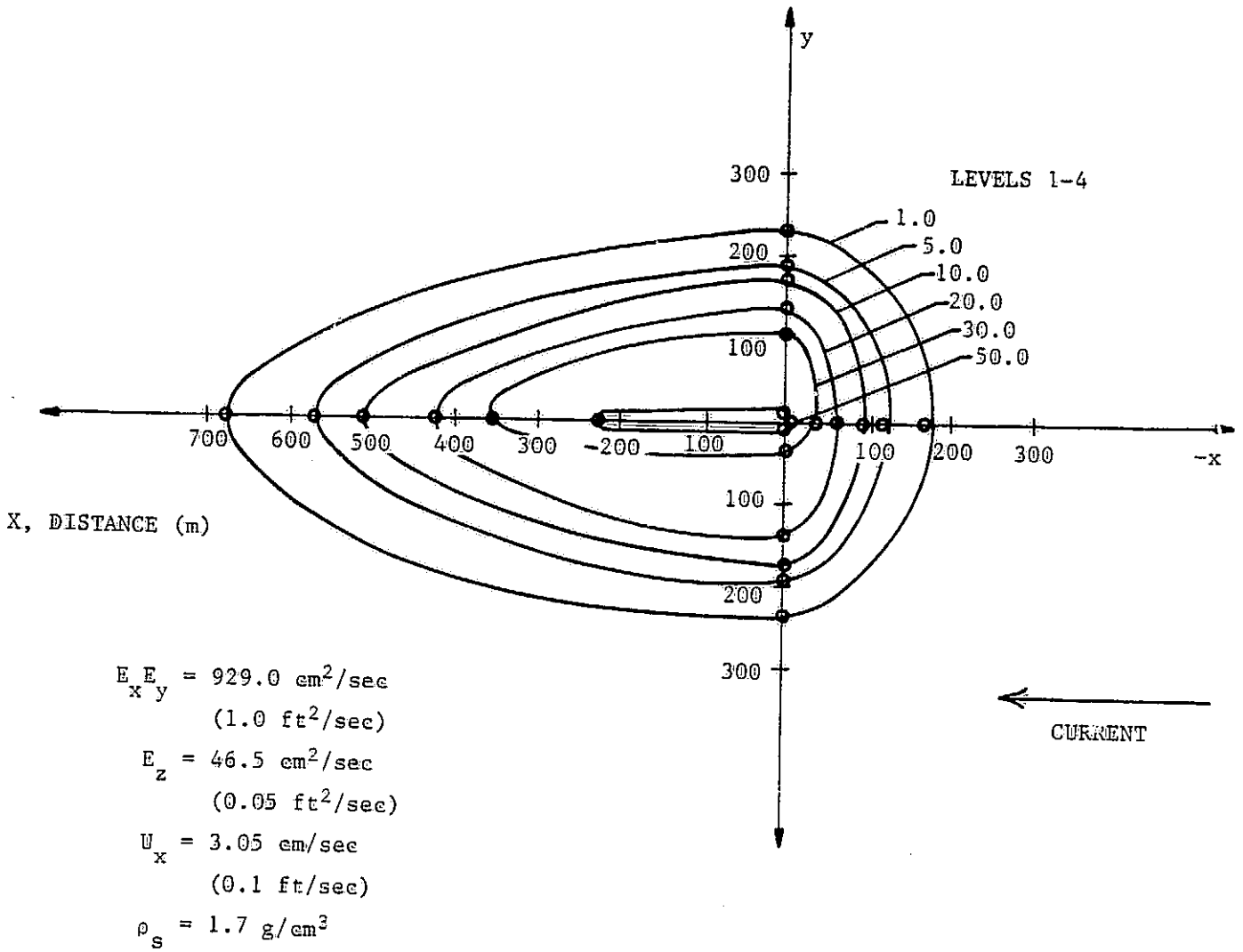


Figure 52. Equiconcentration lines for a continuous release, first case (time = 75 min).

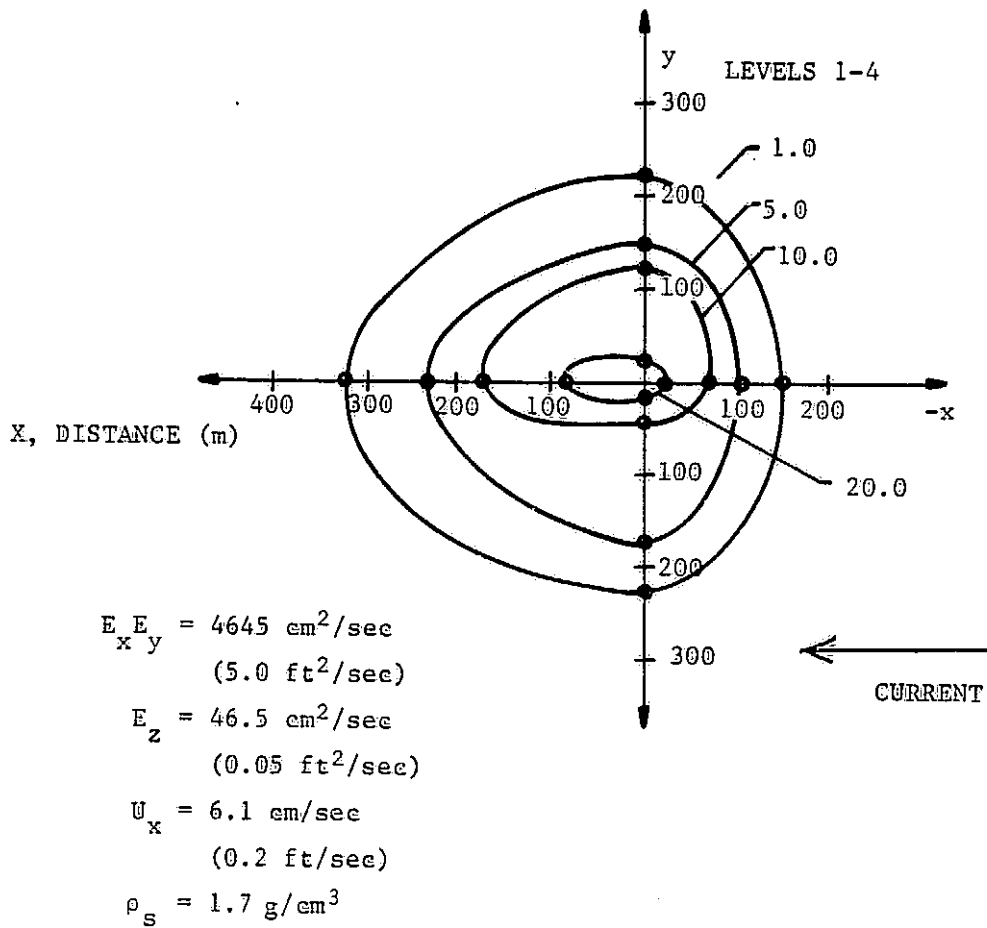


Figure 53. Equiconcentration lines for a continuous release, second case (time = 10 min).

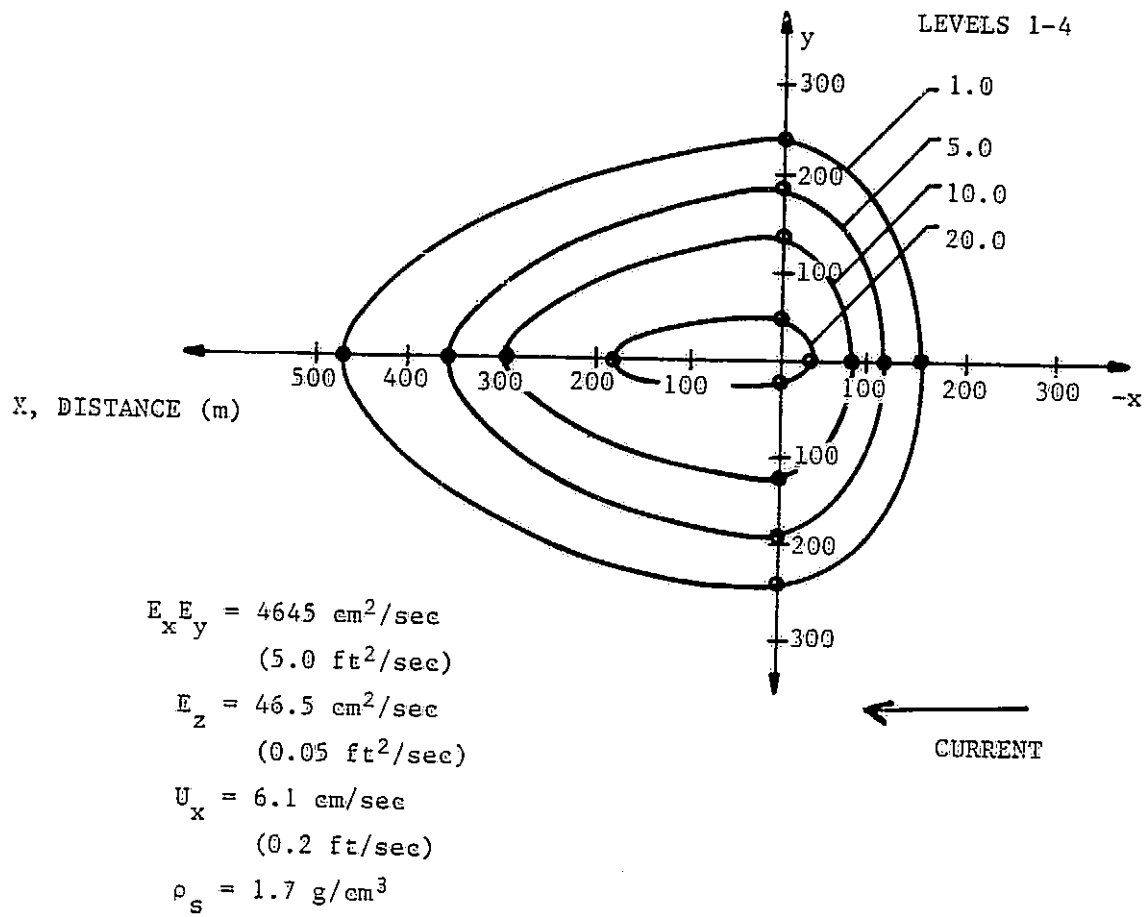


Figure 54. Equiconcentration lines for a continuous release, second case (time = 20 min).

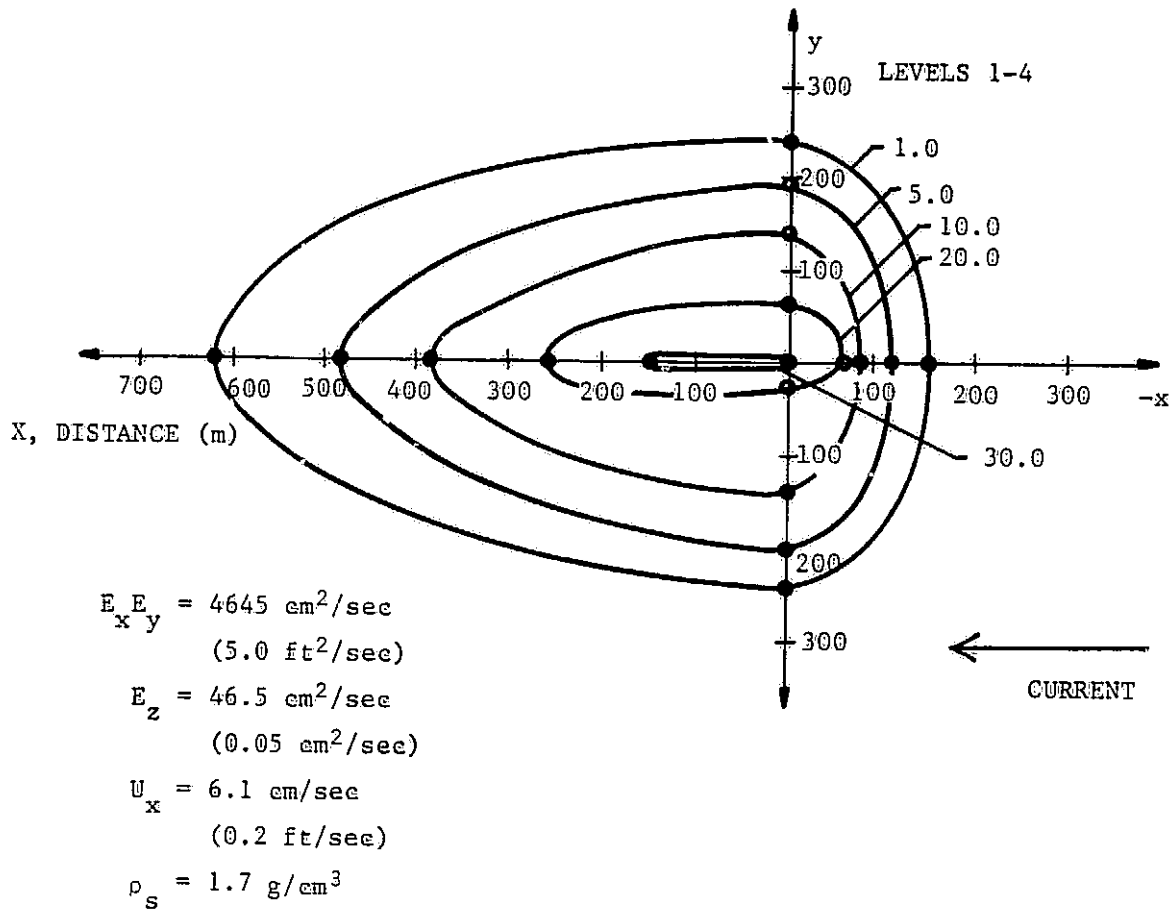


Figure 55. Equiconcentration lines for a continuous release, second case (time = 30 min).

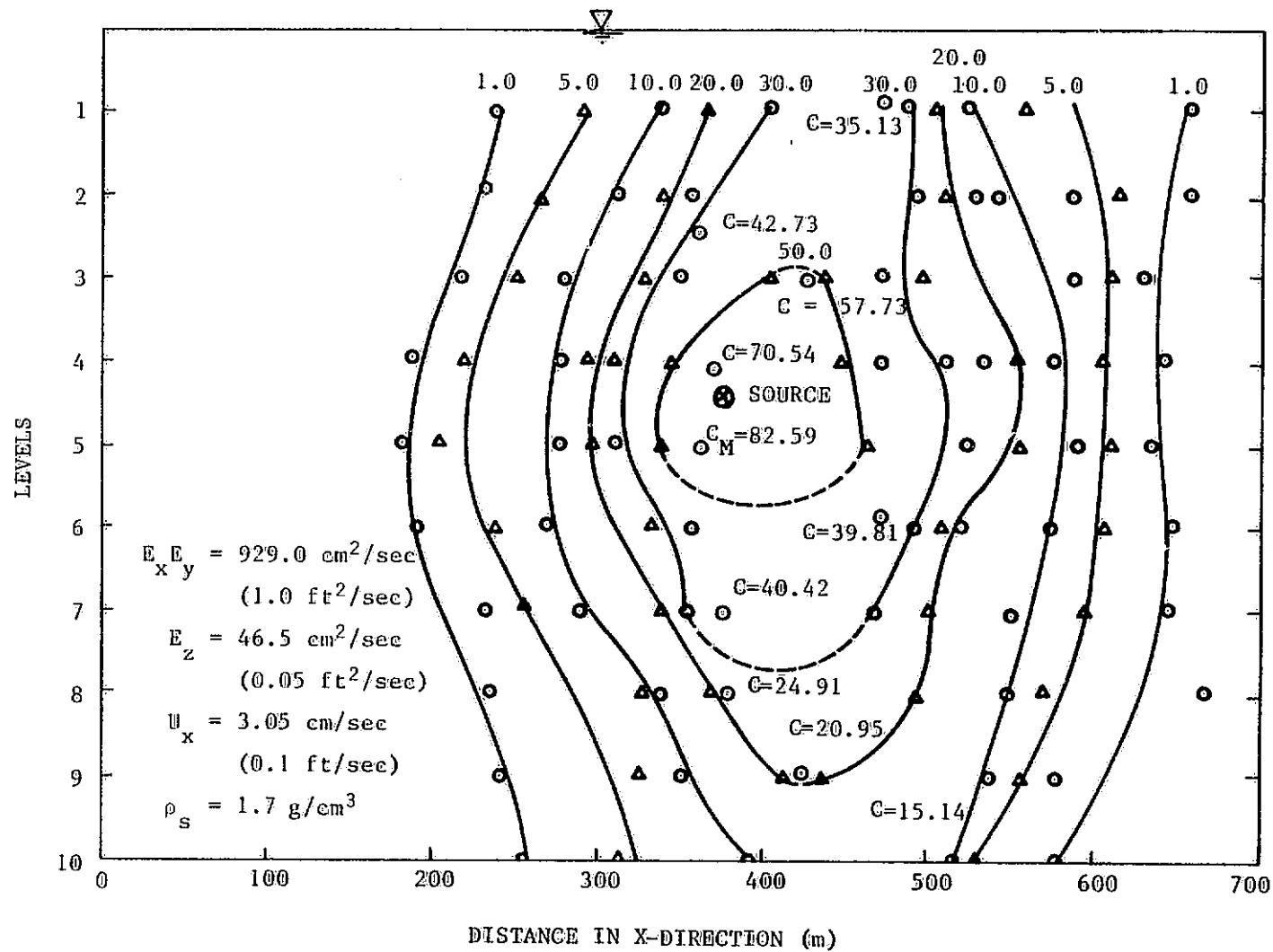


Figure 56. Vertical equiconcentration lines, first case (time = 15 min).

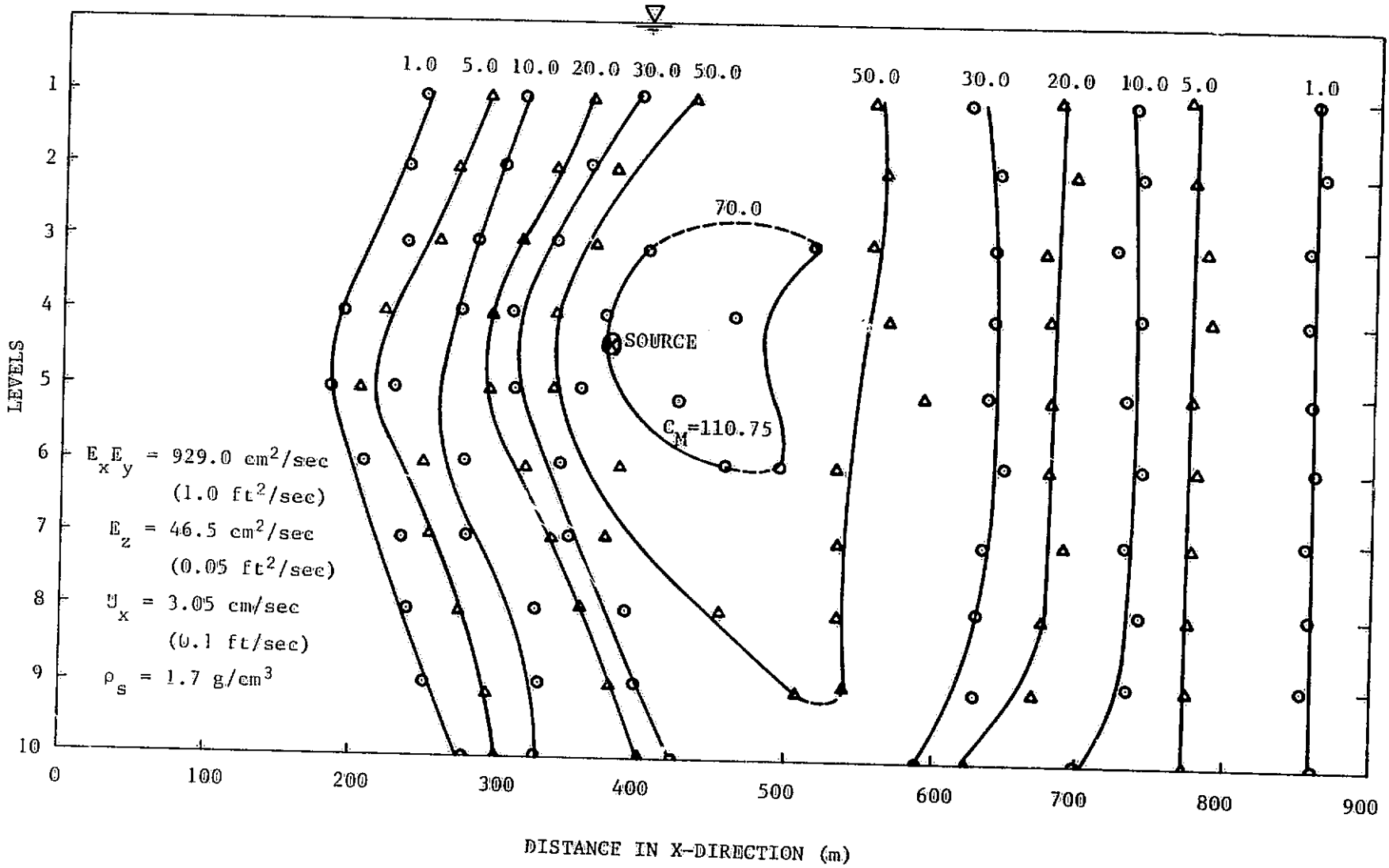


Figure 57. Vertical equiconcentration lines, first case (time = 45 min).

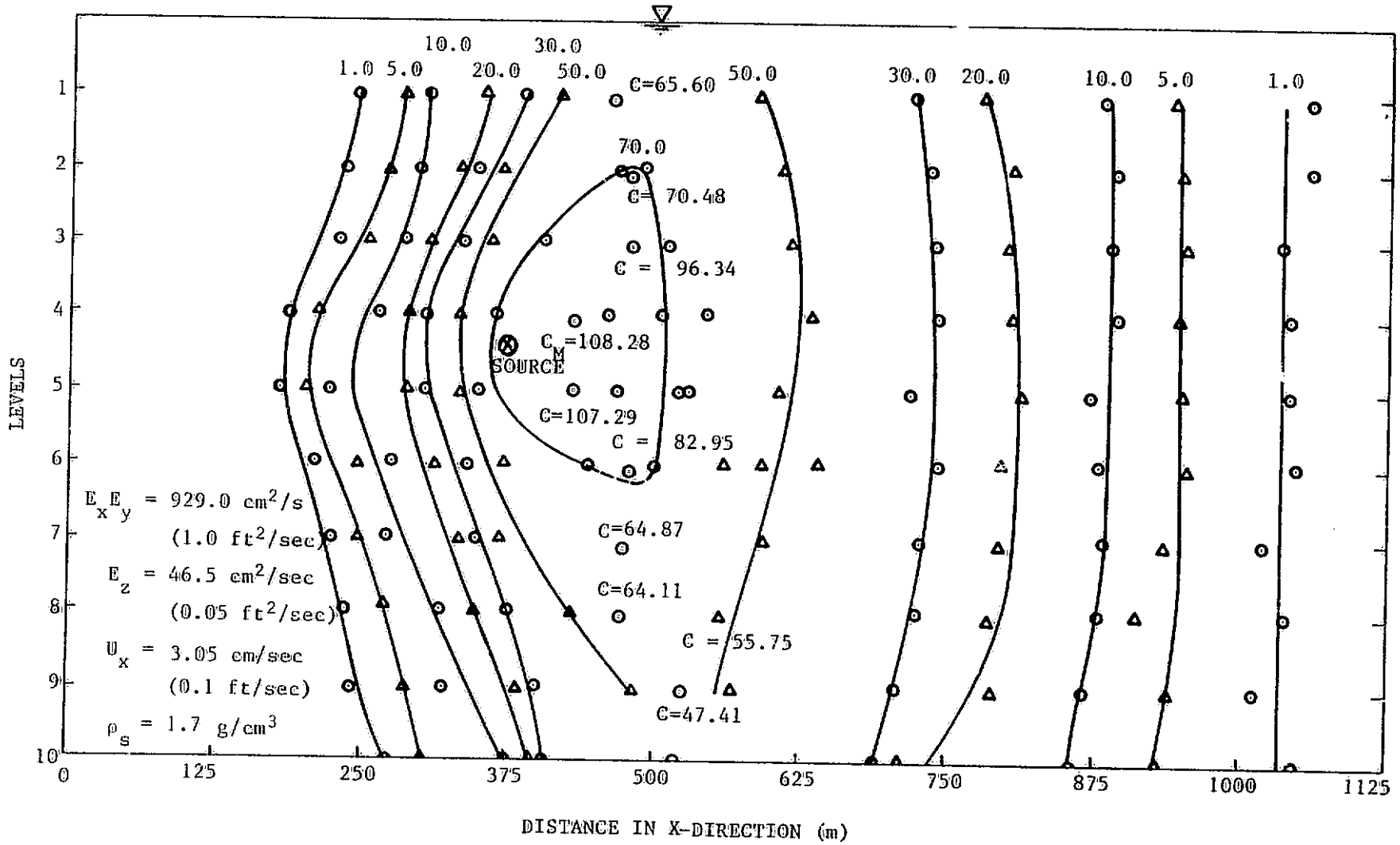


Figure 58. Vertical equiconcentration lines, first case (time = 75 min).

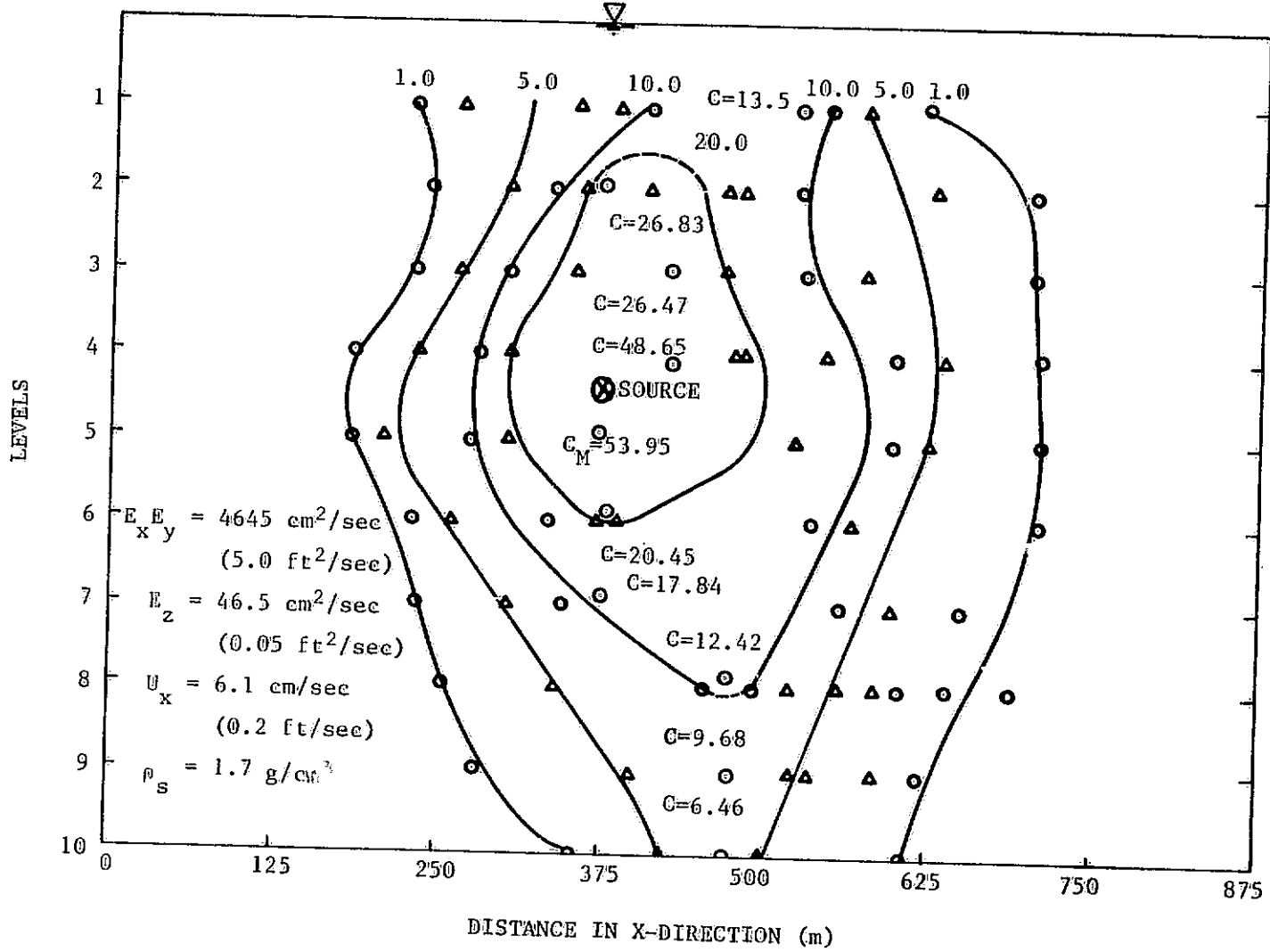


Figure 59. Vertical equiconcentration lines, second case (time = 10 min).

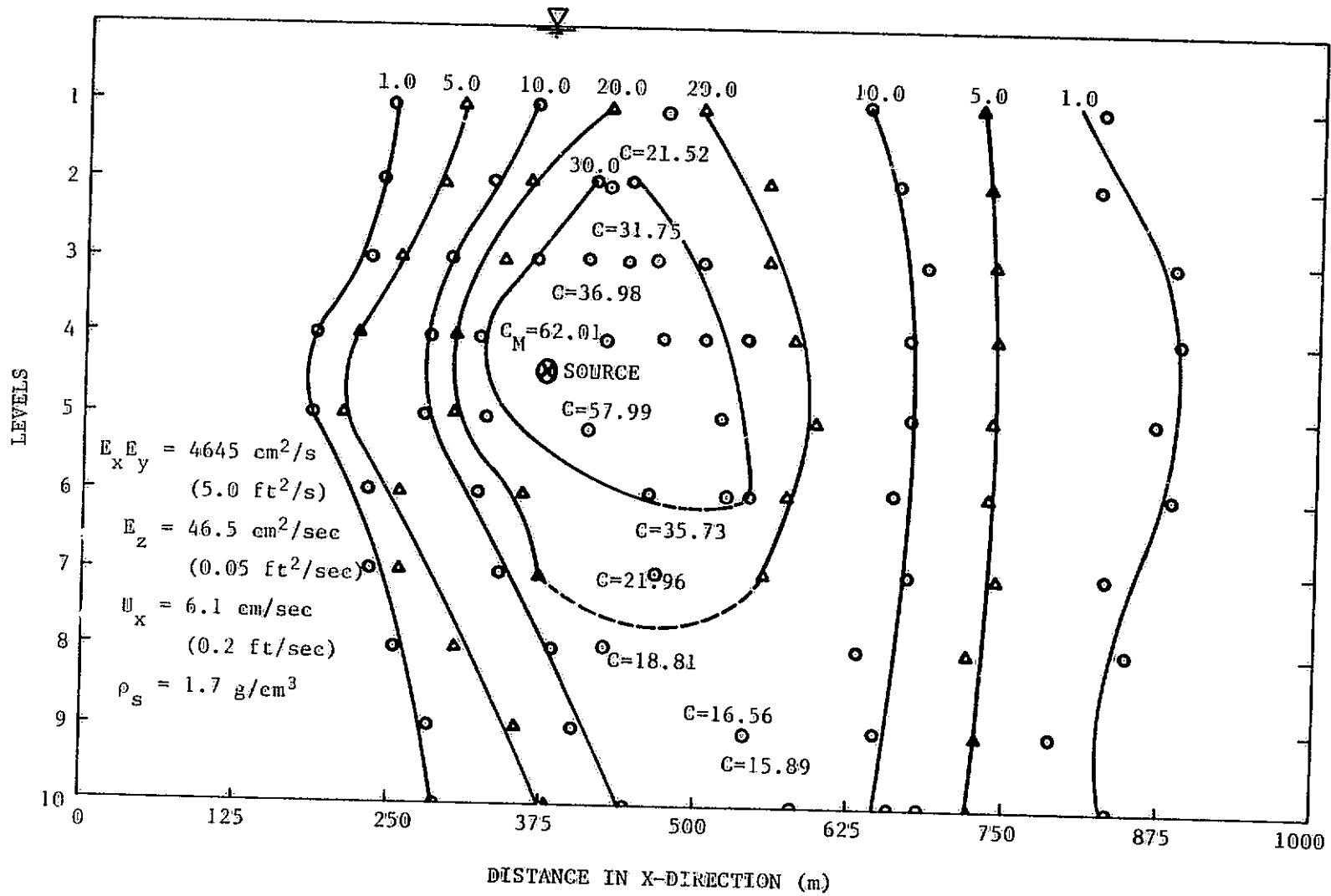


Figure 60. Vertical equiconcentration lines, second case (time = 20 min).

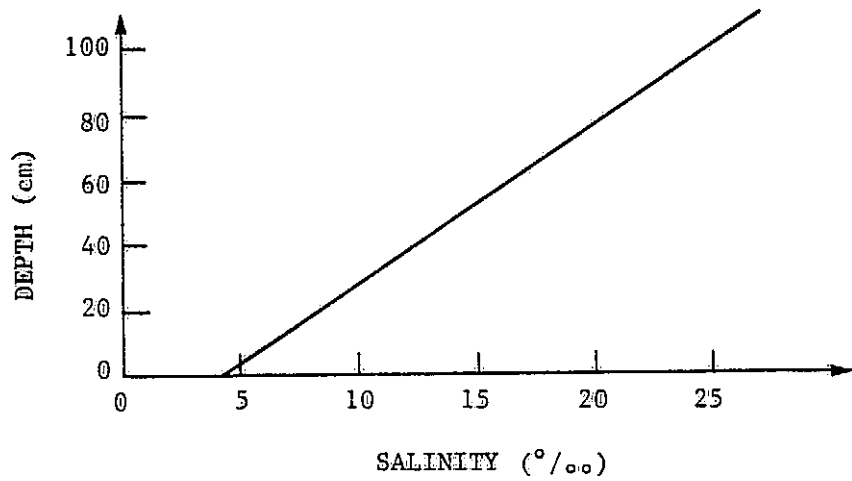


Figure 62. The relationship between water depth and salinity for the case of linear density stratification.

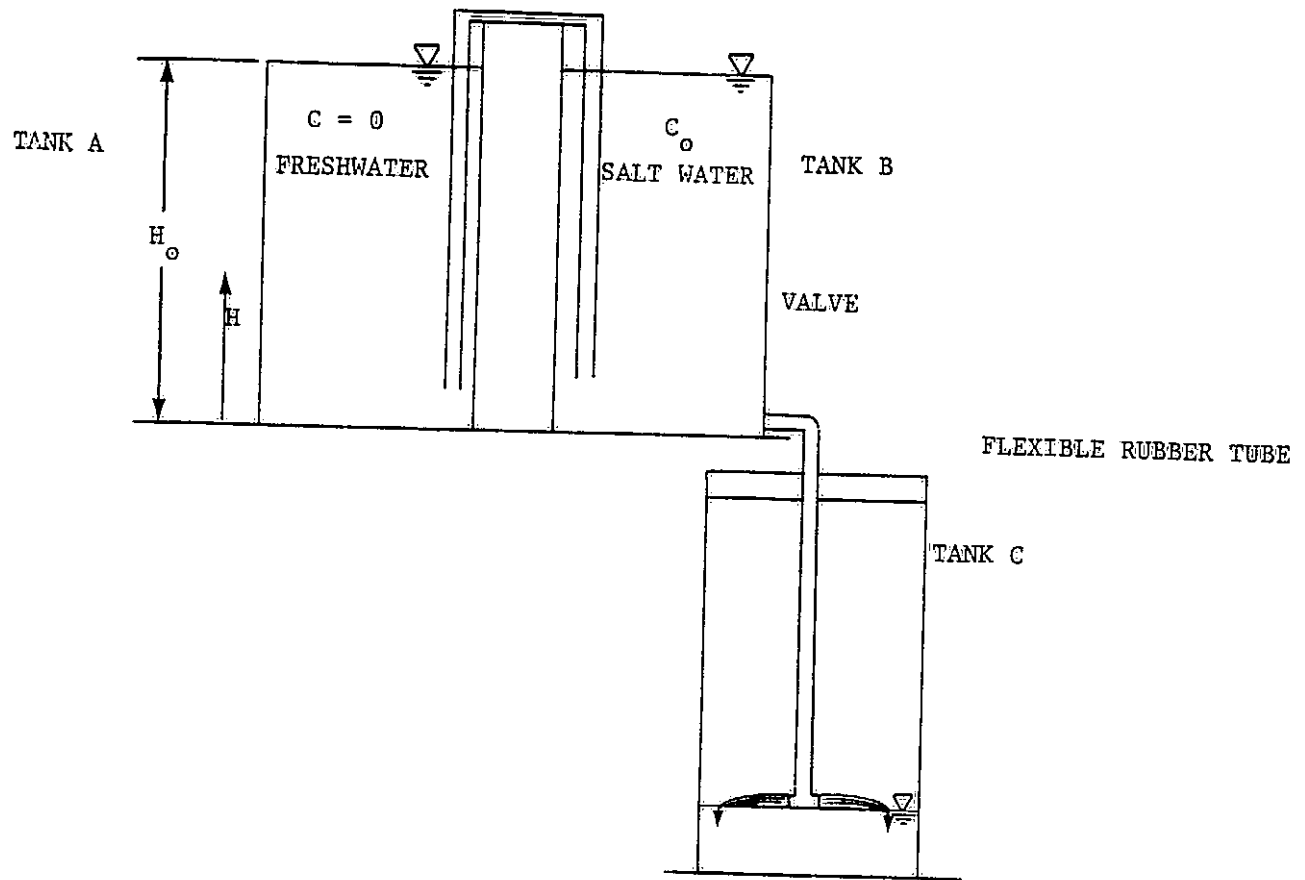


Figure 63. Laboratory setup.

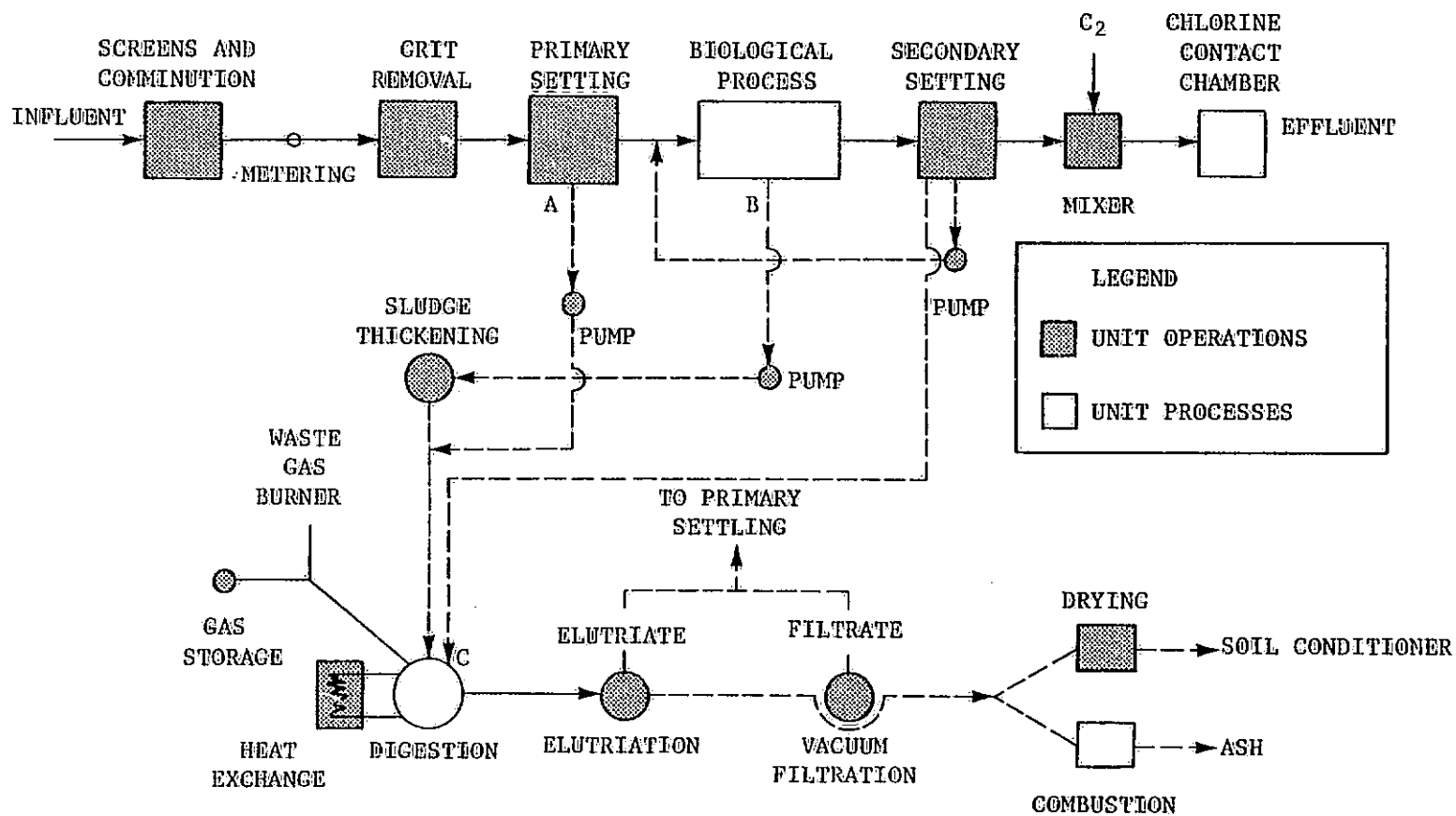


Figure 64. Wastewater treatment plant flowsheet.

REFERENCES

1. Environmental Protection Agency: Ocean Dumping in the United States - 1977. Fifth Annual Report on Administration of Title I, March 1977.
2. Pagoria, P.S.; and Kuo, C.Y.: Interpretation of the Characteristics of Ocean-Dumped Sewage Sludge Related to Remote Sensing. Part II, Final Report under NASA Grant NSG 1441, Feb. 1979.
3. Johnson, R.W.: Quantitative Sediment Mapping from Remotely Sensed Multispectral Data. Presented at the Fourth Annual Remote Sensing of Earth Resources Conference (Tullahoma, TN), Mar. 1975.
4. Johnson, R.W.: Quantitative Mapping of Water Quality Parameters in the James River, Virginia, by Aircraft Remote Sensing. Presented at the 1976 Annual Meeting, Virginia Academy of Science (Fairfax, VA), May 1976.
5. Whitlock, C.H.; and Talay, T.A.: Remote Sensing Observations of Industrial Plumes at Hopewell, Virginia. Presented at the EPA Kepone Seminar II (Easton, MD), Sept. 1977.
6. Johnson, R.W.: Identification and Mapping of Pollution Features in the Coastal Zones. Presented at the 1977 Region 3 Conference and Exhibit (Williamsburg, VA), Apr. 1977.
7. Johnson, R.W.; Ohlhorst, C.W.; and Usry, J.W.: Location, Identification, and Mapping of Sewage Sludge and Acid Waste Plumes in the Atlantic Coastal Zones. Proceedings of the Fourth Joint Conference on Sensing of Environmental Pollutants (New Orleans, LA), Nov. 1977.
8. Johnson, R.W.; and Hall, J.B., Jr.: Remote Sensing Operations (Multi-spectral Scanner and Photographic) in the New York Bight, September 22, 1975. NASA TM X-73993, Feb. 1977.
9. Johnson, R.W.; Duedall, I.W.; Glasgow, R.M.; Proni, J.K.; and Nelsen, T.A.: Quantitative Mapping of Suspended Solids in Wastewater Sludge Plumes in the New York Bight Apex. J. Water Pollution Control Fed. (Washington, DC), Oct. 1977.
10. Svehla, R.; Raquet, C.; Shook, D.; Salzman, J.; Coney, T.; Wachter, D.; and Gedney, R.: Remote Sensing Study of Maumee River Effects on Lake Erie. NASA TM X-71780, July 1975.

11. Wazernak, C.T.; and Lyzenga, D.R.: Satellite Remote Sensing Study of the Trans-Boundary Movement of Pollutants. EPA Report 600/3-77-056, May 1977.
12. Scherz, J.P.; Crane, D.R.; and Rogers, R.H.: Classifying and Monitoring Water Quality by Use of Satellite Imagery. International Conference on Environmental Sensing and Assessment (Las Vegas, NV), Sept. 1975.
13. Ketchum, B.H.; and Ford, W.L.: Rate of Dispersion in the Wake of a Barge at Sea. Transactions, American Geophysical Union, Vol. 33, No. 5, Oct. 1952.
14. Ball, J.; and Reynolds, T.D.: Dispersal of Liquid Waste from a Moving Barge. Journal WCPF, Vol. 48, No. 11, Nov. 1976.
15. Young, R.A.: Combined Progress Report on the Second Sludge Tracking Acoustical Experiment (STAX II). NOAA Preliminary Draft, Apr. 1977 (personal communication).
16. Callaway, R.J.; Teeter, A.M.; Browne, D.W.; and Ditsworth, G.R.: Preliminary Analysis of the Dispersion of Sewage Sludge Discharged from Vessels to New York Bight Waters, M.G. Gross, ed., Proceedings of the Symposium on Middle Atlantic Continental Shelf and the New York Bight. Allen Press, 1976.
17. Ditsworth, G.R.; Teeter, A.M.; and Callaway, R.J.: New York Bight Suspended Matter and Oceanographic Data: 1973-1974. EPA Report 600/3-78-002, Feb. 1978.
18. Teeter, A.M.; Callaway, R.J.; and Denbu, D.W.: Dispersion of Sewage Sludge Discharged into New York Bight, Physical Oceanographic Data - December 1974. EPA Report 600/3-78-068a, Sept. 1978.
19. Teeter, A.M.; Callaway, R.J.; and Denbu, D.W.: Dispersion of Sewage Sludge Discharged into New York Bight, Physical Oceanographic Data and Laboratory Analysis - 1975. EPA Report 600/3-78-068b, Sept. 1978.
20. Usry, J.W.; Witte, W.G.; Whitlock, C.H.; and Gurganus, E.A.: Laboratory Upwelled Spectral Signature Measurements of Sewage Sludge for Remote Sensing of Ocean Dumping. Presented at 1977 IEEE Southeast Conference (Williamsburg, VA), Apr. 1977.

21. Johnson, B.H.: Investigation of Mathematical Models for the Physical Fate Prediction of Dredged Material. U.S. Army Corps of Engineers, Waterways Experiment Station, Technical Report D-74-1, Mar. 1974.
22. Koh, R.C.Y.; and Chang, Y.C.: Mathematical Model for Barged Ocean Disposal of Wastes. EPA Report 660/2-73-029, Dec. 1973.
23. Edge, B.L: Hydrodynamic Analysis of Sludge Dumped in Coastal Waters. Chapter 125, Proceedings of the Thirteenth Coastal Engineering Conference, American Society of Civil Engineers, July 1972.
24. Krishnappen, B.G.: Dispersion of Granular Material Dumped in Deep Water. Canada Centre for Inland Waters (Ontario), 1975.
25. Johnson, B.H.; and Holliday, B.W.: Numerical Model Results of Dredged Material Disposal at Ten Proposed Ocean Disposal Sites in the Hawaiian Islands. U.S. Army Corps of Engineers, Waterways Experiment Station, Miscellaneous Paper H-77-6, May 1977.
26. Falk, L.L.; Myers, T.D.; and Thomann, R.V.: Waste Dispersion Characteristics and Effects in an Oceanic Environment. EPA Report 600/2-77-112, June 1977.
27. Deb, A.K.: Mathematical Modelling of Dispersion of Barged Wastes. ASCE Spring Convention and Exhibit, Apr. 24-28, 1978.
28. Rittall, W.F.: A Discussion of a Near Field Dispersion Model for Sludge Discharges to Coastal Waters. In: Proceedings of Pretreatment and Ultimate Disposal of Wastewater Solids, A. Freiburger, ed. EPA Report 902/9-74-002, 1974.
29. Bowers, G.W.; and Goldenblatt, M.K.: Calibration of a Predictive Model for Instantaneously Discharged Dredged Material. EPA Report 600/3-78-089, Sept. 1978.
30. Brandsma, M.G.; and Divoky, D.J.: Development of Models for Prediction of Short-Term Fate of Dredged Material Discharged in the Estuarine Environment. U.S. Army Corps of Engineers, Waterways Experiment Station, Contract Report D-76-5, May 1976.
31. Johnson, B.H.; and Holliday, B.W.: Evaluation and Calibration of the Tetra Tech Dredged Material Disposal Model Based on Field Data. U.S. Army Corps of Engineers, Waterways Experiment Station, Technical Report D-78-47, Aug. 1978.

32. Pavish, D.L.; and Spaulding, M.L.: Development and Application of a Three-Dimensional Numerical Model for Predicting Pollutant and Sediment Transport Using an Eulerian-Lagrangian Marker Particle Technique. NASA Report, July 1977.
33. Browne, D.W.; and Callaway, R.J.: Dispersion of Sewage Sludge Discharged from Sludge Disposal Vessels into New York Bight. EPA Corvallis Environmental Research Laboratory, Data Report I, Vol. 3, June 1974.
34. Burgess, F.J.; and James, W.P.: Air Photo Analysis of Ocean Outfall Dispersion. Water Pollution Control Research Series, 16070 ENS06/71, June 1971.
35. Kuo, C.Y.: Free Falling Particle in Density Stratified Fluid. Puerto Rico Water Resources Research Institute, Report A-032-PR, Dec. 1972.
36. Proni, J.R.; Newmann, F.C.; Young, R.A.; Walter, D.; Sellers, R.; McGillivray, P.; Duedall, I.; Stanford, H.; and Parker, C.: Observations of the Intrusion into a Stratified Ocean of an Artificial Tracer and the Concomitant Generation of Internal Oscillations, 1976 (personal communication).
37. Broecker, W.S.; Feely, H.W.; and Gerard, R.D.: Transport and Transfer Rates in the Waters of the Continental Shelf. ERDA Annual Report (11-1) 2185, June 1975.
38. Yudelson, J.M.: A Survey of Ocean Diffusion Studies and Data. Division of Engineering and Applied Science, California Institute of Technology (Pasadena), Technical Memorandum No. 67-2, Sept. 1967.

APPENDIX

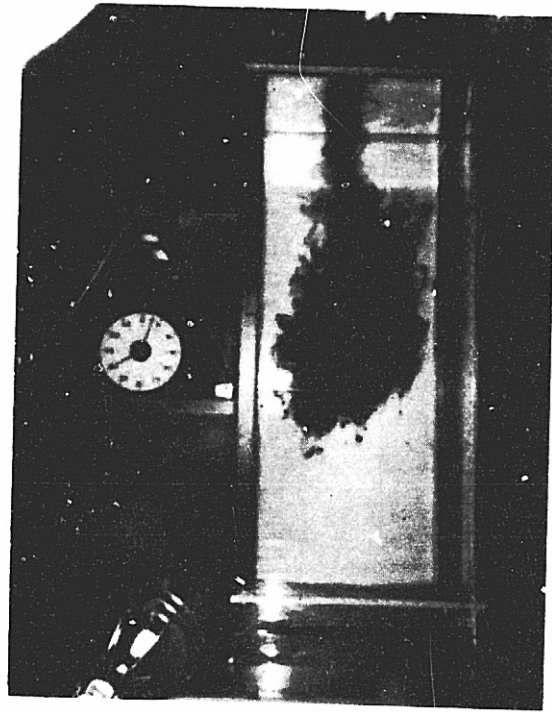


Figure A-1.

Sludge type: primary sludge;
Dumping method: water surface continuous release;
Ambient condition: freshwater;
Time: 2.33 min after release.

ORIGINAL PAGE IS
OF POOR QUALITY

ORIGINAL PAGE IS
OF POOR QUALITY

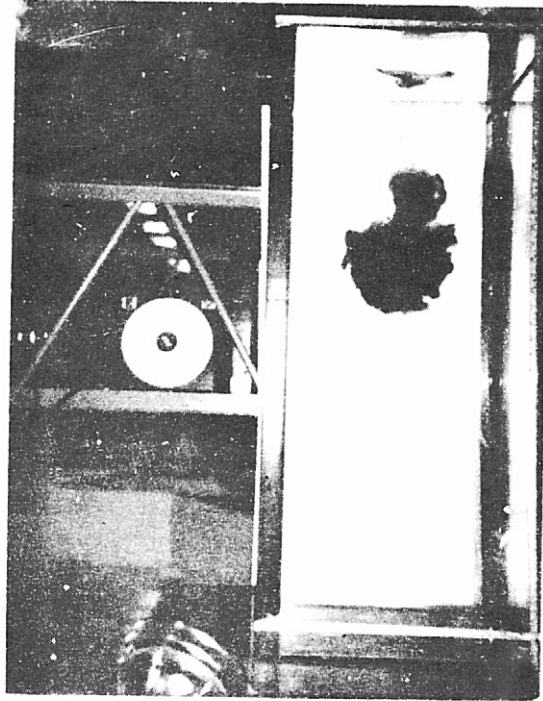


Figure A-2a.

Sludge type: secondary sludge;

Dumping method: water surface continuous dumping;

Ambient condition: freshwater;

Time: 0.38 min after dumping.

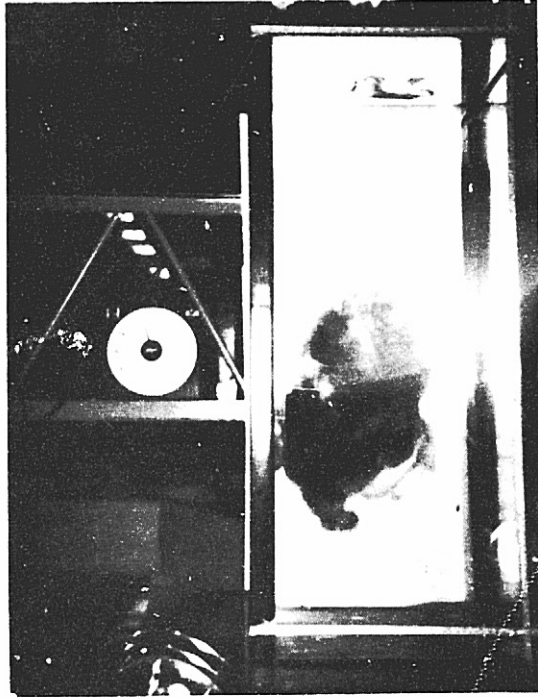


Figure A-2b.

Sludge type: secondary sludge;

Dumping method: water surface continuous dumping;

Ambient condition: freshwater;

Time: 1.05 min after dumping.

ORIGINAL PAGE IS
OF POOR QUALITY

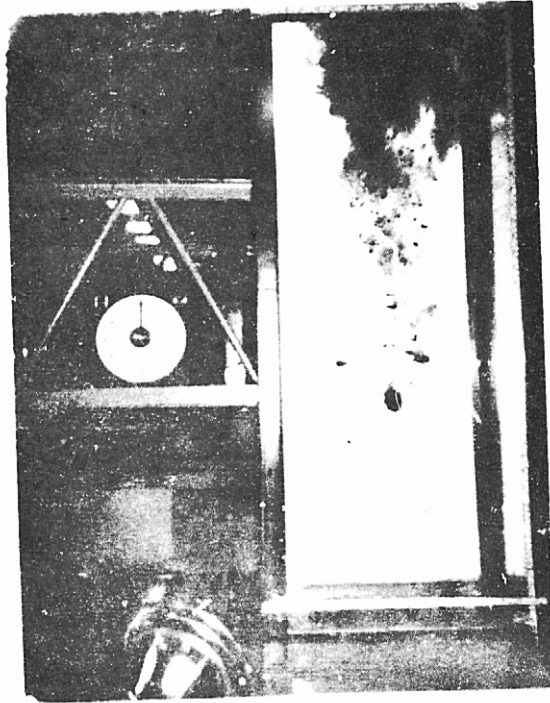


Figure A-3.

Sludge type: primary sludge;
Dumping method: underwater instantaneous release;
Ambient condition: freshwater;
Time: 5.00 min after release.

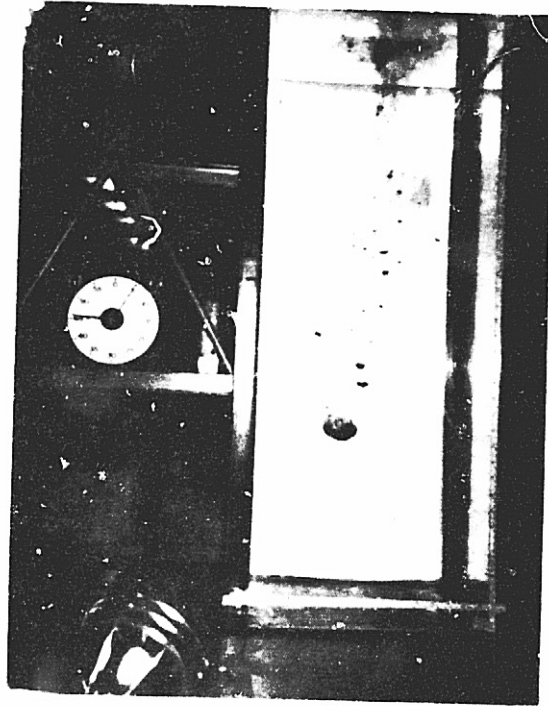


Figure A-4.

Sludge type: primary sludge;
Dumping method: underwater instantaneous release;
Ambient condition: freshwater;
Time: 0.23 min after release.

ORIGINAL PAGE IS
OF POOR QUALITY



Figure A-5.

Sludge type: secondary sludge;
Dumping method: underwater instantaneous release;
Ambient condition: freshwater;
Time: 0.67 min after release.

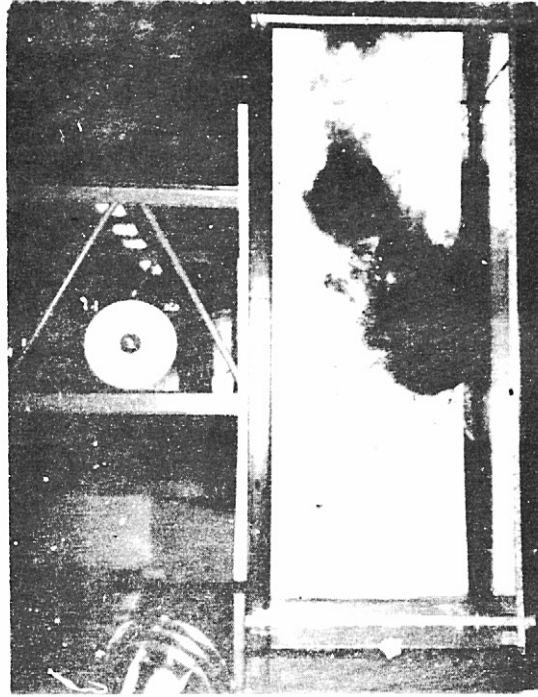


Figure A-6.

Sludge type: primary sludge;
Dumping method: water surface instantaneous release;
Ambient condition: freshwater;
Time: 1.35 min after release.

ORIGINAL PAGE IS
OF POOR QUALITY

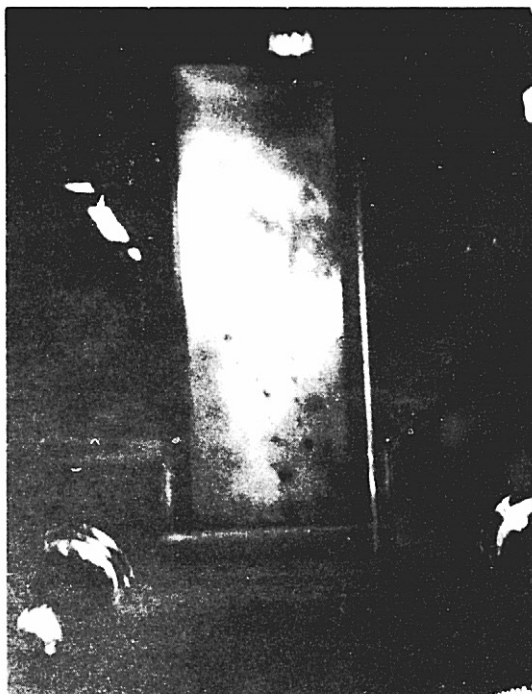


Figure A-7a.

Sludge type: primary sludge;
Dumping method: water surface instantaneous release;
Ambient condition: freshwater;
Time: 0.4 min after dumping.

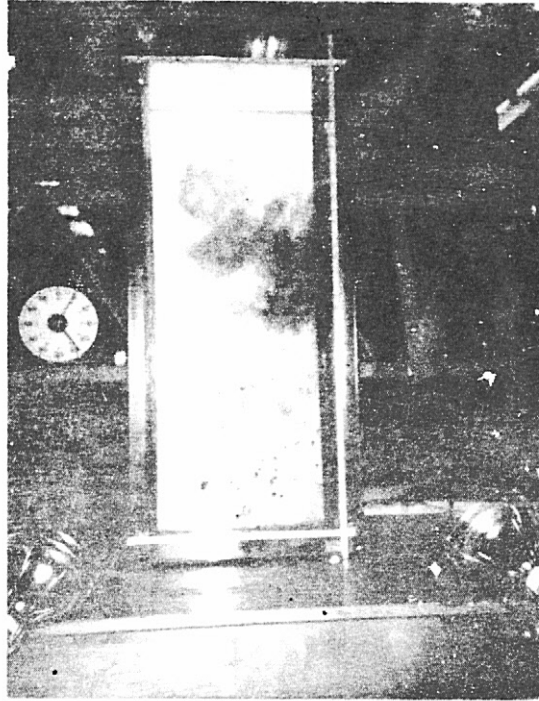


Figure A-7b.

Sludge type: primary sludge;

Dumping method: water surface instantaneous release;

Ambient condition: freshwater

Time: 0.6 min after dumping.

ORIGINAL PAGE IS
OF POOR QUALITY

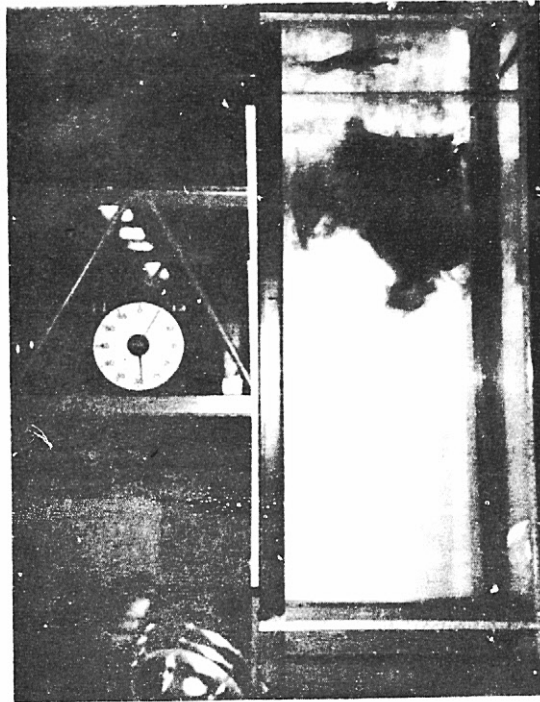


Figure A-8.

Sludge type: secondary sludge;
Dumping method: water surface instantaneous release;
Ambient condition: freshwater;
Time: 0.52 min after release.

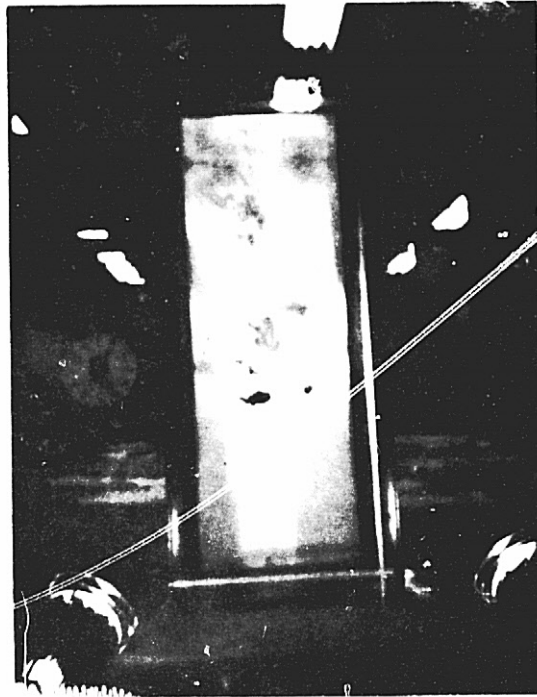


Figure A-9.

Sludge type: primary sludge;

Dumping method: water surface instantaneous release;

Ambient condition: 15⁰/∞∞ salt water;

Time: 0.42 min after release.

ORIGINAL PAGE IS
OF POOR QUALITY

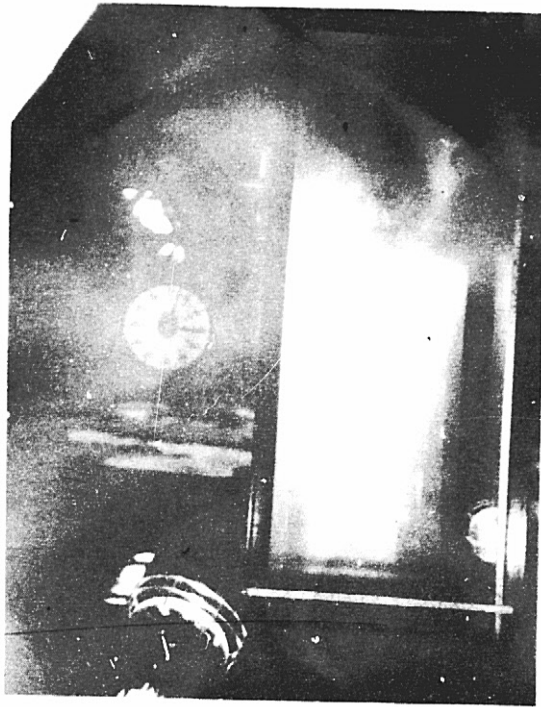


Figure A-10.

Sludge type: secondary sludge;
Dumping method: water surface instantaneous release;
Ambient condition: 15⁰/00 salt water;
Time: 2.75 min after release.



Figure A-11a.

Sludge type: primary sludge;
Dumping method: water surface instantaneous release;
Ambient condition: 2-layer system,
 upper layer: freshwater,
 lower layer: 15^o/oo salt water;
Time: 0.32 min after dumping.

ORIGINAL PAGE IS
OF POOR QUALITY

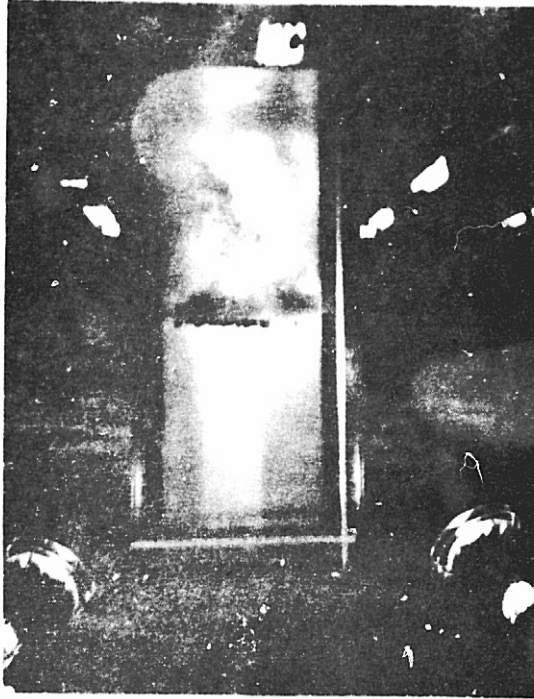


Figure A-11b.

Sludge type: primary sludge;
Dumping method: water surface instantaneous release;
Ambient condition: 2-layer system,
 upper layer: freshwater,
 lower layer: 15⁰/oo salt water;
Time: 0.55 min after dumping.

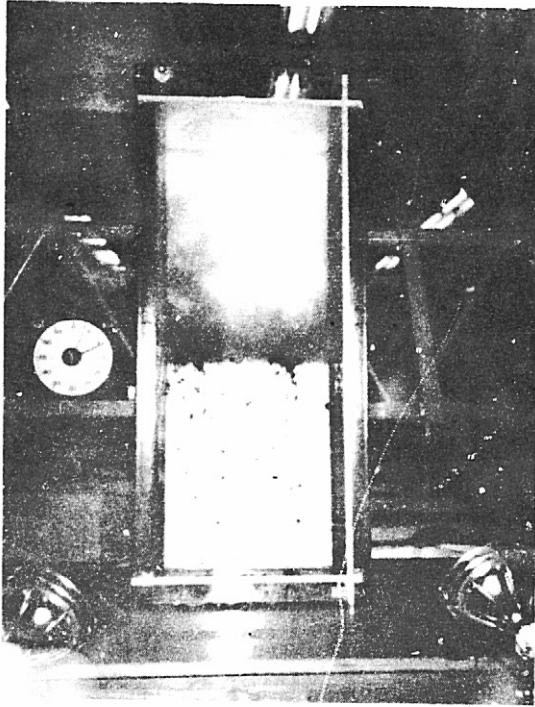


Figure A-11C.

Sludge type: primary sludge;
Dumping method: water surface instantaneous release;
Ambient condition: 2-layer system,
 upper layer: freshwater,
 lower layer: 15⁰/00 salt water;
Time: 1.82 min after dumping.

ORIGINAL PAGE IS
OF POOR QUALITY

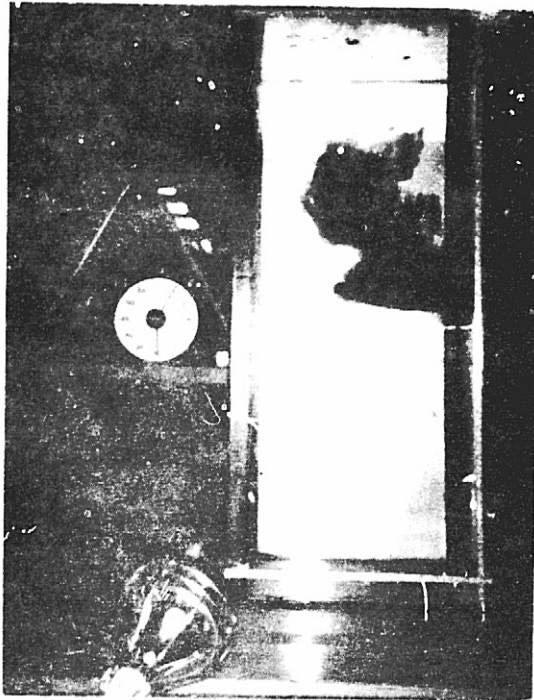


Figure A-12a.

Sludge type: secondary sludge;
Dumping method: water surface instantaneous release;
Ambient condition: 2-layer system,
 upper layer: freshwater,
 lower layer: 15⁰/100 salt water;
Time: 0.52 min after dumping.

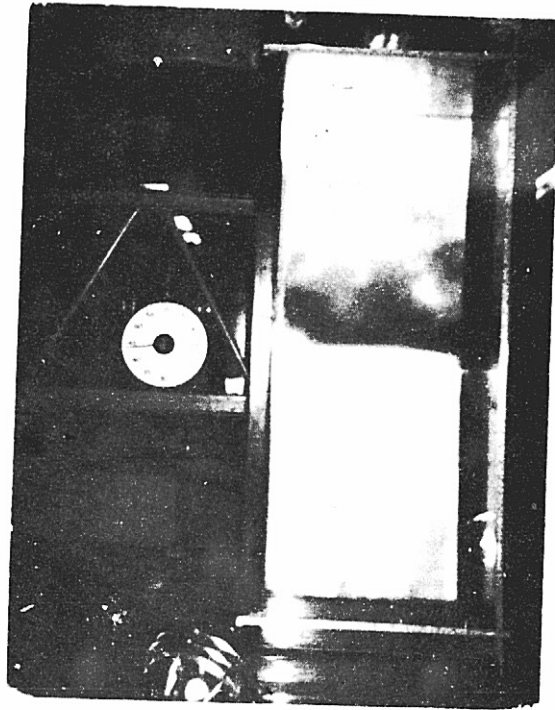


Figure A-12b.

Sludge type: secondary sludge;
Dumping method: water surface instantaneous release;
Ambient condition: 2-layer system,
 upper layer: freshwater,
 lower layer: 15⁰/00 salt water;
Time: 3.27 min after dumping.

ORIGINAL PAGE IS
OF POOR QUALITY.

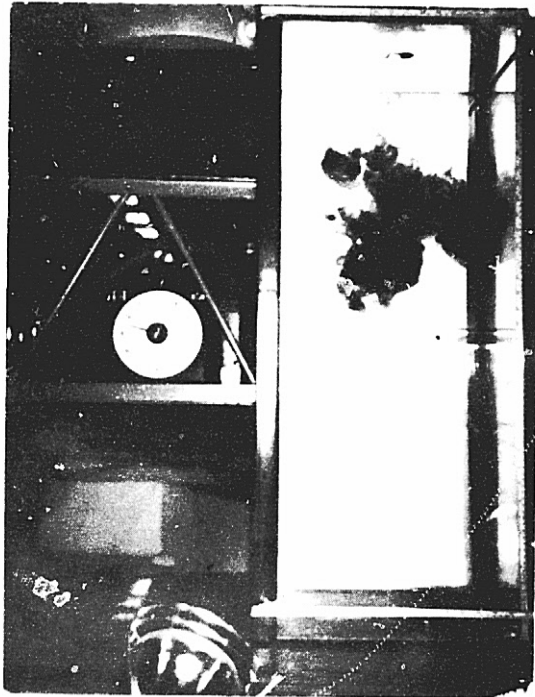


Figure A-13a.

Sludge type: secondary sludge;
Dumping method: water surface instantaneous release;
Ambient condition: 2-layer system,
 top: freshwater,
 bottom: 25⁰/∞ salt water;
Time: 0.27 min after dumping.

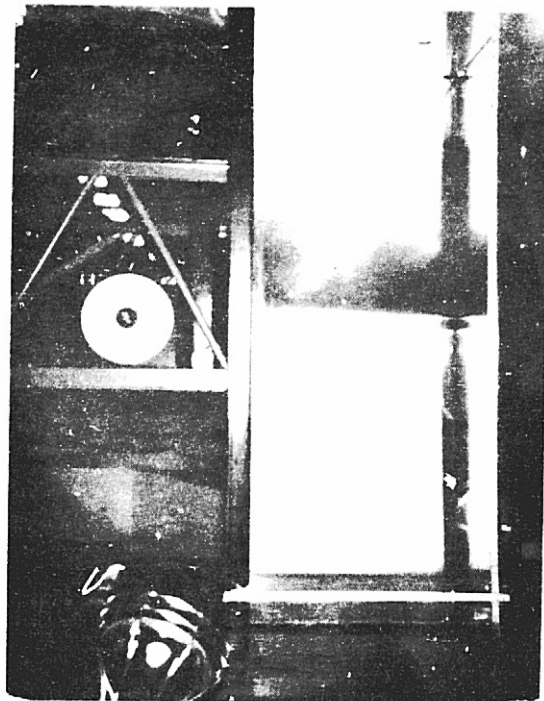


Figure A-13b.

Sludge type: secondary sludge;
Dumping method: water surface instantaneous release;
Ambient condition: 2-layer system,
 top: freshwater,
 bottom: 25^o/oo salt water;
Time: 1.87 min after dumping.

ORIGINAL PAGE 19
OF POOR QUALITY

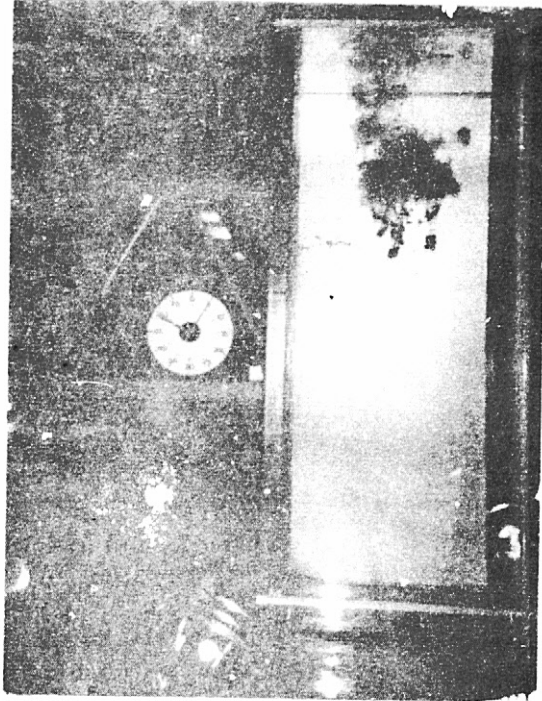


Figure A-14a.

Sludge type: primary sludge;

Dumping method: water surface instantaneous release;

Ambient condition: linearly varying density (bottom 25^o/oo);

Time: 0.2 min after dumping.

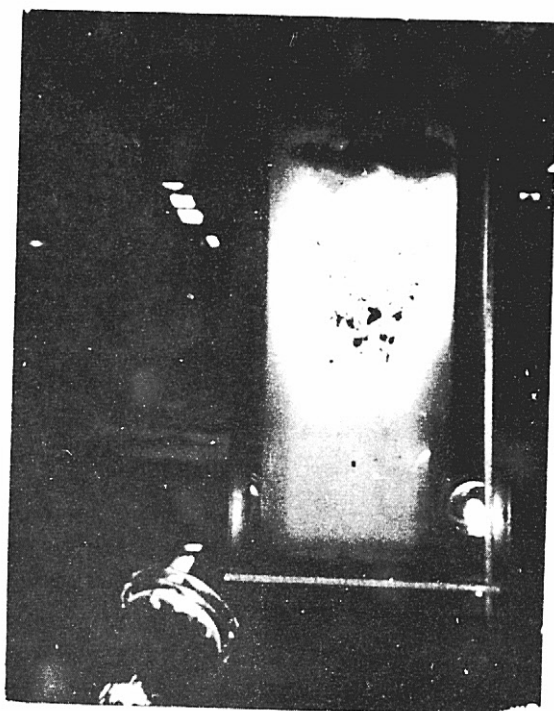


Figure A-14b.

Sludge type: primary sludge;
Dumping method: water surface instantaneous release;
Ambient condition: linearly varying density (bottom 25⁰/00);
Time: 1.08 min after dumping.

ORIGINAL PAGE IS
OF POOR QUALITY



Figure A-14C.

Sludge type: primary sludge;
Dumping method: water surface instantaneous release;
Ambient condition: linearly varying density (bottom $25^{\circ}/\infty$);
Time: 2.93 min after dumping.

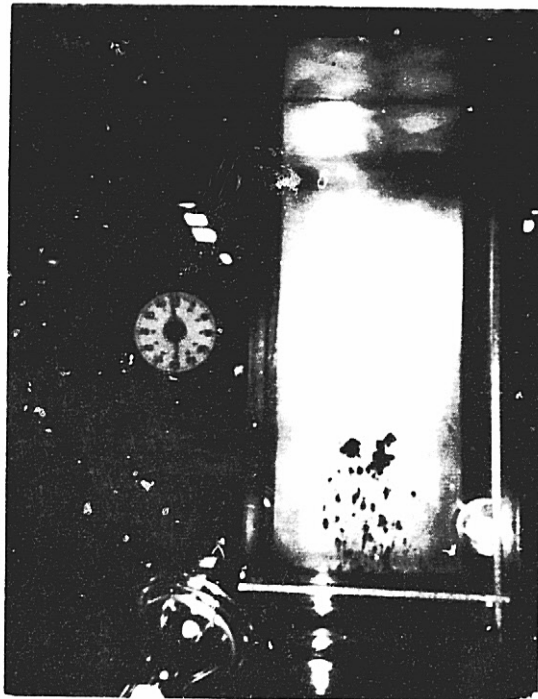


Figure A-14d.

Sludge type: primary sludge;

Dumping method: water surface instantaneous release;

Ambient condition: linearly varying density (bottom $25^{\circ}/_{00}$);

Time: 6.52 min after dumping.

ORIGINAL PAGE IS
OF POOR QUALITY

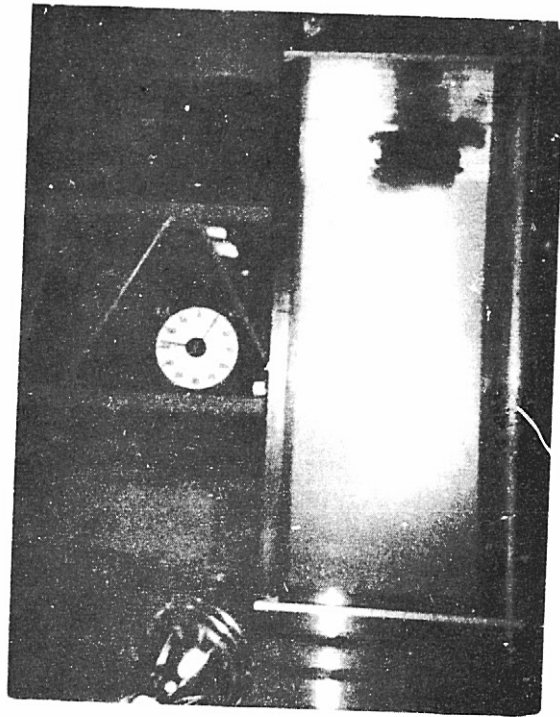


Figure A-15a.

Sludge type: secondary sludge;
Dumping method: water surface instantaneous release;
Ambient condition: linearly varying density (bottom $25^{\circ}/_{00}$);
Time: 0.23 min after dumping.

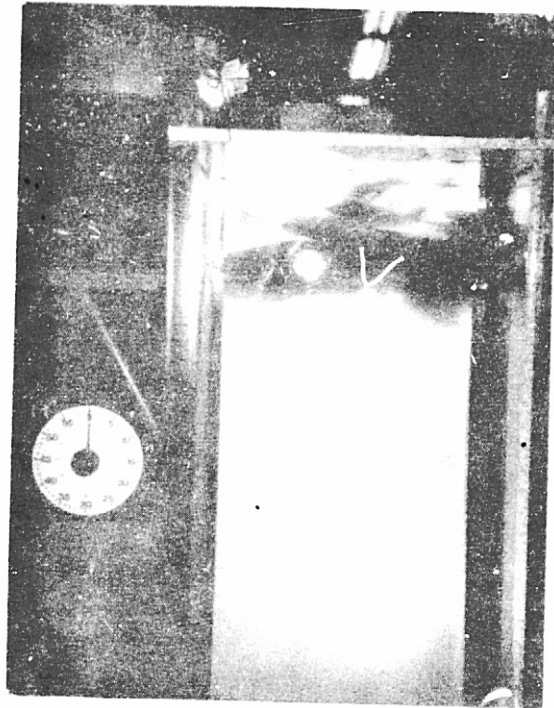


Figure A-15b.

Sludge type: secondary sludge;
Dumping method: water surface instantaneous release;
Ambient condition: linearly varying density (bottom $25^{\circ}/\text{cc}$);
Time: 5 min after dumping.